UNIVERSITY OF CRETE
DEPARTMENT OF CHEMISTRY

SYNTHETIC, SPECTROSCOPIC, STRUCTURAL, AND SPECIATION STUDIES IN THE Co(II) – N,N – BIS(PHOSPHONOMETHYL)GLYCINE SYSTEM

ANCA MATEESCU

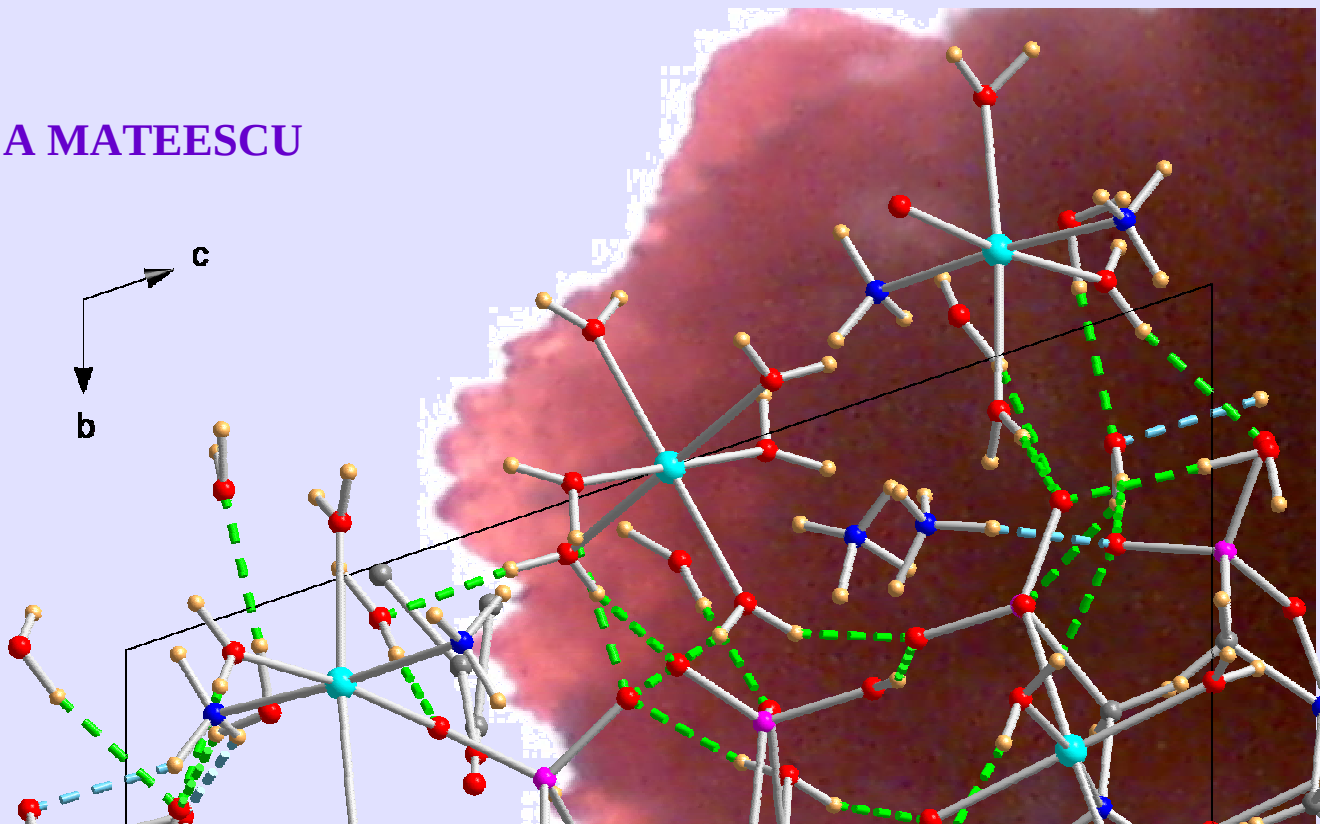

SYNTHETIC, SPECTROSCOPIC, STRUCTURAL, AND SPECIATION STUDIES IN THE Co(II) – N,N – BIS(PHOSPHONOMETHYL)GLYCINE SYSTEM.

ANCA MATEESCU

Supervisor: Assoc. Prof. Athanassios Salifoglou

UNIVERSITY OF CRETE, DEPARTMENT OF CHEMISTRY

COMMITTEE MEMBERS: *Athanassios Coutsolelos*, Department of Chemistry,University of Crete

Apostolis Rizos, Department of Chemistry, University of Crete

Athanassios Salifoglou, Aristotle University of Thessalonik

ABSTRACT

CHAPTER 1

COBALT: THE ELEMENT IN NATURE AND IN THE LAB

CHAPTER 2

EXPERIMENTAL TECHNIQUES AND METHODS USED FOR CHARACTERIZATION OF THE COMPLEXES

CHAPTER 3

COMPLEX FORMATION OF Co(II) WITH THE ORGANO PHOSPHONATE LIGAND NTA2P (N,N-BIS(PHOSPHONOMETHYL) GLYCINE) AT LOW pH

CHAPTER 4

AN UNUSUAL COMPLEX OF Co(II) WITH THE ORGANO PHOSPHONATE LIGAND NTA2P (N,N- BIS (PHOSPHONOMETHYL) GLYCINE)

CHAPTER 5

POTENTIOMETRIC AND SPECTROPHOTOMETRIC MEASUREMENTS OF Co(II) WITH NTA AND ITS PHOSPHONIC DERIVATIVES

CHAPTER 6

GENERAL CONCLUSIONS

SYNTHETIC, SPECTROSCOPIC, STRUCTURAL AND SPECIATION STUDIES IN THE Co(II)- N,N –BIS(PHOSPHONOMETHYL) GLYCINE SYSTEM.

ABSTRACT

Cobalt plays important roles in biological systems, despite its low availability in the earth's crust. The most common examples are vitamin B_{12} and coenzyme B_{12}, a cofactor required for a group of enzymatic systems of central importance in biochemistry. Its involvement in (bio)chemical processes contributing to the integrity of the physiology of humans underscores its ability to promote (bio)chemistry with molecular targets of variable mass and biological properties. Given the fact that organic phosphonates are widespread substrates-ligands in biological fluids, we sought to investigate the relevant chemistry with Co(II).

In an effort to unravel the aqueous chemistry of Co(II) in the presence of phosphonate ligands, two new Co(II)- N,N-bis(phosphonomethyl) glycine acid, aqueous soluble, complexes were synthesized, isolated and characterized. Aqueous reactions of $Co(NO_3)_2 \cdot 6H_2O$ with N,N-bis(phosphonomethyl) glycine acid led to the isolation of complex $[Co(C_4H_9O_8NP_2)_2(H_2O)_2] \cdot 2H_2O$ (**1**) at low pH. At higher pH values 5.5-6 aqueous reactions of $Co(CH_3COO)_2 \cdot 6H_2O$ with N,N-bis(phosphonomethyl) glycine acid in the presence of ammonia led to the isolation of complex $(NH_4)_4[Co(H_2O)_6][Co\{N(CH_2COO)(CH_2PO_3)_2\}(H_2O)_2]_2[Co(H_2O)_2\{N(CH_2COO)(CH_2PO_3H)(CH_2PO_3)\}Co(NH_3)_2(H_2O)_3]_2 \cdot 10\ H_2O \cdot 1.36\ CH_3CH_2OH$ (**2**). The complexes were further characterized analytically, spectroscopicaly (FTIR, UV-vis, EPR), and electrochemically (cyclic voltammetry). Speciation studies were carried out for nitrilotriacetic acid (NTA) and its phosphonic derivatives (N-(phosphonomethyl)-iminodiacetic acid (NTAP), N,N-bis(phosphonomethyl)glycine (NTA2P) and nitrilo-tris(methylphosphonic acid) (NTA3P)). Such information are vital in trying to understand the interactions of soluble and bioavailable forms of Co(II) in biological interactions in human organisms.

– CHAPTER 1 –

COBALT: THE ELEMENT IN NATURE AND IN THE LAB

1.1 GENERAL REMARKS ABOUT COBALT

Of all the inorganic elements in the periodic table, only a small number are utilized in biological systems. Most frequently encountered are the alkali and alkali-earth ions Na(I), K(I), Mg(II), Ca(II) required to neutralize the charge of simple inorganic anions such as phosphate and sulfate as well as more complex species such as nucleoside triphosphates, DNA, and RNA. Many first-row transitional-metal ions are also of key importance in biology, with the most predominant and widely known being iron, copper, and zinc. The bioinorganic chemistry of cobalt, vanadium, manganese, and nickel, is also being rapidly developed as we become increasingly aware of the important roles of these less common elements.[1]

Cobalt is a brittle, hard, transition metal with magnetic properties similar to those of iron. It is one of those trace metals, which is present in the human body, with its chemical forms in small amounts being essential to many life forms, including humans.

The metal crystallises in two allotropic forms: the α form and the β form. The α form is close-packed and the β form is face-centered cubic. Cobalt has two oxidation states that exist in solution: cobaltous Co(II) and cobaltic Co(III). Cobaltous Co(II) solutions are usually pink and have the ion octahedrally solvated. They are usually quite stable to air oxidation. Tetrahedral configurations are also found in solution, with the square or trigonal pyramidal configurations being more rarely encountered. Cobalt Co(III) is a powerful oxidizing agent and its salts decompose water. Co(III) complexes may be pink, yellow, blue, violet or purple. They are quite stable as they form inert complexes.

The following represents the electronic configuration of cobalt, its associated term symbol for the ground state neutral gaseous atom and its oxidation states.

- **Ground state electron configuration**: [**Ar**] **3d**^{7} **4s**^{2} (**group number: 9, period number: 4, block: d-block**).
- **Term symbol**: $^4\mathbf{F}_{9/2}$

- **Oxidation States**: *Co(-I)* (rare) - $[Co(CO)_4]^{1-}$; *Co(0)* (rare) - $[Co_2(CO)_8]$; *Co(I)* (rare) - $[Co(NCCH_2)_5]^{1+}$; *Co(II)* - CoO, $Co(OH)_2$, CoF_2, $CoCl_2$, $[Co(H_2O)_6]^{2+}$ (aq), salts and complexes; *Co(III)* - $Co(OH)_3$, CoF_3, $[Co(H_2O)_6]^{3+}$ (aq), $[Co(NH_3)_6]^{3+}$; *Co(IV)* - CoS_2, $[CoF_6]^{2-}$, *Co(V)* – K_3CoO_4.

1.2 COBALT IN ABIOTIC SYSTEMS

Cobalt is present in the earth's crust at concentrations reaching 20 mg/Kg (i.e. 0.0029%). It is only the thirtieth most abundant element and apart from Sc, cobalt is the rarest of the first row transition elements. Only a few important cobalt ores exist, although over 200 cobalt-containing minerals are known. About 33,000 tons of cobalt are produced annually. Native cobalt is unknown in terrestrial minerals, but it is sometimes present in small amounts (usually less then 2%) in native nickel-iron alloys of both terrestrial and meteoric origin. Cobalt occurs in compounds with arsenic, oxygen, nickel and sulfur as in the following minerals: smaltite – $(Co,Ni)As_2$ (cubic crystal form), safforite – $(Co,Fe)As_2$ (orthorhombic crystal form), skutterudite - $(Co,Ni)As_3$ (cubic crystal form), cobalite - CoAsS (cubic crystal form), carollite - Co_2CuS_4 (isomeric crystal form), linnaeute – $(Co,Ni)_3S_4$ (ortogonal crystal form), erythrite – $Co_3(AsO_4)_2 \cdot 8H_2O$ (monoclinic crystal form).

Values for abundances are difficult to determine with high certainty. In Table 1, values for the abundance of cobalt are given in units of ppb (parts per billion; 1 billion = 10^9).[2-4]

Table 1. Abundance of cobalt in the universe.

Abundance	ppb by weight
Sun	4000
Meteorite (carbonaceous)	600,000
Crustal rocks	30,000
Sea water	0.08
Stream	0.2
Lithosphere	0.02
Human	20

1.2.1 USES OF COBALT

The early uses of cobalt were all centered around its oxides and salts. It was not until 1900 that an appreciable demand was created for the metal. The more important uses of cobalt in its various forms include: a) the pure metal, which is encountered only in plating processes originating from electrodeposition, b) the commercial metal, which is used in compounding alloys, both ferrous and nonferrous, and c) the metal as a binder in the production of cemented carbide cutting tools. It is also used in many alloys, in permanent magnets, ceramics and special glasses, jet turbines and gas turbine generators, razor blades and catalytic converters. Of the several known cobalt isotopes, the radioactive cobalt-60 is the most important one. It has a half-life of 5.7 years and produces intensive gamma radiation. Cobalt-60 is used extensively in industry and in radioisotope therapy.

Colors. Cobalt salts are used for the production of brilliant and permanent blue colours in porcelain, glass, pottery, and tiles.

Enamels. In the manufacture of porcelain-enamelled articles, cobalt oxide is often used to promote adhesion of the glass to the metal, or to secure a desirable blue-colored enamel. Cobalt as a coloring compound is used in blue and black cover coats.

Cobalt Soaps. Since cobalt, in the metallic state, does not react satisfactorily with ordinary acids, various inorganic cobalt compounds are used to prepare the cobalt salts of higher fatty acids, naphthenic acids and resin acids. These salts have enjoyed a very wide use as catalysts for the acceleration of the drying process (the process by which the liquid unsaturated oils change to solid elastic films) in soybean and similar unsaturated oils.

Catalysts. Cobalt compounds have been used as catalysts for a number of organic reactions. The most common application has been in the catalytic combination of carbon monoxide and hydrogen, as best exemplified by the Fischer-Tropsch synthesis. Cobalt nitrate is generally used for preparing the catalyst.

Hygrometric Indicators. Cobalt salts, especially the chloride, have proved to be very useful as visual indicators of humidity, the blue anhydrous form becoming red when the humidity is sufficiently high.

1.3 COBALT IN BIOLOGICAL SYSTEMS

Our bodies contain a significant number of elements in the periodic table, even mercury from dental work, metal ions from cooking pots, and assorted pesticides from the epidermal surface of unwashed fruits. The strength, of protein-metal ion bonds are such that any metallic cation that finds its way into our bodies will spend a large part of its time bound to amino acids and proteins. Cobalt is present in a variety of aliments, with quantities varying from 150 μg to 600 μg. Cobalt is absolved and distributed to different tissues. When not found in the vitamin B_{12} corrinoid ring, cobalt exists in biological systems as Co(II), an ion able to accommodate four, five, or six donor atoms in a variable coordination polyhedron.[5]

Essential metals are micronutrients required in small amounts. Cobalt, encountered in minute quantities in the human body (0.7 mg for an average person of 70 Kg), is involved in key biomolecules, regulating processes in human physiology. As a metal ion, Co(II) assumes forms, which are dictated by the nature of organic binders in biological fluids and the conditions under which metal ion-ligand interactions arise. As a metal cofactor, cobalt enters key biomolecules, such as B_{12} coenzyme and vitamin B_{12}, and establishes the role of a regulator in a number of biological processes including metallohydrolases, like methionine aminopeptidase, nitrile hydratases, ribonucleotide reductase, glutamate mutase and others.[6-10]

Absence or deficit of cobalt could be the cause for a number of physiological aberrations, such as pernicious anemia.[11] In the case of anemia, it was recognized that cobalt-carrying vitamine B_{12} deficiency was the culprit of the clinical symptomatology. In the case of exposure of the human body to large amounts of cobalt, the consequences are dire, resulting in toxic effects manifested in heart disease and excessive formation of red corpuscles. A large excess of cobalt in the body also decreases the ability of the thyroid to accumulate iodine.[12,13]

The existence of soluble, bioavailable forms of this metal ion in human fluids is essential to the participation of cobalt as a metal cofactor in biomolecules. Because both high molecular mass as well as low molecular mass molecules exist with potential binding properties toward metal ions, it is very likely that interactions with both types of moieties take place with Co(II).[7,8,14,15] Among the potential Co(II) low molecular mass binders in such fluids are organic acids, amino acids, small peptides and other molecules like the one mentioned previously, possessing phosphonate moieties.[16-18] The latter groups characterize

biological sites in small molecules and proteins or enzymes with key roles in signal transduction, and enzyme inhibition.[19,20] Structures of cobalt Co(II) complexes with phosphonic acids have been reported in the past.[21-24] Of the low molecular mass ligands available in human fluids, citric acid is widely known for its abundance in biological fluids, such as human plasma at relatively high concentrations (ca. 0.1 mM).[25] A dinuclear cobalt Co(II)–citrate complex as well as a monomer complex have already been reported.[26,27]

Structures of cobalt complexes with the amino acids glutamic and aspartic,[28,29] histidine,[30] glycine,[31,32] phenylalanine,[33] alanine,[34] methionine, *S*-methyl-cysteine,[29] and asparagine[35] have been reported.[36,37] The structure of cobalt bound to the dipeptide gly-gly has also been reported.[38] Less information exists on the other hand about the electronic and magnetic properties of cobalt–amino acid compounds, although amino acid compounds of a simpler metal like copper have received much more attention. This is because Co(II) and Co(III) ions have the more complex $3d^7$ and $3d^6$ ground configurations, respectively, with higher complications introduced by the orbital and spin degeneracy of the ground state. A study on cobalt Co(II) and the amino acid L-threonine revealed that the Co(II) ion is in a deformed octahedral environment, sitting on a 2-fold symmetry axis. Magnetic measurement data reflect the molecular character of a compound with weak exchange interactions. EPR measurements in polycrystalline and single-crystal samples indicate a distorted axial symmetry around the Co(II) ion, as expected from the structural results.[39]

1.3.1. COBALT AND VITAMIN B_{12}

In 1948, an "anti-pernicious anemia factor" was isolated and named vitamin B_{12}. Vitamin B_{12} is unusual in several ways. It is the only vitamin known to contain a metal. It is essential for all higher animals but it is not found in higher plants, nor can it be synthesized by animals. While most vitamins can be made by a wide variety of plants and specific animals, no plant or animal has been shown capable of producing $B_{12,}$ and the exclusive source of this vitamin appears to be tiny microorganisms like bacteria, yeasts, molds, and algae.

Like most vitamins, B_{12} can occur in a variety of forms and take on a variety of names. Names for B_{12} include: cobrynamide, cobinamide, cobamide, cobalamin, hydroxycobalamin, aquocobalamin, nitrocobalamin and cyanocobalamin. Each of these designations contains a

form of the word “cobalt”, since cobalt is the metal ion found in the center of the vitamin. The term cobalamin is generally used to describe a cobalt derivative of the corrin ring system that carries a benzimidazole ligand on one face and one of a number of possible ligands (R) on the other. Of these, the two alkyl derivatives (methyl and adenosyl) are the most important ones.

The core of cabalamin (vitamin B_{12}) (Fig. 1) consists of a corrrin ring with a central cobalt ion. The corrrin ring, like a porphyrin ring has four pyrrole units. Two of them are directly bonded to each other, whereas the others are joined through methane bridges, as in porphyrins. A cobalt atom is bonded to the four pyrrole nitrogens. The fifth substituent is a derivative of dimethylbenzimidazole that contains ribose 3-phosphate and aminoisoparopanol. One of the nitrogen atoms of dimethylbenzimidazole is linked to cobalt. The amino group of aminoisoparopanol is an amide linkage with a side chain. The sixth substituent of the cobalt atom can be $–CH_3$, OH^-, or 5’-deoxyadenosyl unit. The cobalt atom in cobalamin can have an oxidation state +1, +2, or +3. The cobalt atom is in the +3 state in hydroxocobalamin (where OH^- occurs in the sixth coordination) site. This form called B_{12a} (Co(III)), is reduced to a divalent state, called B_{12r} (Co(II)) by a flavoprotein reductase. The B_{12r} (Co(II)) form is reduced by a second flavoprotein reductase to B_{12s} (Co(I)).

$$B_{12a}\ (Co(III)) \rightarrow B_{12r}\ (Co(II)) \rightarrow B_{12s}\ (Co(I))$$

The B_{12s} form is the substrate for the final enzymatic reaction that yields the final coenzyme. Co(I) attacks the 5’ carbon atom of ATP and displaces the triphosphate group to form 5’- deoxyadenosylcobalamin, also known as coenzyme B_{12}.[40]

Cobalamin is absorbed through a specialized transport system. The stomach secretes a glycoprotein, called the intrinsic factor, which binds cobalamin in the intestinal lumen. Pernicious anemia is caused by a deficiency of that intrinsic factor, which leads to impaired absorption of cobalamin.

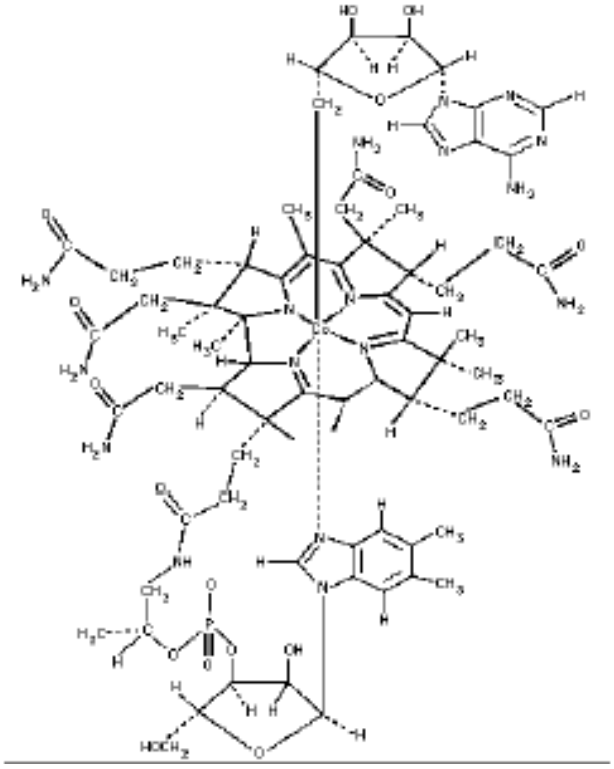

Fig. 1 Structure of vitamin B_{12}

A tissue deficiency of this vitamin causes pernicious anemia, which in its completely developed stages is characterised by macrocytosis, megaloblastic bone marrow, neurological and mental changes, endocrine dysfunction, disturbance in fat metabolism, mucous membrane disorders and occasionally other disturbances.

A deficiency may result either from a diet insufficient in vitamin B_{12} or from inability to use that which has been ingested because of a lack of intrinsic factor. Oral administration of small doses with intrinsic factor or massive oral administration doses without intrinsic factor produce rapid remissions of all symptoms of pernicious anemia with few exceptions.

Treatment with vitamin B_{12} is of value in nutritional macrocytic anemia and megaloblastic anemia of infancy and herpes zoster. It has also been reported to be useful in certain skin and liver diseases and a variety of other diseases, in which results are not well defined.

Estimates of the human daily requirement of vitamin B_{12} is less than 3μg.[41] Children because of their higher metabolic rate may require several times this amount. It is one of the least toxic of therapeutic agents and doses of 100 mg/kg (intraperitoneal) in rates and 10 mg orally in humans have shown no toxic effects. Vitamin B_{12} appears to be essential for the growth of all animals and is responsible for most, if not all, of the "animal protein factor", a factor which permits growth of animals or chicks on rations containing no animal protein

1.3.2 FUNCTIONS OF VITAMIN B_{12}

Vitamin B_{12} is involved in carbohydrate and fat metabolism, reduction of sulfides to sulfhydryl compounds, nucleic acid metabolism, protein metabolism, transmethylation and other one-or two-carbon atom transfers.

– Developing red blood cells

Perhaps the most well known function of vitamin B_{12} involves its role in the development of red blood cells. As red blood cells mature, they require information provided by molecules of DNA. Without B_{12}, synthesis of DNA becomes defective and so does the information needed for red blood cell formation. The cells become oversized and poorly shaped and begin to function ineffectively.

– Developing nerve cells

A second major function of B_{12}, less clearly understood than the first, involves its participation in the development of nerve cells. A coating, which encloses the nerves, called the myelin sheath forms less successfully whenever B_{12} is deficient. Although the vitamin plays an indirect role in this process, supplementation of B_{12} has been shown to be effective in relieving pain and other symptoms in a variety of nervous system disorders.

– Other roles

Protein, the component of food required for growth and repair of cells, depends upon B_{12} for proper cycling through the body. Many of the protein key components, amino acids, become unavailable for use in the absence of B_{12}.

1.3.3 DEFICIENCY SYMPTOMS

Although B_{12} is not the only nutrient deficiency that can contribute to occurrence of the following symptoms, B_{12} deficiency should be considered as a possible underlying factor whenever any of the symptoms mentioned below are present. Symptoms potentially associated with vitamin B_{12} deficiency include: fatigue, memory problems, difficulty swallowing, depression, decreased reflexes, nervousness, weakness, weak pulse, numbness in feet.

1.3.4 RADIOACTIVE FORMS OF VITAMIN B_{12}

Radioactive forms of vitamin B_{12} are useful for assays and for the study of the behaviour of the substance in biological systems. Vitamin B_{12} containing Co^{60} is the most extensively used form and is prepared by fermentations in which radioactive cobalt is added.

1.3.5 OCCURRENCE

Vitamin B_{12} occurs in practically all-animal products, in the form of a protein complex. It is present in larger amounts in those products that are rich in protein. Liver, kidney and some types of seafood are the richest sources in vitamin B_{12}. Fermented materials, such as rumen contents, are particularly rich sources of vitamin B_{12}. Vitamin B_{12} is also known to be produced by many actinomycetes and other bacteria. In general, plant material contains little or no vitamin B_{12}. An exception is the algae. It has been suggested that these plants may be the source of the relatively large amounts of vitamin found in some shell and fish. Table 2 lists the contents of vitamin B_{12} – active substances in a variety of natural materials.

Table 2. Table of Food Sources of Vitamin B12.

Food	Vitamin B_{12} (Micrograms)	Food	Vitamin B_{12} (Micrograms)
Beef liver	60.0	Milk (1 Cup)	0.9
Salmon	4.9	Tuna	0.9
Beef meat	2.1	Yogurt	0.9
Clams	1.1	Pork meat	0.6
Oysters	1.0	Chicken meat	0.3

1.4 GENERAL REMARKS ABOUT PHOSPHONATES

Phosphonic acids are organic compounds containing one or more C—$PO(OH)_2$ groups. Phosphonates are clearly distinguished from phosphates by their direct C --- P bonds. Many of the phosphonates and especially their hydroxo and amino derivates, have biological activity or can serve as sequestering ligands in metal ion removal, both in biology and in industry. Phosphonates generally have their greatest affinity for metal ions when present as fully dissociated species (highly alkaline solutions). They are especially effective in strongly complexing hydrolyzed cations, such as Al(III), Tl(III), Au(III), Zr(IV), Th(IV), Pt(II),Co(II), etc.

Phosphonate compounds, especially the ones containing more than one phosphonate groups, are effective chelating agents. Chelating agents have the potential to perturb the natural speciation of metals and to influence metal bioavailability.[42] They also have the potential to remobilize metals from sediments and aquifers, posing a potential risk to groundwater and drinking water.[43]

Natural and synthetic aminophosphonic molecules are very effective ligands, in many cases with high specificity for metal ions. This class of compounds includes a variety of herbicides, plant growth regulators, antibiotics and inhibitors of metalo-enzymes.[44] As potent metal ion binders, these molecules could be involved in interactions relevant to the fate of metal ions in the natural environment or biological systems. Numerous studies aimed at

understanding the chelating properties of this class of ligands and determining the stability of the complexes formed.[45-51]

1.5 USE AND PROPERTIES OF PHOSPHONATES

Bis(phosphonates) were first synthesized in 1897 by Von Baeyer and Hofmann (1897). An example of such a bis(phosphonate) is HEDP (1-Hydroxyethane(1,1-diphosphonic acid)). The work of Schwarzenbach *et al*. (1949) established phosphonic acids as effective complexing agents. The introduction of an amine group into the molecule to obtain —NH_2—C—$PO(OH)_2$ increases the metal binding abilities of the phosphonate. Examples of such compounds are NTA3P (or NTMP) (Nitrilo tris(methylene phosphonic acid), EDTMP (1,2-Diamino (methylene phosphonic acid) DTPMP (Diethylenetriamine (methylene phosphonic acid) and NTA2P (N,N,-bis(phosphonomethyl) glycine. (see Table 3.). Certain phosphonates are quite common among different organisms, from prokaryotes to eubacteria, fungi, mollusks and insects. Until now no bis- or poly-phosphonates have been found to occur naturally.

Phosphonates have very important properties: a) they are effective chelating agents for di- and trivalent metal ions, and b) they are quite stable at high temperature, low and high pH and in the presence of oxidants. An important industrial use of phosphonates is in cooling waters, desalination systems, and in oil fields to inhibit scale formation. In pulp and paper manufacturing and in textile industry, phosphonates are used as peroxide bleach stabilizers, acting as chelating agents for metals that could inactivate the peroxide. In detergents, they are used as a combination of chelating agent, scale inhibitor and bleach stabilizer.[52] Phosphonates are also increasingly used in medicine to treat various bone and calcium metabolism diseases and as carriers for radionuclides in bone cancer treatments.[53-55] Human toxicity is low, which can be seen in the fact that phosphonates are used to treat various diseases. The toxicology studies show that at concentrations found in wastewater (0.01–1.0 M) no toxic effect on aquatic organisms and humans is expected.

Aminopolycarboxylates and their mixed carboxylic-phosphonic derivatives are widely used for various purposes, covering fields from analytical chemistry, paper and textile industry, to medicine. Many of the aminophosphonic acids display diverse and useful biological properties. The aminophosphonic acids are probably the most important substitutes

for the corresponding amino acids in biological systems.[56-58] They find applications for instance, in medicine as antibacterial agents, antibiotics, enzyme inhibitors, plant growth regulators, NMR imaging agents, and pharmacological agents.[59-62] Aminophosphonic acids are also found as constituents of natural products. Being structural analogs of amino acids, they can act as their antagonists and compete with their carboxylic counterparts for metal ions or the active sites of enzymes or other cellular receptors. Containing strong metal binding donor groups, aminophosphonates are able to chelate essential or toxic metal ions.

Table 3. Structure of some phosphonic acids

Abbreviation	Structure
HEDP	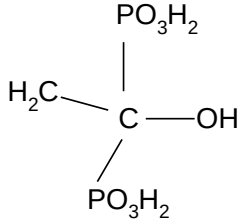
NTA3P	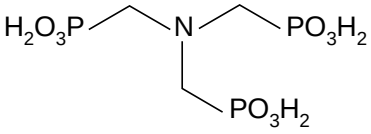
EDTMP	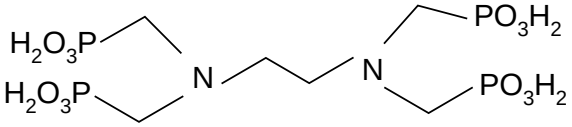
DTPMP	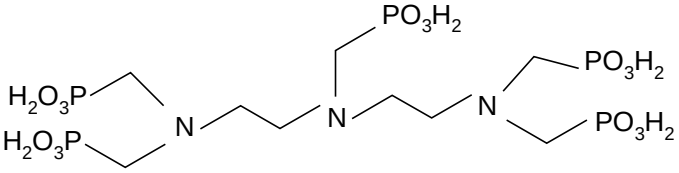
NTA2P	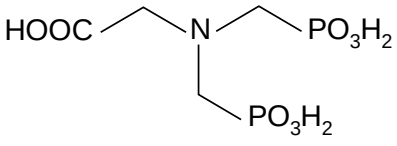

1.6 SCOPE AND GOALS OF THIS RESEARCH WORK

The ability of ligands, containing phosphonate groups, to interact with metal ions has been well established. Complexation of different trace metals, which are found in human fluids, including cobalt, to such phosphonate groups begets solubility, potential bioavailability and likely absorption to biological sites in need of those essential metals. The existence of bioavailable species arising from such interactions at physiological pH values, as well as throughout the biologically relevant pH range, is of major significance. Knowledge of cobalt speciation pattern with phosphonate containing ligands is essential in understanding the role of this metal ion in processes that either support normal biological functions or impart aberrations to human physiology.

The use of a diphosphonate ligand, such NTA2P exemplifies quite well structural attributes of phosphonic analogs of amino acids, for which structurally characterized complexes with Co(II) in aqueous media are limited. Prompted by the need to investigate biological interactions at the chemical level and discover potential biologically relevant Co(II)-phosphonate species, we have launched pertinent synthetic research efforts on the Co(II)- N,N-bis(phosphonomethyl) glycine (NTA2P) binary system. Toward this end we report herein the synthesis, isolation, spectroscopic, structural characterization as well as EPR and cyclic voltammetry studies of two new species between cobalt (II) and N,N-bis(phosphonomethyl) glycine acid at two different pH values. Also solution speciation studies (pH-metric and spectrophotometric measurements) were carried out for Co (II) – NTA and its phosphonic derivatives (NTAP, NTA2P, NTA3P). The solution speciation studies have put forward proposals for Co(II)-((N,N,-bis(phosphonomethyl) glycine) species being present in solution.

1.7 LITERATURE

1. Cowan, J. A. *Inorganic Biochemistry,* VCH Publisher, Inc., New York, **1993**
2. Kaye, G. W. C.; and Laby, T. H. in *Tables of Physical and Chemical Constants*, Longman, London, UK, 15th edition, **1993**.
3. Cox, P. A. in The Elements: *Their Origin, Abundance, and Distribution*, Oxford University Press, Oxford, UK, **1989**.
4. Selbin, J. *J. Chem. Ed.* **1973**, *50*, 306
5. Sigel, H. *Metals* I*ons in Biological Systems*, Marcel Dekker, INC New York and Basel, **1986**, volume 20.
6. Taylor, D. M.; Williams, D. R. *Trace Element Medicine and Chelation Therapy*. Royal Society of Chemistry, Cambridge, **1995**.
7. Balachandran, S.; Vishwakarma, R. A.; Monaghan, S. M; Prelle, A.; Stamford, N. P. J.; Leeper, F. I.; Battersby, A. R. *J. Chem. Soc., Perkin Trans.* **1994,** *1*, 487-491.
8. Battersby, A. R. *Acc. Chem. Res*. **1993,** *26*, 15-21.
9. Debussche, I.; Conder, M.; Thihaut, D.; Cameron, B.; Crouzet, J.; Blanche, F. *Bacteriol*. **1992**, *33*, 7445-7451.
10. Roderick, S. L., Matthews, B. W. *Biochemistry*, **1993**, *32*, 3907-3912.
11. Hamilton, F. M. N.; Gropper, S. A. S. In *The Biochemistry of Human Nutrition*, West Publishing Company, New York, **1987**, 298-301.
12. Helis, H. M.; de Meester, P.; Hodgson, D. J. *J. Am. Chem. Soc*. **1977**, 99, 3309-3312.
13. Waldbott, G. L. In *Health Effects of Enviromental Pollu*tion Mosby, Inc; St. Louis, MO, **1973**.
14. Payne, M. S.; Wu, S.; Fallon, R. D.; Tudor, G.; Stieglitz, B.; Turner, I. M., Jr.; Nelson, M. *Biochemistry* **1997**, 36, 5447-5454.
15. Lippard, S. J.; Berg, J. M. In *Principals of Bioinorganic chemistry*, **1994**, chapter 11, pp 336-347.
16. (a) Kiss, T. In *Biocoordination Chemistry,* K. Burger, Ed. Ellis Ilorwood: Chichester, U.K., **1990**, *56*. (b) Perrin, D. D.; Agarwal R.P. In *Metal Ions* in *Biological Systems,* New York, **1973**, Vol. 2, p. 168. (c) Perrin, D. D. *Nature* **1965**, *206*, 170.
17. Martin, R. B. *J. Inorg. Biochem,* **1986**, *28*, 181-187

18. May, P. M.; Linder, P. W.; Williams D. R. *J. Chem. Soc. Dalton Trans.* **1977**, 558-595.
19. Sanna, D.; Bodi, I.; Bouhsina, S.; Micera, G.; Kiss, T. *J. Chem. Soc. Dalton., Trans*. **1999**, 3275-3282.
20. Kafarski, P.; Mastalerz, P. *Beitr. Wirkstofforsch*. **1984**, *21*, 1.
21. Cao, D. K.; Gao, S.; Zhenga, L. M. *Journal of Solid State Chemistry* **2004**, *41*, 3366-3374.
22. Jankovics, H.; Daskalakis, M.; Raptopoulou, C. P.; Terzis, A.; Tangoulis, V.; Giapintzakis, J.; Kiss, T.; Salifoglou, A. *Inorg. Chem.* **2002**, *41*, 3366-3374.
23. Mao, J. G.; Clearfield, A. *Inorg. Chem*. **2002**, *41*, 2320-2324.
24. Song, J. L.; Prosvirin, V.; Zhao, H. H.; Mao, J. *Eur. J. Inorg. Chem.* **2004**, 212.
25. Martin R. B. *J. Inorg. Biochem*. **1986**, *28*, 181-187.
26. Kotsakis, N. ; Raptopoulou, C. P.; Terzis, A.; Tangoulis, V.; Giapintzakis, J. Jakusch, T. ; Kiss, T ; Salifoglou, A. *Inorg. Chem.* **2003**, *42*.
27. Matzapetakis, M. ; Dakanali, M. ; Raptopoulou, C. P. ; Tangoulis, V. ; Terzis, A. ; Giapintzakis, J. ; Salifoglou, A. J. *Biol. Inorg. Chem.,* **2000**, *5*, 469-474.
28. (a) Doyne, T.; Pepinsky, R. *Acta Crystallogr*. **1957**, *10*, 438-439. (b) Pepinsky, R.; Turley, J. W.; Okaya, Y.; Doyne, T.; Vand, V.; Shimada, A.; Lovell, F. M.; Sogo, Y. *Acta Crystallogr*. **1957**, *10*, 811-812.
29. Isago, T.; Igi, K.; Hidaja, J. *Bull. Chem. Soc. Japan* **1979**, *52*, 407-414.
30. (a) Harding, M. M.; Long, H. A. *J. Chem. Soc. (A)* **1968**, 2554-2559. (b) Candlin, R.; Harding, M. M. *J. Chem. Soc. (A)* **1970**, 384-393.
31. Clegg, W.; Lacy, O. L.; Straughan, B. P. *Acta Crystallogr*. **1987**, *43*, 794-797.
32. Ravikumar, K.; Rajan, S. S. *Z. Kristallogr*. **1985**, *171*, 201-207.
33. Demaret, A.; Abello, L.; Fourati, M.; Lapluye, G. *J. Chem. Res. (S)* **1978**, 354-355.
34. Herak, R.; Prelesnik, B.; Krstanovic, I. *Acta Crystallogr*. *B* **1978**, *34*,91-95.
35. Sekisaki, M. *Bull. Chem. Soc. Jpn.* **1979**, *52*, 403-406.
36. Allen, F. H. *Acta Crystallogr.* **2002**, *B58*, 380-388.
37. Bruno, I. J.; Cole, J. C.; Edington, P. R.; Kessler, M.; Macrae, C. F.; McCabe, P.; Pearson, J.; Taylor, R. *Acta Crystallogr.* **2002**, *B58*, 389-397.
38. Solujic, L. R.; Herak, R.; Prelesnik, B.; Celap, M. B. *Inorg. Chem.* **1985**, *24*, 32-37.
39. Rizzi, A. C.; Brondino, C. D.; Calvo, R.; Baggio, R.; Garland, M. T.; Rapp, R. E. *Inorg. Chem.* **2003**,*42*, 4409-4416.

40. Stryer, L. *Biochemistry,* second edition, W. H. Freeman, New York, **1995**, 537 – 540.
41. Hamilton, E. M. N.; Gropper, S. A. S. *The Biochemistry of Human Nutrition,* West Pub Company, New York, **1987**, 298-301.
42. Anderson, R. L.; Bishop, W. E.; Campbell, R. L.; *CRC Critical Rev. Toxicol.* **1985**, *15*, 1–102
43. Hering, J. G. in *Metal Speciation and Contamination of Soils* (eds H.E. Allen, C. P. Huang, G. W. Bailey and A. R. Bowers), **1995.**
44. Kiss, T. in *Biocoordination Chemistry,* ed. K. Burger, Ellis Horwood, Chichester, **1990**, p.56
45. Carter, R. P.; Carroll R. L.; Irani, R. P. *Inorg. Chem.* **1967**, *6*, 939.
46. Lundager Madsen, H. E.; Christensen, H. H; Gottlieb-Peterson, C. *Acta Chem. Scand., Ser. A,* **1978**, *32*, 79.
47. Wozniak M.; Novogrocki, G. *Talanta* **1979**, *26*, 1135.
48. Appleton, T. G.; Hall J. R.; McMahon, I. J. *Inorg. Chem*. **1986**, *25*, 726.
49. Radomska, B.; Matczak-Jon E; Wojciechowski, W. *Inorg. Chim. Acta* **1986**, *124,* 83.
50. Kiss, T.; Balla, J.; Nagy, G.; Kozlowski, H.; Kowalik, J. *Inorg. Chim. Acta* **1987**, *138*, 25.
51. Appelton, T. G.; Byriel, K.A.; Hall, J. R.; Kennard, C. H. L.; Lynch, D. E.; Sinkinson J.A.; Smith, G. *Inorg. Chem.* **1994**, *33*, 444
52. Wanner B. L. in *Biodegradation* **1994**, *5,* 175–184
53. Fleisch, H. Recent. *Results Cancer Res.* **1989**, *116*, 1–28
54. de Klerk, J. M. H.; van Dijk, A.; van Het Schip, A. D.; Zonnenberg, B. A.; van Rijk, P. P. *J. Nucl. Med*. **1992**, *33*, 646–651.
55. de Witt, G. C.; May, P. M.; Webb, J.; Hefter, G. *BioMetals* **1996**, *9,* 351-361.
56. Baylis, E. K.; Campbell, C. D.; Dingwall, J. G. *J. Chem. Soc., Perkin Trans*. **1984**, 2445.
57. Kafarski, P.; Lejczak, B. *Phosphorus Sulfur* **1991**, *63*, 193.
58. Hanessian, S.; Bennani, Y. L. *Synthesis* **1995**, 1272.
59. Kiss, T.; Jezowski-Bojezuk, M.; Kozlowski, H.; Kafarski, P.; Antezak, K. *J. Chem. Soc., Dalton Trans.* **1991**, 2275.
60. Allen, M. C.; Fuhrer, W.; Tuck, B.; Wade, R.; Wood, J. M. *J. Med. Chem*. **1989**, *32*, 1652.
61. Atherton, F. R.; Hassal C. H.; Lambert, R.W. *J. Med. Chem.* **1986**, *29*, 29.
62. Sawada, K.; Ichikawa T.; Uehara, K. *J. Chem. Soc., Dalton Trans.* **1996**, 3077.

– CHAPTER 2 –

EXPERIMENTAL TECHNIQUES AND METHODS USED FOR CHARACTERIZATION OF THE COMPLEXES

2.1 DIFFRACTION

Introduction

The diffraction of radiation by crystals and fibers has provided an enormous amount of valuable information on biological structures. Light, X-rays, neutrons and electrons have all been used to produce diffraction patterns. The most widely used approach has been X-rays, because of their availability and penetration potential as well as the fact that their wavelength is small compared with those used in molecular studies.

Physical Basis of Diffraction

Diffraction is the name given to phenomena occurring when a wave passes through an object and spreads beyond the object. Different diffracted waves interfere with each other and produce an interference pattern. If the atoms are arranged in a periodic fashion, as in crystals, the diffracted waves will consist of sharp interference maxima (peaks), with the same symmetry as in the distribution of atoms. Measuring the diffraction pattern, therefore, allows us to deduce the distribution of atoms in a material. A crystal lattice is a regularly represented arrangement of atoms. The unit cell of a lattice is the smallest and simplest unit from which the three-dimensional periodic pattern can be produced. For a given set of lattice planes, with an inter-planar distance of d, the condition for diffraction (peak) to occur can be simply written as:

$$n\lambda = 2d\sin\theta \qquad (1)$$

which is known as Bragg's law.

In equation (1), n is an integer, d is the spacing between the lattice planes in the crystal, and θ is the angle of incidence of the beam with wavelength λ.

Lattice Planes

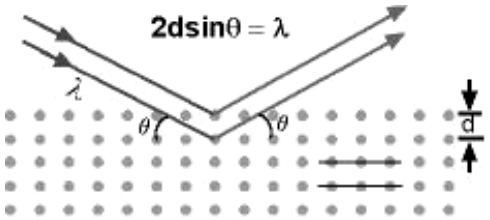

Bragg's Law

Experimental Measurement of Diffraction

Sources of Radiation

X-rays are electromagnetic radiation of exactly the same nature as light, but of very much shorter wavelength. For diffraction applications, only short wavelength X-rays (hard X-rays), in the range of a few Ångstroms to 0.1 Ångstrom (1 keV - 120 keV), are used. X-rays are produced generally by either X-ray tubes or synchrotron radiation sources. X-rays are generated when a focused electron beam, accelerated across a high voltage field, bombards a stationary or rotating solid target. As electrons collide with atoms in the target and slow down, a continuous spectrum of X-rays is emitted. The high energy electrons also eject inner shell electrons in atoms through the ionization process. When a free electron fills the shell, an X-ray photon, with energy characteristic of the target material, is emitted. Common targets used in X-ray tubes include Cu and Mo, which emit x-rays with energies 8 keV and 14 keV and corresponding wavelengths of 1.54 Å and 0.8 Å, respectively.

Experimental Setup

Diffraction can occur whenever Bragg's law is satisfied. With monochromatic radiation, an arbitrary setting of a single crystal in an X-ray beam will not generally produce any diffracted pattern. There would, therefore, be very little information in a single crystal diffraction pattern by using monochromatic radiation. This problem can be overcome by continuously varying λ or θ over a range of values, to satisfy Bragg's law. Practically, this is done by:

- using a range of X-ray wavelengths (i.e. white radiation),
- by rotating the crystal or using a powder or polycrystalline specimen.

In the rotating crystal method, a single crystal is mounted with an axis normal to the monochromatic X-ray beam. A cylindrical film is placed around it and the crystal is rotated

about the chosen axis. As the crystal rotates, sets of lattice planes will at some point enter the correct Bragg angle for the monochromatic incident beam, and at that point a diffracted beam will form. The reflected beams are located on the surface of imaginary cones. When the film is laid out flat, the generated diffraction spots lie on horizontal lines.

Powder XRD (X-ray Diffraction) is perhaps the most widely used X-ray diffraction technique for characterizing materials. As the name suggests, the sample is usually in a powdery form, consisting of fine grains of single crystalline material to be studied. The technique is also used widely for studying particles in liquid suspensions or polycrystalline solids (bulk or thin film materials).

Powder diffraction data can be collected using either transmission or reflection geometry. Since the particles in the powder sample are randomly oriented, these two methods will yield the same data. The powder method is used to determine the value of the lattice parameters accurately. Lattice parameters reflect the magnitudes of the unit vectors a**,** b and c, which define the unit cell for the crystal. For every set of crystal planes, by chance, one or more crystals will be in the correct orientation to give the correct Bragg angle to satisfy Bragg's equation. Every crystal plane is, thus, capable of diffraction. Each diffraction line is made up of a large number of small spots, each from a separate crystal. Each spot is so small as to give the appearance of a continuous line.

X-ray Crystallography

X-ray crystallography is a standard technique for delineating crystal structures. Its basic theory was developed soon after X-rays were first discovered more than a century ago. However, over the years it has gone through continual development in data collection, instrumentation and data reduction methods. In recent years, the advent of synchrotron radiation sources, area detector-based data collection instruments, and high speed computers, has dramatically enhanced the efficiency of crystallographic structural determination. Today, X-ray crystallography is widely used in materials and biological research. Structures of very large biological machinery (e.g. protein and DNA complexes, virus particles) have been solved using this method.

In X-ray crystallography, integrated intensities of the diffraction peaks are used to reconstruct the electron density map within the unit cell in the crystal. To achieve high accuracy in the reconstruction, which is done by Fourier transformations of the diffraction intensities with appropriate phase assignment, a high degree of completeness as well as redundancy in diffraction data is necessary, meaning that all possible reflections are measured multiple times to reduce systematic and statistical error. The most efficient way to do this is by using an area detector, which can collect diffraction data in a large solid angle. The use of high intensity X-ray sources, such as synchrotron radiation, is an effective way to reduce data collection time.

2.2 INFRARED SPECTROSCOPY

Introduction

The energy of most molecular vibrations corresponds to that of the infrared region of the electromagnetic spectrum. Absorption of IR is restricted to compounds with small energy differences in the possible vibrational and rotational states. These vibrations can be detected and measured directly in an infrared spectrum. Of the entire infrared spectrum, only the range 1400 – 4000 cm^{-1} is useful in readily deriving any information. However, the 600 – 1400 cm^{-1} region contains many bands including those from skeletal vibrations. Therefore, this region is sometimes helpful in "fingerprinting" molecules.

Physical Basis of Infrared Spectra

A molecule absorbs only those frequencies of IR light that match vibrations that cause a change in the dipole moment of the molecule. Molecules are flexible, moving collections of atoms. The atoms in a molecule are constantly oscillating around average positions. Bond lengths and bond angles are continuously changing due to this vibration. All of the motions can be described in terms of two types of molecular vibrations. One type of vibration, **a stretch**, produces a change of bond length. A stretch is a rhythmic movement along the line between the atoms so that the interatomic distance is either increasing or decreasing.

The second type of vibration, **a bend**, results in a change in bond angle. Each of these two main types of vibration can have variations. A stretch can be symmetric or asymmetric. Bending can occur in the plane of the molecule or out of plane; it can be **scissoring**, like blades of a pair of scissors, or **rocking**, where two atoms move in the same direction.

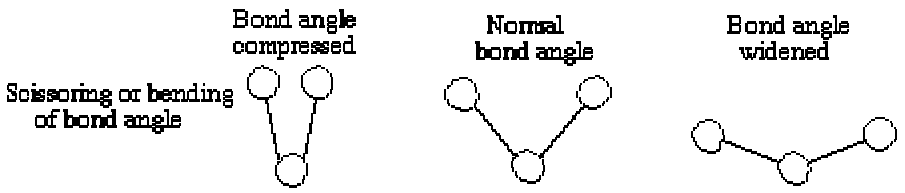

The motions or oscillations, which are induced by certain vibrational modes within the material, can interact with a beam of infrared radiation directed onto the material: energy is exchanged between the beam and material when the frequencies are synchronous or "in resonance." A simple way of relating energetics and structure is provided by an example of the potential-energy curve of a diatomic molecule. The curve in Fig. 1 shows how the energy of a molecule changes as the distance between its nuclei changes. At the minima of the potential-energy curve, the attraction due to various dispersive forces is balanced by the forces from charge repulsion. The vibrations of the bond can be analyzed in terms of the molecule's undergoing simple harmonic oscillations about its equilibrium bond length. The vibrational frequency, ν_{vib}, is given by:

$$\nu_{vib} = \frac{1}{2\pi}\sqrt{\frac{k}{\mu}} \qquad (2)$$

where k is the force constant of the bond and μ ($\mu = \frac{m_1 m_2}{m_1 + m_2}$) is the reduced mass of the molecule.

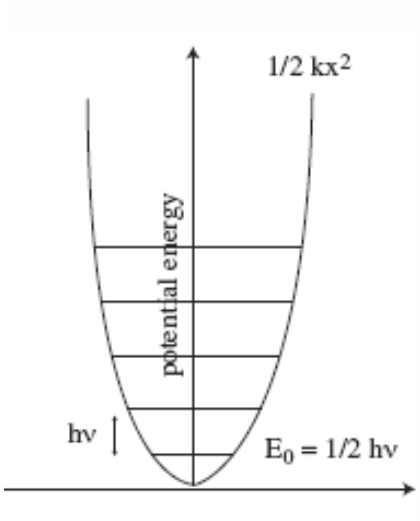

Fig. 1 Harmonic oscillator potential well and energy levels.

Real molecules do not obey the laws of simple harmonic motion exactly. Quantum mechanics tells us that only certain values of the energy are allowed. These values are represented by the horizontal line on the Morse curve, in Fig. 2. Values of energy in between these energy levels are not permitted and the spacing between energy levels becomes smaller at higher energy values. As the energy increases, the atoms move further away from their equilibrium positions and enter a non-parabolic region of the Morse curve. Therefore, the vibrations can no longer be treated as simple harmonic but they are described as anharmonic oscillators. When the Morse potential is used to calculate the allowed energy levels of the system, we find:

$$E_v = \omega_e(v+1/2) - \omega_e\chi_e(v+1/2)^2 \quad (3)$$

where v can have values 0, 1, 2, …., and $\omega_e\chi_e$ is a small anharmonic correction.

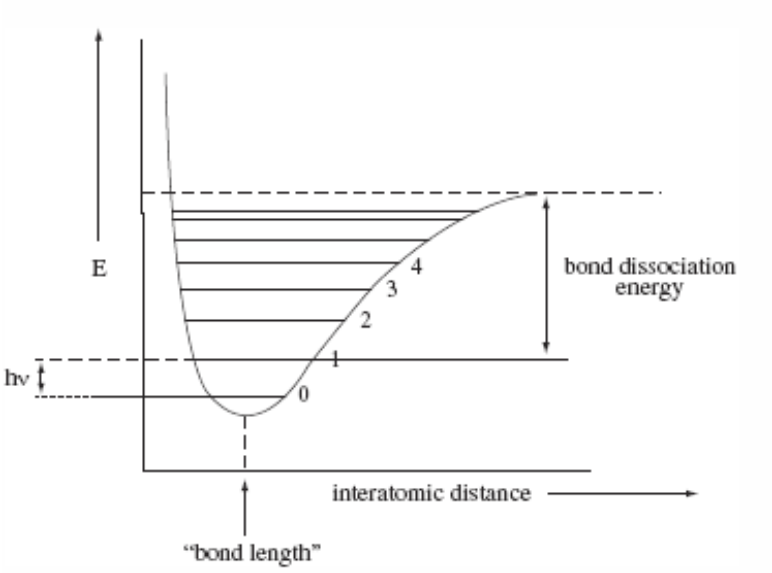

Fig. 2 The Morse potential.

Measurement of Infrared Spectra

In Infrared Spectroscopy, light of all different frequencies passes through a sample and the intensity of the transmitted light is measured at each frequency. Typically, the sample is a solution in a cell transparent to the IR radiation. NaCl and KBr windows are most frequently used for this purpose. At frequencies corresponding to the vibrational energies of the sample,

some light is absorbed and less light is transmitted than at frequencies, which do not correspond to the vibrational energies of the molecule. In order to compensate for absorption and scattering of the light by the solvent and sample cell, the incident light is split into two beams, one which goes through the sample, and the other one which passes through a reference, usually consisting of pure solvent. Transmittance is then defined as I_s/I_r, where I_s is the intensity of light passing thought the sample, and I_r is the intensity of light passing thought the reference cell (Fig. 3).

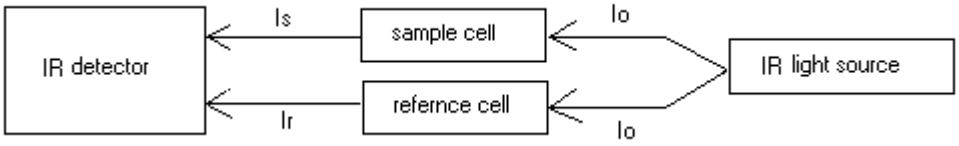

Fig. 3 Schematic representation of an infrared experiment.

With Fourier-Transform InfraRed spectroscopy (FTIR), the intensity of the infrared beam is measured before and after it interacts with the sample, as a function of the light's frequency. An infrared spectrum usually consists of a plot of the absorption of radiation as a function of wavenumbers and is characterized only in terms of positions of the maxima of each of the absorption bands ν_{max}, expressed in cm^{-1}. From this plot, we can determine the identities, surrounding environments and concentrations of the chemical bonds in the sample. This technique considerably improves the sensitivity over scanning or dispersive infrared spectroscopy. The enhanced sensitivity of Fourier Transform (FT) and FTIR spectroscopic techniques allows weak signals to be measured with high precision. Examples of such weak signals originate in low concentrations of active species in a sample or signals from samples that are poor reflectors or transmitters.

2.3 ULTRAVIOLET AND VISIBLE ABSORPTION SPECTROSCOPY

Introduction

The visible region of the spectrum comprises photon energies of 36 to 72 kcal/mole, and the near ultraviolet region out to 200 nm, extends this energy range to 143 kcal/mole. Ultraviolet radiation, having wavelengths less than 200 nm, is difficult to handle and is seldom used as a routine tool for structural analysis. The energies noted above are sufficient to promote or excite a molecular electron to a higher energy orbital. Consequently, absorption spectroscopy carried out in this region is sometimes called electronic spectroscopy.

Physical Basis of Ultraviolet Absorption Spectroscopy

The absorption of UV or visible radiation corresponds to the excitation of outer electrons. There are three types of electronic transitions, which can be considered;

- Transitions involving π, σ, and *n* electrons
- Transitions involving charge-transfer electrons
- Transitions involving *d* and *f* electrons

When an atom or molecule absorbs energy, electrons are promoted from their ground state to an excited state. In a molecule, the atoms can rotate and vibrate with respect to each other. These vibrations and rotations also have discrete energy levels, which can be considered as being packed on top of each electronic level.

Absorption of ultraviolet and visible radiation in organic molecules is restricted to certain functional groups (*chromophores*) that contain valence electrons of low excitation energy. The spectrum of a molecule containing these chromophores is complex. This is because the superposition of rotational and vibrational transitions onto the electronic transitions gives a combination of overlapping lines. This appears as a continuous absorption band.

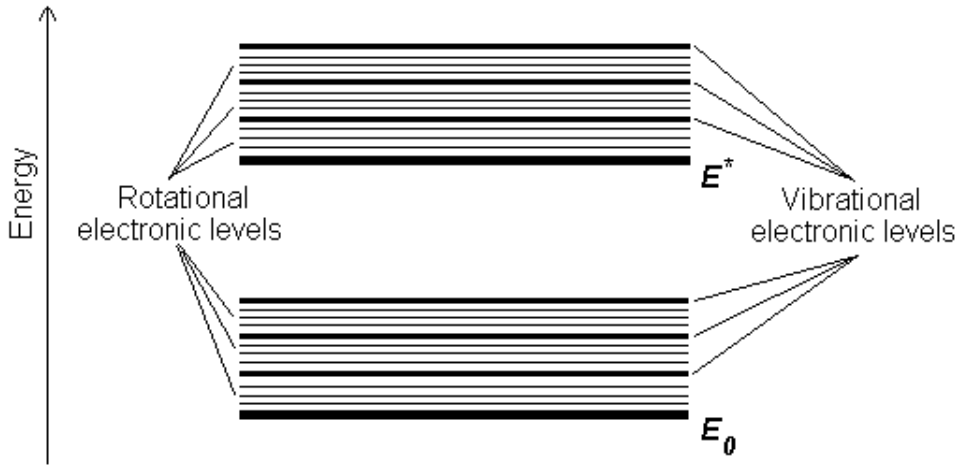

Possible *electronic* transitions of π, σ, and *n* electrons are:

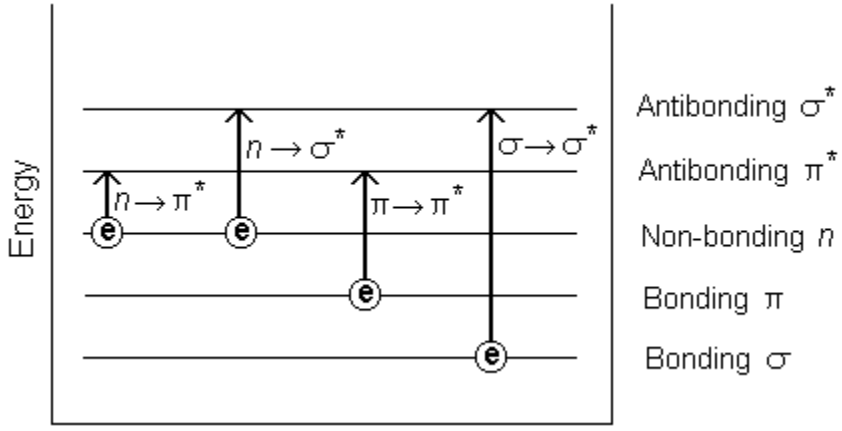

$\sigma \rightarrow \sigma^*$ Transitions

An electron in a bonding σ orbital is excited to the corresponding antibonding orbital. The energy required is large. Absorption maxima due to $\sigma \rightarrow \sigma^*$ transitions are not seen in typical UV-Vis. spectra (200 - 700 nm)

$n \rightarrow \sigma^*$ Transitions

Saturated compounds containing atoms with lone pairs (non-bonding electrons) are capable of $n \rightarrow \sigma^*$ transitions. These transitions usually need less energy than $\sigma \rightarrow \sigma^*$ transitions. They can be initiated by light whose wavelength is in the range 150 - 250 nm.

n $\rightarrow \pi^*$ *and* $\pi \rightarrow \pi^*$ *Transitions*

In its majority, the absorption spectroscopy of organic compounds is based on transitions of *n* or π electrons to the π^* excited state. This is because the absorption peaks for these transitions fall in an experimentally convenient region of the spectrum (200 - 700 nm). These transitions need an unsaturated group in the molecule to provide the π electrons.

Charge - Transfer Absorption

Many inorganic species show charge-transfer absorptions. These species are called *charge-transfer complexes*. For a complex to demonstrate charge-transfer behavior, one of its components must have electron donating properties and another component must be able to accept electrons. Absorption of radiation, then, involves the transfer of an electron from the donor to an orbital associated with the acceptor. Molar absorptivities from charge-transfer absorption are large (greater that 10,000 L mol^{-1} cm^{-1}).

d-d Transitions

The spectra of transition metal complexes can be interpreted in terms of d-d transitions. The intensities and band positions depend on the metal, the ligand, and the arrangement of the ligands.

Measurement of UV Spectra

When sample molecules are exposed to light, having an energy that matches a possible electronic transition within the molecule, some of the light energy will be absorbed as the electron is promoted to a higher energy orbital. An optical spectrometer records the wavelength(s) at which absorption occurs, together with the degree of absorption at each wavelength.

The diagram of the components of a typical spectrometer is shown in Fig. 4. A beam of light from a visible and/or UV light source is separated into its component wavelengths by a prism or diffraction grating. Each monochromatic (single wavelength) beam, in turn, is split into two equal intensity beams by a half-mirrored device. One beam, the sample beam passes

through a small transparent container (cuvette) containing a solution of the compound being studied in a transparent solvent. The other beam, the reference, passes through an identical cuvette containing only the solvent. The intensities of these light beams are then measured by electronic detectors and compared. The intensity of the reference beam, which should have suffered little or no light absorption, is defined as $\mathbf{I_0}$. The intensity of the sample beam is defined as **I**. Over a short period of time, the spectrometer automatically scans all the component wavelengths in the manner described. The ultraviolet (UV) region scanned is normally from 200 to 400 nm, and the visible portion is from 400 to 800 nm.

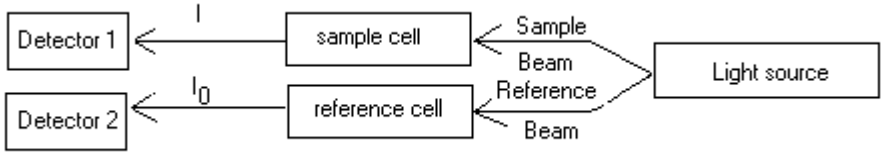

Fig. 4 Schematic representation of a UV-Visible experiment.

If the sample compound does not absorb light at a given wavelength, $I = I_0$. However, if the sample compound absorbs light, then I is less than I_0, and this difference may be plotted on a graph versus wavelength. Absorption may be presented as transmittance ($T = I/I_0$) or absorbance ($A = \log I_0/I$). If no absorption has occurred, T = 1.0 and $A = 0$.

Since the absorbance of a sample analyte is proportional to its molar concentration in the sample cuvette, a corrected absorption value known as the molar absorptivity is used when comparing the spectra of different compounds. This is defined as:

$$\varepsilon = A/ c\, l \qquad (4)$$

where: A = absorbance, c = sample concentration in moles/liter, l = length of light path through the cuvette in cm.

2.4 ELECTRON PARAMAGNETIC RESONANCE SPECTROSCOPY

Introduction

Electron Paramagnetic Resonance (EPR), also known as Electron Spin Resonance (ESR) and Electron Magnetic Resonance (EMR), is the name given to the process of resonant absorption of microwave radiation ($\approx 10^{10}$ Hz) by ions or molecules, with at least one unpaired electron spin, and in the presence of a static magnetic field (≈ 0.3 T). It has a wide range of applications in chemistry, physics, biology, and medicine.

Physical Basis of Electron Paramagnetic Resonance

EPR is a magnetic resonance technique very similar to NMR, Nuclear Magnetic Resonance. However, instead of measuring the nuclear transitions, one detects the transitions of unpaired electrons in an applied magnetic field. The physical basis of the technique is the interaction between the magnetic moment of the electron and the applied magnetic field.

Like a proton, the electron has a spin, which gives it a magnetic property known as a magnetic moment. The magnetic moment makes the electron behave like a tiny bar magnet. When an external magnetic field is applied, the paramagnetic electrons can either orient in a direction parallel or antiparallel to the direction of the magnetic field. This creates two distinct energy levels for the unpaired electrons and allows us to measure them as they are driven between the two levels.

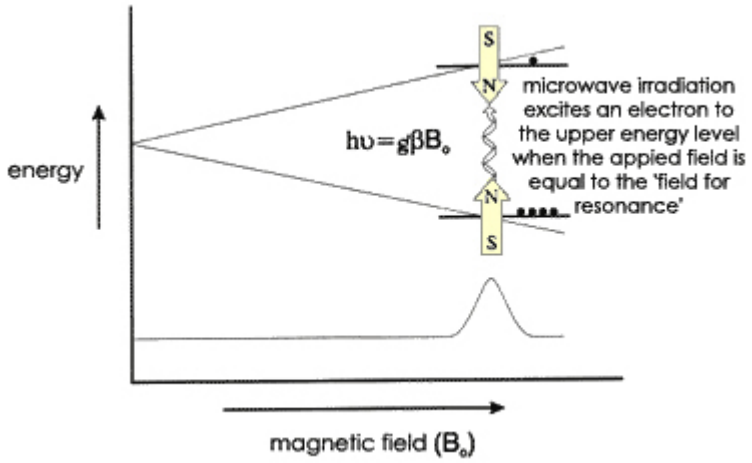

Initially, there will be more electrons in the lower energy level (parallel to the field) than in the upper level (antiparallel). A fixed frequency of microwave irradiation is used to excite some of the electrons in the lower energy level to the upper energy level. In order for the transition to occur, the external magnetic field must be at a specific strength, such that the energy level separation between the lower and upper states is exactly matched by the microwave frequency. In order to achieve this condition, the external magnet's field is swept while exposing the sample to a fixed frequency of microwave irradiation. The condition where the magnetic field and the microwave frequency are "just right" to produce an EPR resonance (or absorption) is known as the resonance condition and is described by equation (5):

$$h\nu = g\beta B_0 \qquad (5)$$

where β is the Bohr magneton, B_0 is the applied (or external) magnetic field at resonance and g is the electron g-factor, which for a free electron is 2.0023. The g-value is used to characterized the position of a resonance. It is a measure of the local magnetic field experienced by the electron.

Measurement of EPR spectra

EPR spectra are usually displayed as the first derivatives of the absorption spectrum. A spectrum is characterized by four main parameters: intensity, linewidth, the g-value (which defines position), and multiplet structure. The intensity of an EPR spectrum in solution can give information on the concentration, the linewidth on any dynamic process, the g-value on the immediate environment of the unpaired electron, and the multiplet structure on the interaction of the unpaired electron spins with nuclear spins. The g-values are usually anisotropic, which means that the spectra depend on the angle between the molecular axes and the applied magnetic field. Fig. 5 is a diagram of a typical EPR spectrometer.

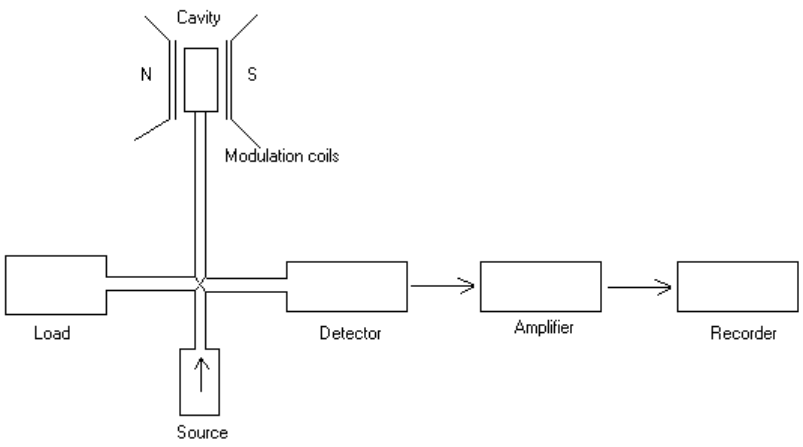

Fig. 5 Schematic representation of an EPR spectrometer.

An approximately monochromatic radiation falls on a sample in an appropriate cell, and one looks for changes in the intensity of the transmitted (or reflected) radiation by means of a suitable detector. Two primary classes of fixed –frequency spectrometers exist: a) continuous or b) pulsed. Microwaves are conducted along hollow tubes whose dimensions are related to the microwave wavelengths. The resonator in a microwave spectrometer is called a cavity. The cavity containing the sample is placed in a magnetic field that is swept through the resonance condition. Sample can be aqueous or solid and typically have volumes in the 10-500 μl range.

2. 5 CYCLIC VOLTAMMETRY

Introduction

A simple potential waveform that is often used in electrochemical experiments is the linear waveform i.e., the potential is continuously changed as a linear function of time. The rate of change of potential with time is referred to as the scan rate (v). The simplest technique that uses this waveform is linear sweep voltammetry. The potential range is scanned in one direction, starting at the initial potential and finishing at the final potential. A more commonly used variation of the technique is *cyclic voltammetry*, in which the direction of the potential is reversed at the end of the first scan. Thus, the waveform is usually of the form of an isosceles triangle (see below). This has the advantage that the product of the electron transfer reaction that occurred in the forward scan can be probed again in the reverse scan. In addition, it is a powerful tool for the determination of formal redox potentials, detection of chemical reactions that precede or follow the electrochemical reaction and evaluation of electron transfer kinetics.

Principles of Cyclic Voltammetry

An example waveform that can be used in cyclic voltammetry is shown below:

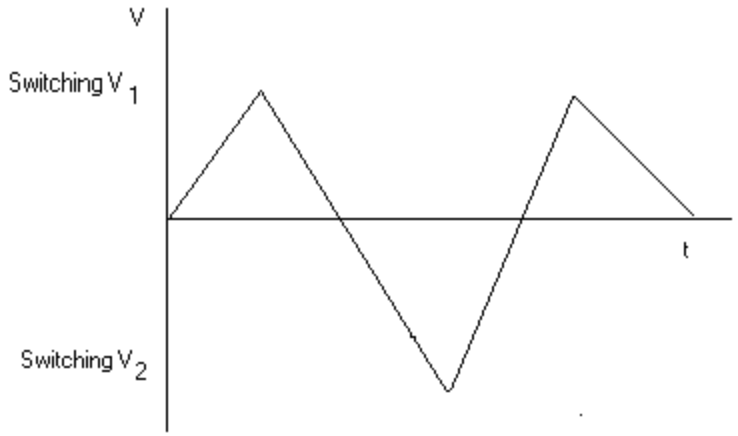

The voltage is first held at the initial potential, where no electrolysis occurs and hence no Faradaic current flows. As the voltage is scanned in the positive direction, the reduced compound is oxidized at the electrode surface. At a particular set value, the scan direction is reversed and the material that was oxidized in the outward excursion is then reduced. Once the voltage returns to the initial value, the experiment can be terminated. A further voltage excursion can take place to more negative (more reducing) values. This may be useful in probing for other species present in the sample or for investigating any electroactive products formed as a result of the first voltage excursion. The peak current, i_p, is described by the Randles-Sevcik equation:

$$i_p = 2.69 \cdot 10^5 n^{3/2} \cdot A \cdot C \cdot D^{1/2} \cdot v^{1/2} \quad (6)$$

where n is the number of moles of electrons transferred in the reaction, A is the area of the electrode, C is the analyte concentration (in moles/cm^3), D is the diffusion coefficient, and v is the scan rate of the applied potential.

A typical cyclic voltammogram recorded for a reversible single electrode transfer reaction is shown in below:

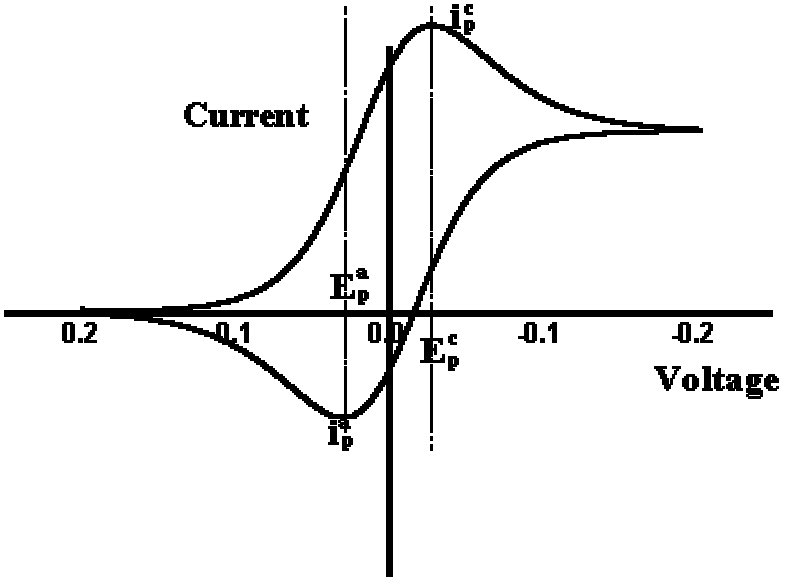

For a *reversible* electrochemical reaction the cyclic voltammogram recorded has certain well-defined characteristics.

1) The voltage separation between the current peaks is:

$$\Delta E = E_p^a - E_p^c = \frac{60}{n} mV$$

2) The positions of peak voltage do not alter as a function of voltage scan rate.

3) The ratio of the peak currents is equal to one, at all scan rates.

$$\left| \frac{i_p^a}{i_p^c} \right| = 1$$

4) The current function is constant with scan rate.

$$\frac{i_p}{\sqrt{v} c_o} = \text{constant}$$

where v- scan rate, c_o – concentration of species

Experimental Setup

A simple electrochemical cell consists of two electrodes and an electrolyte. An electrode is the interface at which dissolved substrates may pick up or lose electron(s). An electrolyte is needed in order to provide electrical conductivity between the two electrodes. In a cell used in cyclic voltammetry, there are always three electrodes due to the difficulties arising from the concurrent measurement of current and potential (see diagram below). The first of the three electrodes is the indicating electrode, also known as the test or *working electrode*. This is the electrode, at which the electrochemical phenomena (reduction or oxidation) being investigated are taking place. The second functional electrode is the *reference electrode*. This is the electrode, whose potential is constant enough that it can be taken as the reference standard against which the potentials of the other electrodes present in the cell can be measured. Commonly used reference electrodes are the silver-silver chloride electrode (Ag/AgCl/4M KCl, E=0.222 V) or the Saturated Calomel Electrode (Hg/HgCl/KCl). The final functional electrode is the *counter or auxiliary electrode*, which serves as a source or

sink for electrons so that current can pass from the external circuit through the cell. In general, neither its true potential nor current is ever measured or known.

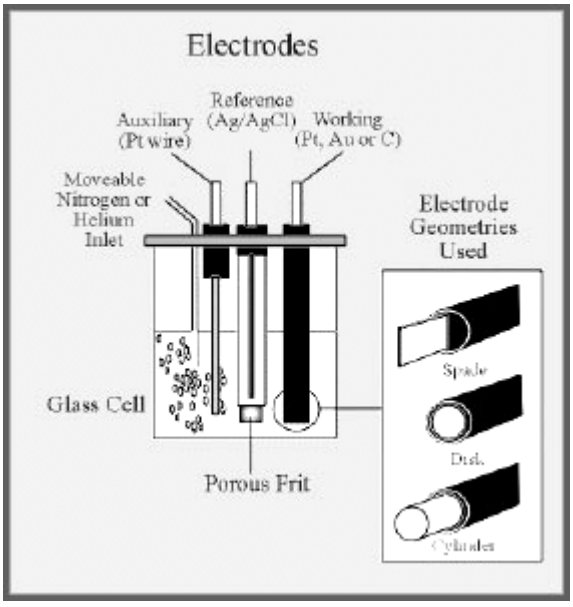

Fig. 6 Electrochemical cell used in cyclic voltammetry.

2.6 POTENTIOMETRY

Introduction

Potentiometry is the field of electrochemical chemistry, in which the potential is measured under conditions of no current flow. The measured potential may then be used to determine the analytical quantity of interest, generally the concentration of some component of the analyte solution. In potentiometry, the potential difference (voltage) between two electrodes is measured. To keep the measurement simple, one of the electrodes is always the reference electrode. The saturated calomel electrode (SCE) and the silver - silver chloride (Ag/AgCl) are the two most common references electrodes used.

Principles of Potentiometry

Potentiometric titrations are titrations, where there is a voltage change that signals the endpoint of a titration. The potentiometric system is used to establish the endpoint and, therefore, many of the limitations of direct potentiometry are insignificant.

The potential that develops in the electrochemical cell is the result of the free energy change that would occur if the chemical phenomena were to proceed until the equilibrium condition had been satisfied.

$$\Delta G = -nFE \quad (7)$$

where ΔG is the free energy, n is the number of electrons transferred, F is Faraday's constant.

For electrochemical cells, the potential difference between the cathodic electrode potential and the anodic electrode potential is the potential of the electrochemical cell.

$$E_{cell} = E_{cathode} - E_{anode} \quad (8)$$

If the reaction proceeds under standard state conditions, this equation allows the calculation of the standard cell potential. When the reaction conditions are not standard state, however, one must utilize the Nernst equation to determine the cell potential.

$$E_{cell} = E^0 - \frac{RT}{nF}\ln(K_{eq}) \quad (9)$$

Physical phenomena, which do not involve explicit redox reactions, but whose initial conditions have a non-zero free energy, will also generate a potential. An example of this would be ion concentration gradients across a semi-permeable membrane. It can also be

potentiometric phenomena, and that is the basis of measurements that use ion-selective electrodes.

$$E_{mem} = (cons\tan t) - \frac{RT}{z_i F}\ln(a_i) \qquad (10)$$

Ion-Selective Electrode (ISE)

Direct potentiometry is mostly based on membrane type electrodes. The most common and the earliest membrane electrode is the glass electrode used for measuring pH. This type of electrode is often called an ion selective electrode (ISE). The selectivity comes from the membrane, which is selectively permeable to the ions of interest. In all types of ISEs, the electrode contains an internal solution with the ions of interest. These ions are attracted to the inside of the membrane and the same type of ions are attracted to the outside of the membrane from the solution being studied. This results in the generation of a potential across the membrane. An Ion-Selective Electrode produces a potential that is proportional to the concentration of an analyte. Making measurements with an ISE is, therefore, a form of potentiometry. The most common ISE is the pH electrode, which contains a thin glass membrane that responds to the H^+ concentration in a solution.

The potential difference across an ion-sensitive membrane is:

$$E = K - (2.303RT/nF)\log(a) \qquad (11)$$

where K is a constant to account for all other potentials, R is the gas constant, T is temperature, n is the number of electrons transferred, F is Faraday's constant, and a is the activity of the analyte ion. A plot of measured potential versus $\log(a)$ will therefore give a straight line.

ISEs consist of the ion-selective membrane, an internal reference electrode, an external reference electrode, and a voltmeter. Commercial ISEs often combine the two electrodes into one unit attached to a pH meter.

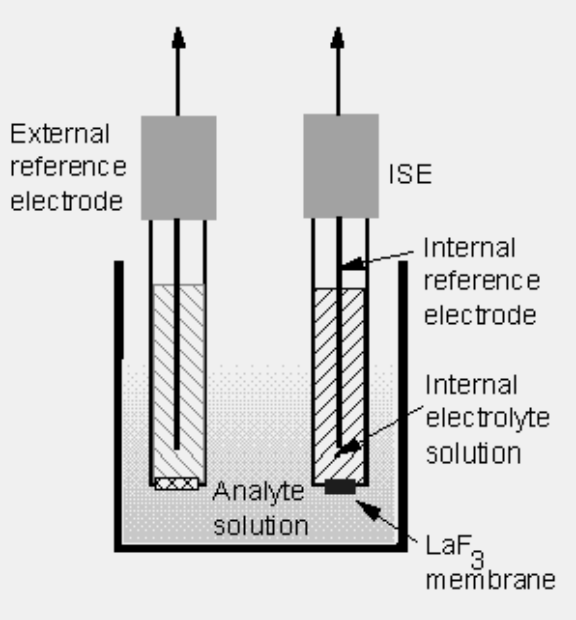

Fig. 7 Schematic representation of an ISE measurement

pH Meter

The pH meter measures the pH of a solution using an ion-selective electrode (ISE) that responds to the H^+ concentration of the solution. The pH electrode produces a voltage that is proportional to the concentration of the H^+ concentration. Taking measurements with a pH meter is, therefore, a form of potentiometry. The pH electrode is attached to control electronics, which convert the voltage to a pH reading. The results are displayed on a meter. A pH meter consists of an H^+-selective membrane, an internal reference electrode, an external reference electrode, and a meter with control electronics and a display. Commercial pH electrodes usually combine all electrodes into one unit attached to the pH meter.

2.7 LITERATURE

1. Cullity, B. D. *Elements of X-ray Diffraction*, Addison-Wesley Publishing Company, Inc., **1978**.
2. Sands, D. E. *Introduction to Crystallography*, Dover Publications Inc., **1993**.
3. Clegg, W.; Blake, A. J.; Gould, R. O.; Main, P. *Crystal Structure Analysis Principles and Practice,* Oxford Science Publications, **2001**
4. Campbell, I. D.; and Dwek, R. A. *Biological Spectroscopy,* The Benjamin/ Cummings Publishing Company, Inc., **1984**.
5. Shriver, D. F.; Atkins, P. W.; Langford, C. H. *Inorganic Chemistry*, Second Edition, Oxford University Press, **1994**.
6. Harris, D.C.; Bertolucci M. D. *Symmetry and Spectroscopy,* Dover Publications, Inc., New York, **1978**.
7. Brown, J. *Molecular Spectroscopy*, Oxford University Press, **1998**.
8. Thomson, M. *Ultraviolet and Visible Spectroscopy*, Second Edition, John Willey & Sons, **1997**.
9. Weil, J.A.; Bolton, J.R.; Wertz, J. E. *Electron Paramagnetic Resonance,* John Wiley & Sons, Inc., **1994**.
10. Wang, I. *Analytical Electrochemistry*, Wiley-VCH, Inc., **1994**.
11. Harris, D. C. *Quantitative Chemical Analysis,* Fourth Edition, W. H. Freeman and Company, New York, **1995**.

– CHAPTER 3 –

COMPLEX FORMATION OF Co(II) WITH THE ORGANOPHOSPHONATE LIGAND NTA2P (N,N- BIS (PHOSPHONOMETHYL)GLYCINE) AT LOW pH.

3.1 INTRODUCTION

The interaction of cobalt with biomolecules carrying phosphonate groups plays an important role in the entrance and circulation of cobalt in biological systems. In an effort to comprehend the chemistry of Co(II) with phosphonate ligands, the organophosphonate ligand N,N-bis(phosphonomethyl) glycine was employed in aqueous reactions with Co(II), ultimately leading to the isolation of complex $\{Co(H_2O)_2\{N(CH_2COOH)(CH_2PO_3H)_2\}\cdot 2H_2O$ (**1**), at pH ≈ 2. The complex was characterized analytically, spectroscopically (FT-IR, UV-Vis, EPR), and electrochemically (cyclic voltammetry).

3.2 EXPERIMENTAL

3.2.1 Material and Methods

All experiments were carried out in the open air, at room temperature. Nano-pure quality water was used for all the experiments. $Co(NO)_3\cdot 6H_2O$, and N,N-bis(phosphonomethyl) glycine used in the synthesis of the title complex were purchased from Aldrich.. Ammonia was supplied by Fluka.

3.2.2. Synthesis

The complex (**1**) was synthesized in aqueous solution, with the initial metal to ligand stoichiometry employed being 1:1. A quantity of 0.17 g (0.58 mmol) of $(Co(NO_3)_2\cdot 6H_2O$ and 0.16 g (0.58 mmol) of N,N-bis(phosphonomethyl) glycine were dissolved in 2.5 mL of nano-pure water. The pH of the resulting solution was 1.5. The derived reaction mixture was stirred at room temperature for 10-15 min. Subsequently, the reaction flask was placed at 4 °C

in the presence of ethanol. A couple of weeks later pink crystals suitable for X-ray diffraction grew out of the solution. The crystalline material was isolated by filtration, and was dried under vacuum. Yield: 0.11 g (~61 %). Anal. Calcd for **1**, **$[Co(C_4H_9O_8NP_2)_2(H_2O)_2] \cdot 2H_2O$** ($C_4H_{17}CoNO_{12}P_2$, MW = 392.06): C, 12.24; H, 4.34; N, 3.57. Found: C, 12.53; H, 4.45; N, 3.54.

The overall stoichiometric reaction leading to complex (**1)** is drawn schematically below:

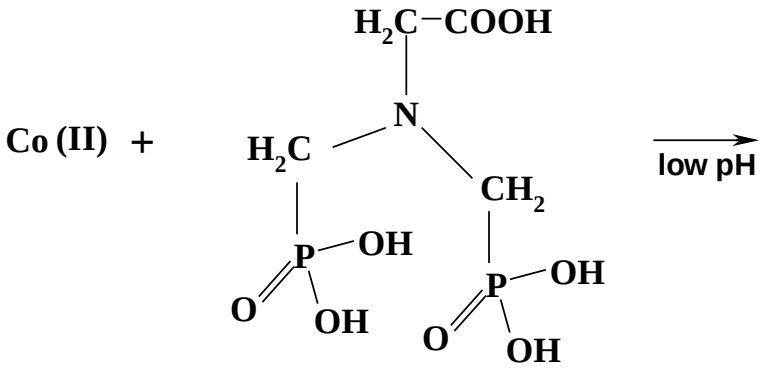

$$[Co(C_4H_9O_8NP_2)(H_2O)_2] \quad + \quad 2\,H^+$$

3.3 RESULTS

3.3.1 X - Ray Crystallographic Structure

The X-ray three-dimensional structure determination of complex **1** was carried out. The compound crystallizes in the monoclinic space group $P2_1$. The ORTEP diagram of complex **1** is shown in Fig.1. Summary of crystal, intensity collection and refinement data for $[Co(C_4H_9O_8NP_2)_2(H_2O)_2] \cdot 2H_2O$ (**2**) are listed in Table 1. A selected list of interatomic distances and bond angles for **1** is given in Table 2. The structure of **1** contains of a mononuclear core unit composed of an octahedral Co(II) ion. The coordination sphere of

Co(II) is generated by two different types of ligands, namely, N,N-bis(phosphonomethyl) glycinate ($^{=}O_3P\text{-}CH_2\text{-}N(CH_2COO^{-})\text{-}CH_2\text{-}PO_3^{=}$ = $NTA2P^{5-}$) and water. The ligand employs both phosphonate groups to coordinate to the metal ion through one of its deprotonated hydroxides, with the remaining hydroxide for each phosphonate group staying in its protonated form as well as the corboxylate group through one of the oxygen. An additional position in the octahedral coordination sphere is occupied by the tertiary amine nitrogen. The corboxylate group bound to the Co(II) ion is in its protonated form. Two water molecules are coordinated to the Co(II) ion, and with the previous $NTA2P^{5-}$ ligand complete the equatorial plane coordination requirements of the octahedral metal ion. One of the water molecules along with the two phosphonate groups and the corboxylate terminal of the H_3NTA2P^{2-} ligand formulate the equatorial plane coordination composition of the octahedral metal ion. The second bound water molecule along with the ammonium nitrogen of the H_3NTA2P^{2-} ligand bound to Co(II) occupy the axial positions in the octahedron. In view of the above description, the mononuclear Co(II) ion resides in a distorted octahedron.

The Co-O bonds lengths fall between 2.012(2) Å and 2.141(2) Å. The Co-N bond length is 2.229(2). The O-Co-O bonds angles are in the range from 87.3(8) - 95.99(8). These bond lengths and angles are similar to those observed in other cobalt(II) phosphonates complexes.[1-4] The Co-O distances in the equatorial plane of the octahedron are of similar length (2.100(2) - 2.141(2) Å), despite the variable nature of the anchor terminal in the two different ligands in the coordination sphere of Co(II), and the fact that they all utilize their oxygens as terminal anchors to the metal ion. In contrast to the equatorial distances, the corresponding axial Co-O bond lengths reflect a more radically varying lengths with the Co-N distance being ~0.1 Å longer than the equatorial ones while the Co-O_w distance is ~0.1 Å shorter that the equatorial ones. It is not unlikely that such bond length variations might be due to Jahn-Teller distortions, which are usually encountered in high-spin Co(II) octahedral species.

The angles within the equatorial plane defined by O(1), O(4), $O_w(1)$, and O(7) are in the range 82.68(8) - 97.58(8)°, with the average being very close to the ideal octahedral angle of 90 °. A similar yet wider angle variation is observed between the axial donor atoms, N and $O_w(2)$, and those in the equatorial plane (range: 78.47(7) - 95.99(8)°).

An interesting attribute of the H_3NTA2P^{2-} ligand participation in the coordination sphere of Co(II) is the presence of a non-protonated central imino moiety in the ligand. As a result, the overall charge of the H_3NTA2P^{2-} ligand coordinated to Co(II) is 2-. Therefore, the overall charge for complex 1 is zero.

Hydrogen bonding interactions are present in the crystal structure of **1** (see Table 3). These interactions involve the coordinated water molecules, the phosphonate oxygen and the hydroxyl moiety on the $NTA2P^{5-}$ ligands. The presence of water molecules of crystallization in **1** is also responsible for the formation of extensive hydrogen bonding network.

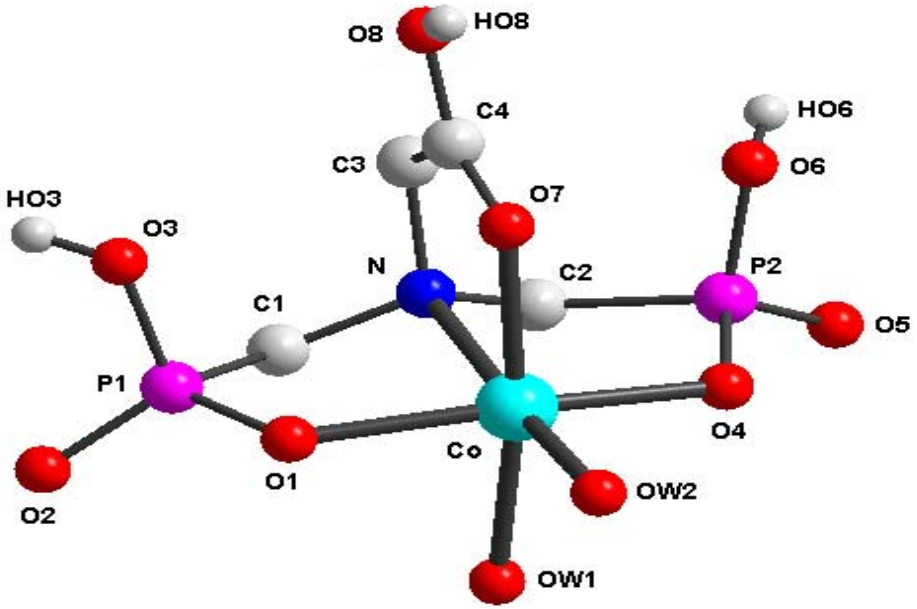

Fig. 1 X-ray structure of $[Co(C_4H_9O_8NP_2)_2(H_2O)_2]$

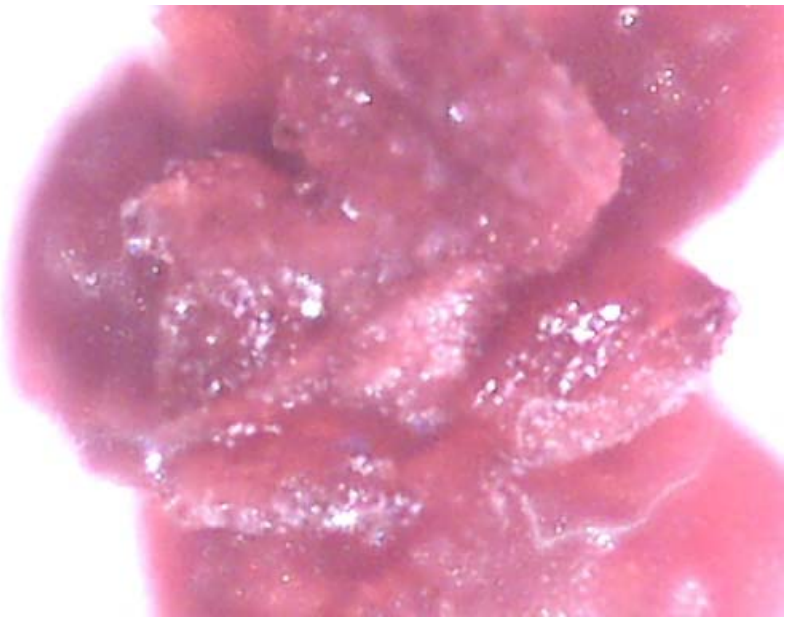

(a)

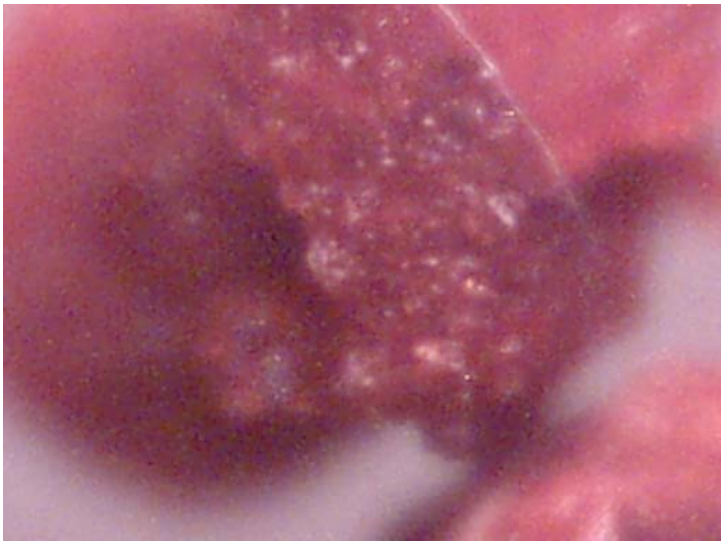

(b)

Optical imagines of complex **1** at (a) x6o and (b) x200 magnitude.

Table 1. Summary of Crystal, Intensity Collection and Refinement Data for $[Co(C_4H_9O_8NP_2)_2(H_2O)_2] \cdot 2H_2O$.

Empirical formula	$C_4H_{17}CoNO_{12}P_2$
Formula weight	392.06
Temperature, K	298
Wavelength	Mo Kα 0.71073
Space group	$P2_1$
a (Å)	7.566(3)
b (Å)	12.721(5)
c (Å)	7.361(3)
β,deg	96.271(13)
V,($Å^3$)	704.2(5)
Z	2
D_{calcd}/D_{measd} (Mg m^{-3})	1.849/1.83
R indices [2468 refs I>2σ(I)](2)	R = 0.0226, R_w = 0.0610
R indices (all data)	R = 0.0226, Rw = 0.061

R values are based on F values, R_w values are based on F^2.

$$R = \frac{\sum \| F_o | - | F_c \|}{\sum (| F_o |)} \quad , \quad R_w = \sqrt{\sum \left[w(F_o^2 - F_c^2)^2 \right] \Big/ \sum \left[w(F_o^2)^2 \right]}$$

(2) [5226 refs I>2σ(I)]

Table 2. Bond lengths [Å] and angles [deg] in complex **1**.

Co-OW2	2.012(2)	O(5)-P(2)-O(6)	111.08(11)
Co-O(1)	2.100(2)	O(4)-P(2)-O(6)	106.57(11)
Co-O(4)	2.101(2)	O(5)-P(2)-C(2)	109.28(11)
Co-OW1	2.127(2)	O(4)-P(2)-C(2)	104.88(11)
Co-O(7)	2.141(2)	O(6)-P(2)-C(2)	107.30(12)
Co-N	2.229(2)	N-C(3)-C(4)	112.2(2)
O(1)-P(1)	1.526(2)	O(7)-C(4)-O(8)	125.7(2)
O(4)-P(2)	1.521(2)	O(7)-C(4)-C(3)	123.3(2)
O(7)-C(4)	1.225(3)	O(8)-C(4)-C(3)	111.0(2)
N-C(3)	1.481(3)		
N-C(2)	1.489(3)		
N-C(1)	1.491(3)		
P(1)-O(2)	1.492(2)		
P(1)-O(3)	1.572(2)		
P(1)-C(1)	1.822(2)		
C(2)-P(2)	1.811(3)		
P(2)-O(5)	1.502(2)		
P(2)-O(6)	1.570(2)		
C(3)-C(4)	1.511(3)		
C(4)-O(8)	1.299(3)		
OW2-Co-O(1)	95.99(8)		
OW2-Co-O(4)	95.41(9)		
O(1)-Co-O(4)	164.81(7)		
OW2-Co-OW1	90.06(9)		
O(1)-Co-OW1	82.68(8)		
O(4)-Co-OW1	87.30(8)		
OW2-Co-O(7)	95.46(9)		
O(1)-Co-O(7)	91.30(8)		
O(4)-Co-O(7)	97.58(8)		
OW1-Co-O(7)	172.24(8)		
OW2-Co-N	173.94(9)		
O(1)-Co-N	84.22(7)		
O(4)-Co-N	85.51(7)		
OW1-Co-N	95.97(8)		
O(7)-Co-N	78.47(7)		
P(1)-O(1)-Co	117.70(9)		
P(2)-O(4)-Co	114.74(10)		
C(4)-O(7)-Co	116.0(2)		
C(3)-N-C(2)	111.9(2)		
C(3)-N-C(1)	111.4(2)		
C(2)-N-C(1)	111.4(2)		
C(3)-N-Co	109.89(14)		
C(2)-N-Co	106.2(2)		
C(1)-N-Co	105.74(14)		
O(2)-P(1)-O(1)	117.37(11)		
O(2)-P(1)-O(3)	112.31(12)		
O(1)-P(1)-O(3)	104.70(11)		
O(2)-P(1)-C(1)	109.52(11)		
O(1)-P(1)-C(1)	104.44(11)		
O(3)-P(1)-C(1)	107.84(11)		
N-C(1)-P(1)	110.6(2)		
N-C(2)-P(2)	109.8(2)		
O(5)-P(2)-O(4)	117.15(11)		

Table 3. Hydrogen bonds in complex **1**

Interaction	D…A (Å)	H…A (Å)	D-H…A (deg)	Symmetry operation
O3-HO3…O5	2.547	1.704	174.9	1-x, -0.5+y, 1-z
O6-HO6…O1	2.559	1.812	174.2	1+x, y, z
O8-HO8…O4	2.593	1.850	158.7	1-x, -0.5+y, -z
OW1-HW1A…OW3	2.720	1.841	166.4	x, y, z
OW1-HW1B…O5	2.922	2.111	166.7	-1+x, y, z
OW2-HW2A…OW4	2.672	1.906	162.6	-x, 0.5+y, -z
OW2-HW2B…O2	2.691	1.845	167.8	x, y, -1+z
OW3-HW3A…O2	2.785	1.970	166.8	-x, 0.5+y, 1-z
OW3-HW3B…O6	2.934	2.187	157.8	1-x, 0.5+y, -z
OW4-HW4A…O3	2.983	2.203	171.8	x, y, z

3.3.2 Electronic spectroscopy

UV/Visible spectra of the crystals were recorded on a Hitachi U-2001 spectrophotometer in the 200-1000 nm range. Two principal regions of adsorption are observed for a high spin octahedral specie.[5,6] A band near 1000-1250 nm can be assigned to the $^4T_{1g}$ ----> $^4T_{2g}$ transition. In addition, a multiple structure band is seen in the visible region at about 500 nm, that can be assigned to $^4T_{1g}$ ----> $^4T_{1g}(P)$. The UV-Vis spectrum of **1** is depicted in Fig. 2. The spectrum exhibits two major peaks at λ_{max} = 550 nm (ε = 6.8 M^{-1} cm^{-1}), and λ_{max} = 517 nm (ε = 9.9 M^{-1} cm^{-1}), a subtly discernible shoulder around 473 nm (ε = 7.6 M^{-1} cm^{-1}), and a distant shoulder around 222 nm (ε = 122.7 M^{-1} cm^{-1}). The absorption features are most likely d-d transitions, typical for a Co(II) d^7 octahedral species. The multiple structured band around 500 nm could be attributed to the $^4T_{1g}$ ----> $^4T_{1g}(P)$ transition. The multiple structures arises from a number of causes, but primarily to admixture of spin forbidden transitions to doublet states mainly derived from ^2G and ^2H. The structure on the visible region may also be due to the spin-orbit coupling, vibrational or low symmetry components, making the analysis of six coordinated cobalt complexes rather difficult. In the absence of detailed studies no further assignments could be proposed.

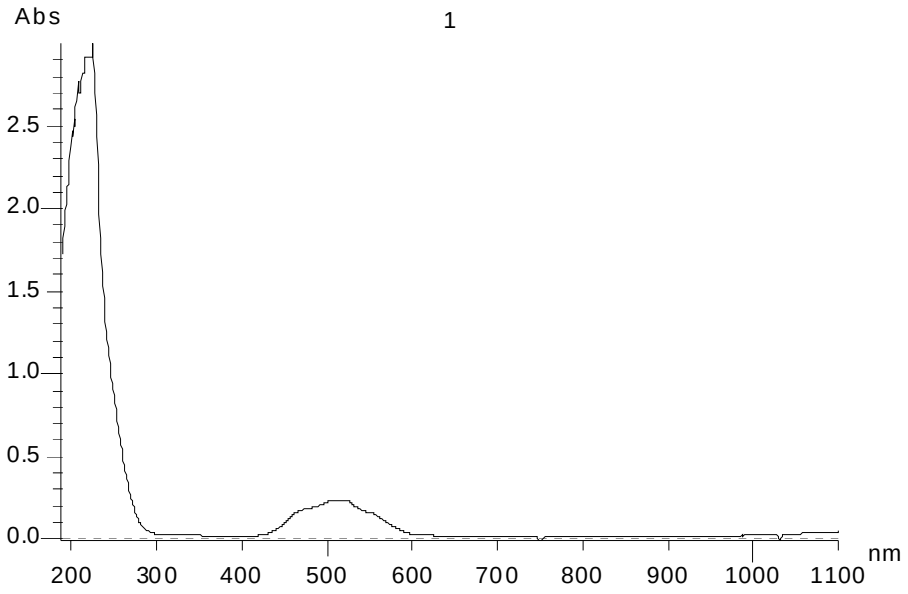

Fig. 2. UV/Visible spectrum of complex **1**, at a concentration c = 0.0238M in the range 200-1100 nm.

3.3.3 FT-IR spectroscopy

FT-infrared measurements were taken on a Perkin-Elmer 1760X FT-IR spectrometer. The FT-infrared spectrum of **1** is depicted in Fig. 3. The FT-infrared spectrum of compound **1** in KBr confirmed the presence of vibrationally active phosphonate groups. Specifically, antisymmetric and symmetric vibrations for the phosphonate groups of the coordinated ligand are present in the spectrum. The antisymmetric stretching vibrations are present for the phosphonates ($\nu_{as}(PO_3)$) in the rang 1105 - 980 cm^{-1}. A symmetric stretching vibration $\nu_s(PO_3)$ is observed in the range 980 - 920 cm^{-1}. The observed PO_3 groups vibrations appear to be shifted to lower frequency values in comparison to the corresponding vibrations in free N,N-bis(phosphonomethyl) glycine acid, thus indicating changes in the vibrational status of the ligand upon coordination to the Co(II) ion (Fig. 4). Antisymmetric as well as symmetric vibrations for the carboxylate group of the coordinated H_3NTA2P^{2-} ligand appear in the spectrum. Specifically, antisymmetric stretching vibrations $\nu_{as}(COO^-)$ are present for the carboxylate groups around 1664 cm^{-1}. Symmetric vibrations $\nu_s(COO^-)$ for the same group are present in the range 1461-1408 cm^{-1}. The frequencies of the observed carbonyl vibrations were shifted to lower values in comparison to the corresponding vibrations in the free H_5NTA2P acid. The difference between the symmetric and antisymmetric stretches, $\Delta(\nu_{as}(COO^-)-\nu_s(COO^-))$, is greater than 200 cm^{-1}, indicating that the carboxylate group of the H_3NTA2P^{2-} ligand was either free or coordinated to the metal ion in a monodentate fashion.[7] This was further confirmed by the X-ray crystal structure of **1**. The broad absorption at 3000 cm^{-1} is due to the O-H stretching vibration of the hydration water molecule.

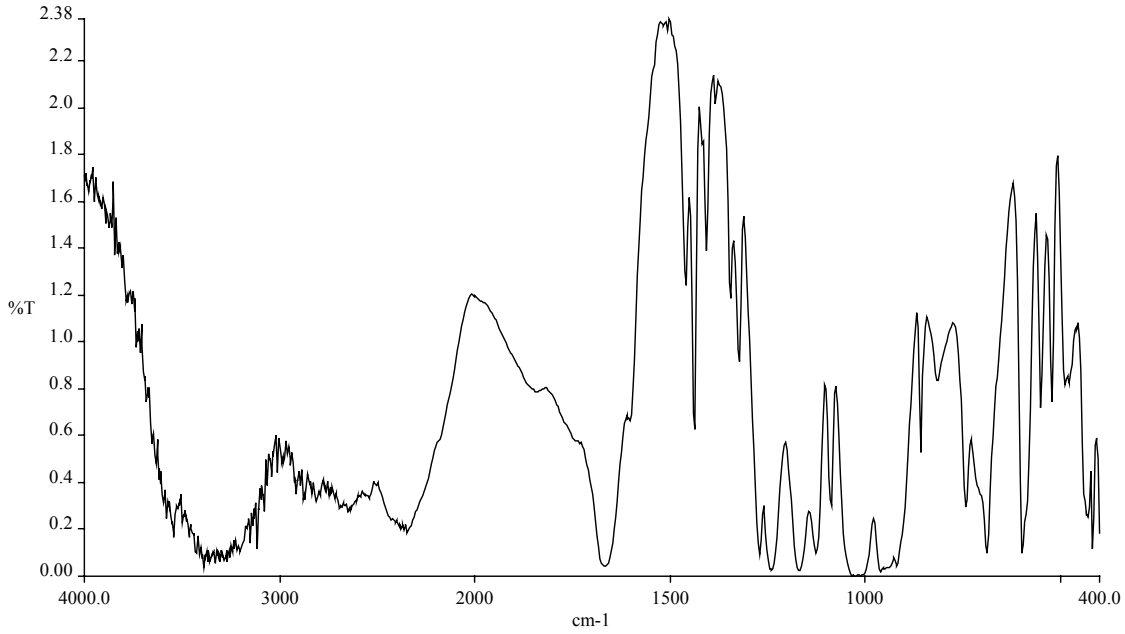

Fig. 3 The FT-infrared spectrum of compound $[Co(C_4H_9O_8NP_2)_2(H_2O)_2] \cdot 2H_2O$.

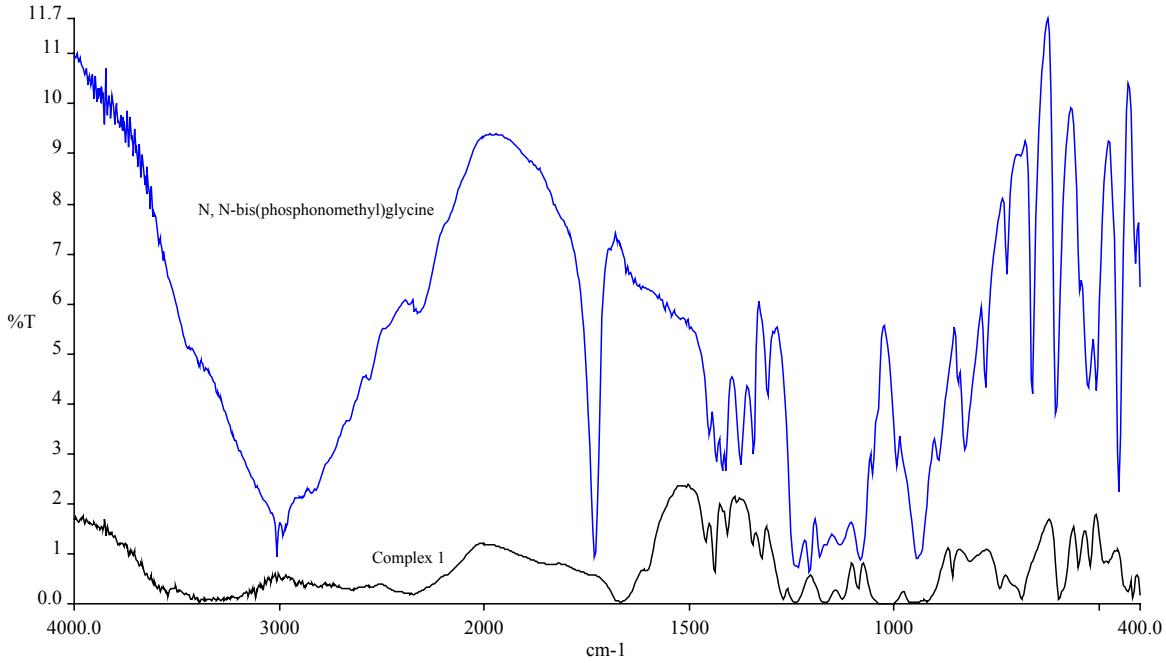

Fig. 4 Comparison between the FT- infrared spectra of compound **1** and N,N-bis(phosphonomethyl) glycine.

3.3.4 EPR spectroscopy

X-Band EPR measurements were carried out in powder samples of **1** as well as in frozen solutions thereof in water and are shown in Fig. 5 and 6, respectively. The EPR spectra of complex **1** in the solid state and in solution were recorded on a Bruker ER 200D-SRC X-band spectrometer.

As a consequence of the fast spin-lattice relaxation time of high-spin Co(II), signals were observed only below 70 K. For the powder spectra, at temperatures T< 23 K, a strong signal appears at low fields and a small broad one at g=2.30. A simulation[8] was carried out in order to derive the effective g-values assuming a Hamiltonian formalism:

$$H = g_z \mu_B H_z S_z + g_x \mu_B H_x S_x + g_y \mu_B H_y S_y \qquad (1)$$

with an effective spin S=1/2 and an anisotropic **g**-tensor and the results are shown in Fig. 7. An isotropic magnetic-field domain line width was used in both cases (lw= 35 G for the powder and lw=75 G for the frozen solution) while the broadness of the spectra reveals the g-strain effects. Gaussian distributions of the g-principal values were used and the results are for the powder ($\Delta g_x = \Delta g_z = 0.78$, $\Delta g_y = 0.23$) and for the frozen solution ($\Delta g_x = \Delta g_y = \Delta g_z = 0.78$). The principal g-values for the powder spectrum are g_x=4.92(1), g_y=2.28(1), g_z=6.33(1) (g_{eff}=4.51) and for the frozen solution g_x=4.20(1), g_y=2.35(1), g_z=5.33(1) (g_{eff} = 3.96).

The dominant broadening effect is realized when the g-strain is converted into B-strain through the relation $\Delta B = -\left(\frac{h\nu}{\mu_B}\right)\left(\frac{\Delta g}{g^2}\right)$, where β_B is the Bohr magneton ($0.92 \cdot 10^{-23}$ J·T).

Thus, the largest and smallest g-values of the powder and solution spectra have field widths that differ by an order of magnitude, rationalizing why the high-field features of the spectrum are so broad.

A very important feature of the Co(II) ion is the value of the effective g-parameter, g_{eff} extracted from the EPR measurements, as a result of which interesting conclusions can be drawn. If the octahedron of a high spin Co(II) system has a small tetragonal or trigonal distortion, additional terms are added in the ground doublet. Provided that these terms are small compared with the spin-orbit coupling of the ground doublet, they may be written into the form:

$$\left| J=\frac{1}{2},\ J_z=\pm\frac{1}{2}\right\rangle + a\left|\frac{3}{2},\pm\frac{1}{2}\right\rangle + b\left|\frac{5}{2},\pm\frac{1}{2}\right\rangle \qquad (2)$$

where α, and even more so b, are small compared to unity. According to Abragam and Bleaney by neglecting terms of order a^2 and b^2, the expressions for the g parameters of the Co(II) system are :

$$g_{\|}=\frac{5}{3}g_S-\frac{2}{3}g_l+\left(\frac{4\sqrt{5}a}{3}\right)(2g_S-g_l),$$
$$g_{\perp}=\frac{5}{3}g_S-\frac{2}{3}g_l-\left(\frac{2\sqrt{5}a}{3}\right)(2g_S-g_l) \qquad (3)$$

where g_S=2.0 and g_l=-3/2.

In Fig. 8, the dependence of the g-parameters on the parameter α of equation 6 is shown. From equation 3 and Fig. 8, it is clear that the value of $g_{eff}=\frac{g_{\square}+2g_{\perp}}{3}\approx\frac{5g_S-2g_l}{3}\approx 4.33$. Therefore, an isotropic g-value $g_{\|}=g_{\perp}=4.33$ corresponds to α=0 (the energy difference between the ground doublet and the excited one is very large), whereas for an admixture of 20%, the values are $g_{\|}$=7.613 and $g_{\perp}$=2.694.

In Table 4 magnetic and EPR parameters are shown for different high-spin Co(II) complexes. It appears that for values of g_{eff}>4.5 (in the EPR spectra of powder samples), the intermolecular interactions contribute significantly to the magnetic behavior of the system. In the case of $Co(C_4H_8NO_3)_2(H_2O)_2$, a weak exchange interaction is proposed between neighboring Co(II) centers in the exchange limit $0.25<|J|<1.2$ cm^{-1} transmitted through hydrogen bonds. For all the other cases (g_{eff}<4.2), no significant intermolecular interactions are observed. The significance of the aforementioned point is also exemplified in the small g_{eff} value of the frozen solution spectrum, where the hydrogen-bonding system breaks apart and no longer exists.

Table 4. EPR properties of various Co(II) corboxylate and mixed corboxylate- phosphonate compounds.

Compounds	g_{eff} [a]	*Model S=3/2* [c]
This work	4.51(1) (p) 3.96(1) (s)	g=2.53(1)
$Co(C_4H_8NO_3)_2(H_2O)_2$ [9]	4.45(1) (p)	g=2.60(1)
$[Co(C_2H_8O_6NP_2)_2(H_2O)_2]$ [10]	4.10(1) (p) 4.10(1) (s)	**[1]** g=2.33 **[2]**($g_{\|}$=1.7,$g_{\perp}$=2.53)
$(NH_4)_4[Co(C_6H_5O_7)]_2$ [11]	4.00(1) (p)	g=2.42
$K_2[Co_2(C_6H_5O_7)_2(H_2O)_4] \cdot 6H_2O$ [12]	3.75(1) (s)	-

The $g_{eff} = g_x+g_y+g_z/3$ is derived from the EPR measurements performed in powder (**p**) or solution (**s**) samples.

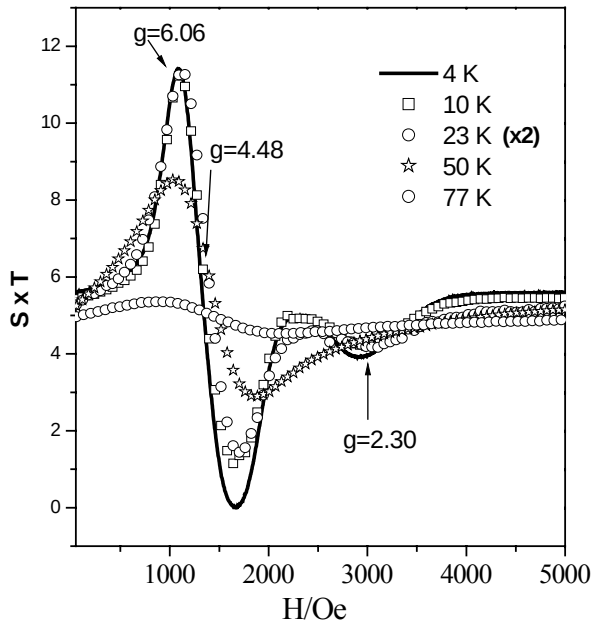

Fig. 5 Temperature dependence of the powder X-Band EPR spectrum (the intensity is multiplied by the temperature) in the field range 0-5000 Oe.

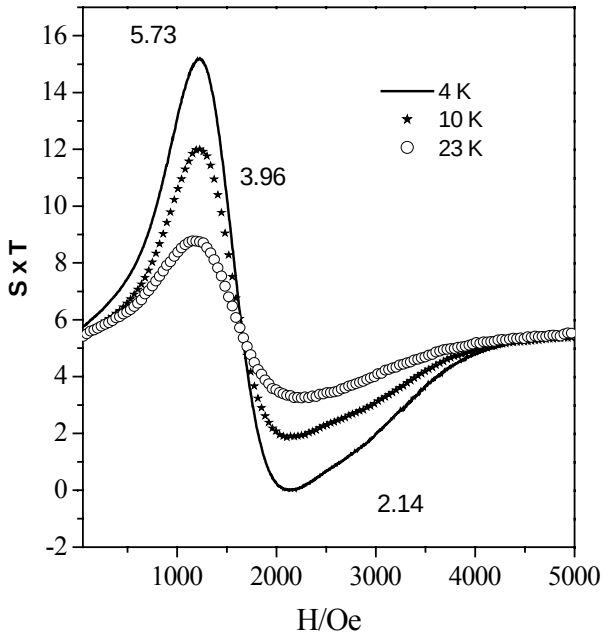

Fig. 6 Temperature dependence of the aqueous solution X-Band EPR spectrum (the intensity is multiplied by the temperature) in the field range 0-5000 Oe.

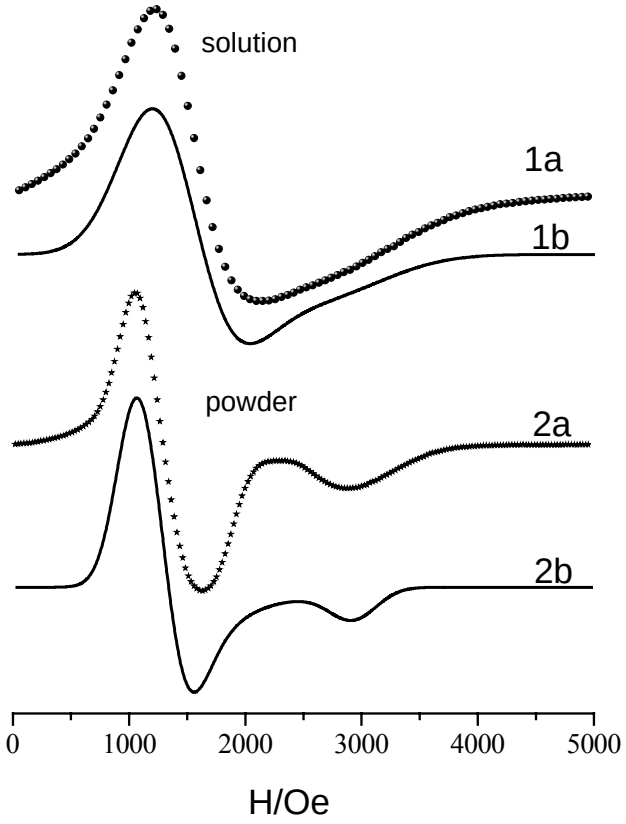

Fig. 7 Simulations of the solution (1a) and powder (2a) EPR spectra are shown as solid lines (1b) and (2b), respectively.

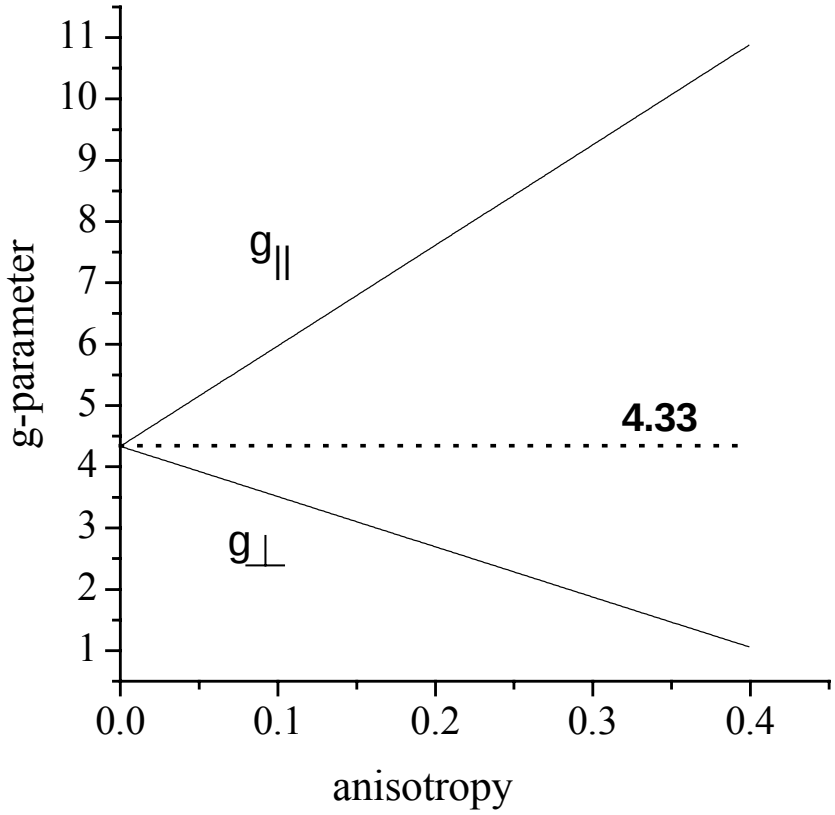

Fig. 8 Anisotropy dependence of the g-parameters ($g_{\|}$ and $g_{\perp}$) of a high-spin Co(II) octahedron resulted from small tetragonal or trigonal distortion

3.3.5 Cyclic Voltammetry

All electrochemical experiments were performed at 25^{o}C using a three-electrode potentiostatic system. The potentials are reported with reference to a Ag/AgCl electrode placed in the same compartment containing the supporting electrode. The aqueous electrolyte solutions were rigorously deoxygenated with argon.

The cyclic voltammogram of complex **1** in the positive potential range is shown in Fig. 9. The E_{pa} and i_{pa} were determined from the cyclic voltammograms at different scan rates (0.5 V/sec, 0.2 V/sec, 0.1 V/sec, 0.05 V/sec). The studied system reflects a one-electron process, which is irreversible. In that only the anodic process is observed. This is based on the following observations: the ratio of the cathodic-to-anodic peak currents i_{pc}/i_{pa} is zero, E_{pa} shifts with scan rate toward more positive potential, and the current function defined as (peak current)/(scan rate)$^{1/2}$(concentration) changes with scan rate. The oxidation wave detected at 1.07 V very likely corresponds to the Co(II)/Co(III) couple. [13] Further work is needed to a\confirm this contention.

In the negative potential range, a well-developed wave is found at $E_{1/2}$= -0.4 V (scan rate 0.1 V/sec) (Fig. 10). Similar waves observed with other cobalt complexes have been attributed either to the reduction of the ligand or to the reduction of the metal center (equilibrium Co(II)/Co(I)).[14,15] As the reduction of the ligand takes place at more negative potentials this wave is assigned to a metal–centered electron transfer corresponding to the couple Co(II)/Co(I). The process is a quasi-reversible one. This is based on the following observations: ΔE varies with scan rate, the current function is not constant, changes with scan rate, the ratio of the peak currents i_{pa}/i_{pc} does not vary much with scan rate ($0<ip_a/ip_c<1$).

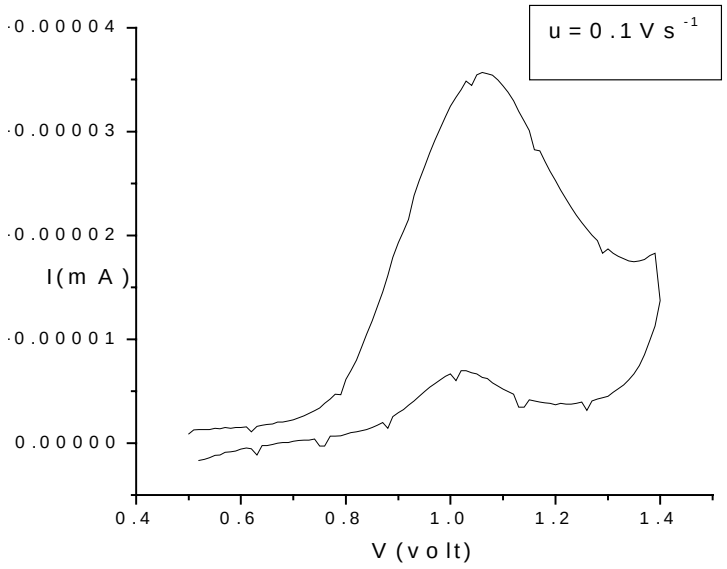

Fig. 9 Cyclic voltammogram (scan rate v =0.1 V s^{-1}) of a 21.9 mM solution of complex **1** in water, with KNO_3 as the supporting electrolyte.

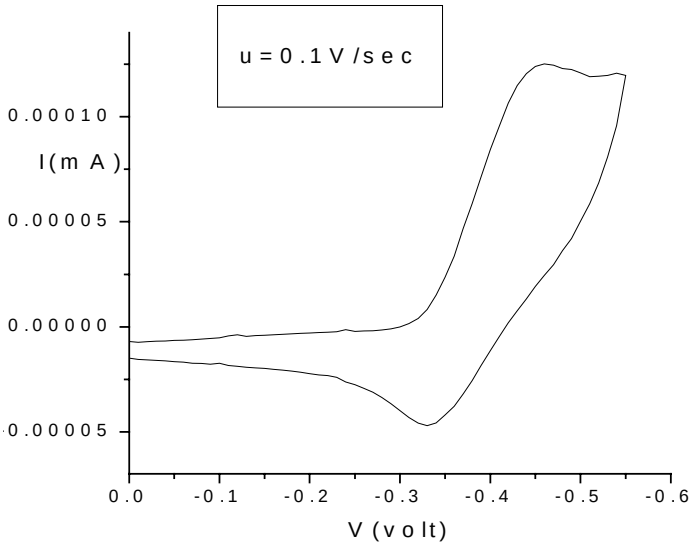

Fig. 10 Cyclic voltammogram (scan rate v = 0.1 V s^{-1}) of a 21.9 mM solution of complex **1** in water, with KNO_3 as the supporting electrolyte.

3.4 DISCUSSION

Though a facile reaction in an aqueous medium, $Co(NO_3)_2$ and $H_2O_3P\text{-}CH_2\text{-}N(CH_2COOH)\text{-}CH_2\text{-}PO_3H_2$ reacted and complex **1** was crystallized and isolated. The pH of the aqueous solutions, in which the reaction was run, was acidic enough (pH = 1.5) to allow for product formation and subsequent isolation of $[Co(C_4H_9O_8NP_2)_2(H_2O)_2] \cdot 2H_2O$ (**1**). The nature of **1** was that of a molecular type of lattice, comprised of mononuclear units linked together through water molecules of crystallization and an extensive network of hydrogen bonds.

The crystallographic data support an octahedral coordination sphere for complex **1**. The ligand employs the two phosphonate groups, the corboxylate group to bind to the metal ion through one of the oxygen of the corresponding groups as well as the amino group. In addition, two water molecules are coordinated to the Co(II) ion to complete the octahedral environment. Variable modes of phosphonate coordination were previously observed in a plethora of metal organophosphonate complexes containing the phosphonate ligand terminals in varying deprotonation states.[16] In the present case, it appears that the coordinated H_5NTA2P ligand loses two of its protons from the two terminal phosphonate groups. Specifically each phosphonate group is singly deprotonated. As a result, the remaining carboxylic acid moiety remains protonated and as such it is anchored to the metal site. The double deprotonation of the H_5NTA2P ligand yields an overall charge of zero for the assembled mononuclear complex, affording the previously mentioned molecular type of lattice in the compound investigated.

The water molecules of crystallization provide an excellent scaffold for hydrogen bond formation throughout the lattice, thus offering their contribution to the stability in the lattice of **1**.

EPR measurements in the solid state and in aqueous solution project the existence a high spin Co(II) complex in solution with $g_{eff} = 4.7$. Such a complex in solution would very likely consist of oxygen ligand octahedral environment of the H_3NTA2P ligand and the two water molecules. To this end, both UV/Visible and EPR data, reflect a species with the formulation of the title complex $[Co(C_4H_9O_8NP_2)_2(H_2O)_2]^0$.

Given that soluble species beget bioavailability for selective candidates eliciting interactions at the cellular and intracellular level, the structural and molecular composition

of complex **1** projects significant features of Co(II) that might be associated with interactions with biological sites. The distinct nature of H_5NTA2P ligand represents both phosphorylated and carboxylic side chains of abutting biomolecular sites capable of interacting concurrently with Co(II), giving rise to soluble species.

3.5 LITE RATURE

1. (a) Fu, R. B.; Wu, X. T.; Hu, S.M.; Zhang, J. J.; Fu, Z. Y.; Du, W. X. *Inorg. Chem. Commun*, **2003**, 6, 827. (b) Fu, R. B.; Wu, X. T.; Hu, S. M.; Zhang, J. J.; Du, W. X.; Xia, S. Q. *Eur. J. Inorg. Chem.* **2003**, 1798.
2. Bao, S. S.; Zheng, L. M.; Liu, Y. J.; Feng, S. H. *Inorg. Chem.* **2003**, 42, 5037.
3. Turner, A.; Jaffres, P. A.; MAcLean, E. J. ; Villemin, D. ; McKee, V. ; Hix, G. B. *Dalton Trans.,* **2003**, 1314.
4. Ferguson, J.; Wood D. L.; Knox, K. *J. Chem. Phys.*, **1963**, 39, 881.
5. Lever, A. B. P. *Inorg. Chem.,* **1965**, 4, 219.
6. Lever, A. B. P.; Ogden D. *J. Chem. Soc.,* **1967**, 2041.
7. Djordjevic C.; Lee, M.; Sinn, E. *Inorg. Chem.* **1989**, *28*, 719-723. b) Deacon, G. B.; Philips, R. *J. Coord. Chem. Rev.* **1980**, *33*, 227-250.
8. Stoll, S. *Spectral Simulations in Solid-State EPR*, Ph.D. thesis, ETH Zürich, **2003**.
9. Rizzi, A. C.; Brondino, C. D.; Calvo, R.; Baggio, R.; Garland, M. T.; and Rapp, R. E. *Inorg. Chem.,* **2003**, *42*, 4409-4416.
10. Jankovics, H.; Daskalakis, M.; Raptopoulou, C. P.; Terzis, A.; Tangoulis, V.; Giapintzakis, J.; Kiss, T.; Salifoglou A. *Inorg. Chem.* **2002**, *41*, 3366-3374.
11. Matzapetakis, M. ; Dakanali, M. ; Raptopoulou, C. P.; Tangoulis, V.; Terzis, A.; Moon, N.; Giapintzakis, J.; Salifoglou, A. *J. Biol. Inorg. Chem.* **2000**, *5*, 469-474.
12. Kotsakis, N. ; Raptopoulou, C. P. ; Tangoulis, V. ; Terzis, A.; Giapintzakis, J.; Jakusch, T.; Kiss, T.; Salifoglou A. *Inorg. Chem.* **2003**, *42*, 22-31.
13. Marquez, V. E.; Anacona, J. R.; Rodriguez Barbarin, C. *Polyhedron,* **2001**, *20*, 1885-1890.
14. Cabort, A.; Michel, A.; Therrien, B.; Stoeckli-Evans, H.; Bernauer, K.; Suss-Fink, G.; Williams, A. F.; Stupka, G. *Inorg. Chim. Acta.,* **2003**, *350*, 193-200.
15. de Bruin, B.; Bill, E. ; Bothe, E. ; Weyhermuller, T.; Wieghardt, K. *Inorg. Chem.,* **2000**, *39*, 2936.
16. (a) Smith, P. H.; Raymomd, K. N. *Inorg. Chem.* **1988**, *27*, 1056-1061. (b) Sergienko, V. S.; Aleksandrov, G. G.; Afonin, E. G. *Kristallografiya* **2000**, *45*, 262-265.

– CHAPTER 4 –

AN UNUSUAL COMPLEX OF Co(II) WITH THE ORGANOPHOSPHONATE LIGAND NTA2P (N,N- BIS (PHOSPHONOMETHYL)GLYCINE)

4.1 INTRODUCTION

The significance of cobalt in human physiology has since long been recognized. Therefore, its speciation in biological fluids constitutes a theme worthy of chemical and biological perusal. The pH acts as a determining factor in the synthesis and isolation of different species of structural diversity. Synthetic efforts targeting soluble species of Co(II) with a representative metal ion binder, the organophosphonate ligand N,N-bis(phosphonomethyl) glycine at pH 5.5-6, led to the isolation of a unique and rare assembly of species. The complex was characterized analytically, structurally, spectroscopically (FT-IR, UV-Visible), and electrochemically (cyclic voltammetry).

4.2 EXPERIMENTAL

4.2.1 Material and Methods

All experiments were carried out in the open air, at room temperature. Nano-pure quality water was used for all the experiments. $Co(CH_3COO)_2 \cdot 6H_2O$, and N,N-bis(phosphonomethyl) glycine used in the synthesis of the title complex were purchased from Aldrich.. Ammonia was supplied by Fluka.

4.2.2. Synthesis

$(NH_4)_4[Co(H_2O)_6][Co\{N(CH_2COO)(CH_2PO_3)_2\}(H_2O)_2]_2[Co(H_2O)_2\{N(CH_2COO)(CH_2PO_3H)(CH_2PO_3)\}Co(NH_3)_2(H_2O)_3]_2 \cdot 10\ H_2O \cdot 1.36\ CH_3CH_2OH$ (**2**).

The complex **2** was synthesized in aqueous solution, with the initial metal to ligand stoichiometry employed being 1:1. A quantity of 0.20 g of $Co(CH_3COO)_2 \cdot 6H_2O$ (0.702mmol) and 0.21 g of N,N-bis(phosphonomethyl) glycine (0.702 mmol) were dissolved in 5.5 mL of nano-pure water. The reaction mixture was allowed to stir at room temperature overnight. Next day, the solution was clear and its color was pink. The pH of the resulting solution was raised to 5.5-6 with aqueous ammonia. The

ammonia was instrumental in two aspects: (i) it helped adjust the pH of the reaction mixture for optimal isolation of the product and (ii) it provided the necessary ligands for Co(II) and the counterions needed to balance the arisen charge. These points were subsequently proven by X-ray crystallography. Stirring continued for an additional 30 min. Isolation of the resulting product was achieved by addition of ethanol (as a precipitating agent) at 4°C. Addition of ethanol resulted in the deposition of pink crystals fifteen days later. The crystalline material was isolated by filtration, and was dried under vacuum. Yield: 0.13 g (65.7 %). Anal. Calcd for **2**, $(NH_4)_4[Co(H_2O)_2\{N(CH_2COO)(CH_2PO_3H)(CH_2PO_3)\}Co(NH_3)_2(H_2O)_3]_2[Co(H_2O)_6][Co\{N(CH_2COO)(CH_2PO_3)_2\}(H_2O)_2]_2 \cdot 10\ H_2O \cdot 1.36\ CH_3CH_2OH$ ($Co_7C_{18.72}H_{122.16}N_{12}O_{63.36}P_8$, MW = 2190.11): C, 10.26; H, 5.57. Found: C, 10.18; H, 5.89. Elemental analyses were performed by Quantitative Technologies, Inc.

The overall stoichiometric reaction leading to complex **2** is shown schematically below:

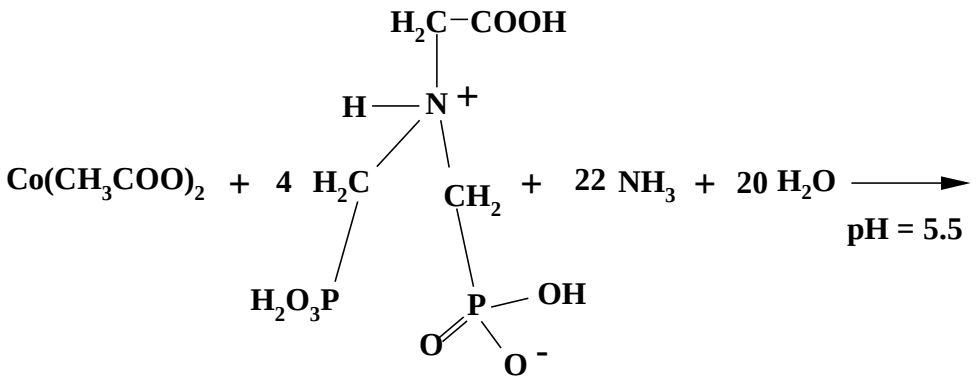

$$(NH_4)_4[Co(H_2O)_6][Co\{N(CH_2COO)(CH_2PO_3)_2\}(H_2O)_2]_2 \cdot$$

$$[Co(H_2O)_2\{N(CH_2COO)(CH_2PO_3H)(CH_2PO_3)\}Co(NH_3)_2(H_2O)_3]_2$$

$$+ \ 14\ (CH_3COO)(NH_4)$$

4.3 RESULTS

4.3.1 X-Ray Crystallographic Structure

$(NH_4)_4[Co(H_2O)_6][Co(H_2O)_2\{N(CH_2COO)(CH_2PO_3H)(CH_2PO_3)\}Co(NH_3)_2(H_2O)_3]_2$ $[Co\{N(CH_2COO)(CH_2PO_3)_2\}(H_2O)_2]_2 \cdot 10\ H_2O \cdot 1.36\ CH_3CH_2OH$ (2). The X-ray crystal structure of **2** reveals the presence of a diversely populated crystal lattice. The compound crystallizes in the triclinic system $P\bar{1}$. The ORTEP diagram of **2** is shown in Fig.1. Summary of crystal, intensity collection and refinement data for $(NH_4)_4[Co(H_2O)_6][Co(H_2O)_2\{N(CH_2COO)(CH_2PO_3H)(CH_2PO_3)\}Co(NH_3)_2(H_2O)_3]_2[Co\{N(CH_2COO)(CH_2PO_3)_2\}(H_2O)_2]_2 \cdot 10\ H_2O \cdot 1.36\ CH_3CH_2OH$ (**2**) are listed in Table 1. Selected interatomic distances and bond angles for compound **2** are listed in Table 2. The structure consists of discrete assemblies of mononuclear and dinuclear complexes of Co(II). Specifically:

1) a mononuclear core unit composed of an octahedral Co(II) ion, $[Co(H_2O)_6]^{2+}$, a known species, the structure of which had been reported in the past, often as a counterion on simple as well as complex molecular assemblies.

2) $[Co\{N(CH_2COO)(CH_2PO_3)_2\}(H_2O)_2]^{3-}$, a mononuclear species consisting of an octahedral Co(II) central metal ion. The coordination sphere of Co(II) is generated by two different types of ligands, namely, N,N-bis(phosphonomethyl) glycinate ($^{=}O_3P$-CH_2-N(CH_2COO^-)-CH_2-$PO_3^{=}$ = NTA2P^{5-}) and water. In particular, one NTA2P^{5-} ligand employs a) both phosphonate groups to coordinate to the metal ion through one of its deprotonated hydroxides, with the remaining hydroxide for each phosphonate group staying in the deprotonated form, and b) the tertiary nitrogen atom to promote further increase in the coordination number of the Co(II) ion. In addition, two water molecules are coordinated to the Co(II) ion, and with the previous NTA2P^{5--} ligand complete the equatorial plane coordination requirements of the octahedral metal ion. In view of the above description, the mononuclear Co(II) ion appears to be confound in a tetragonally distorted octahedron. Two of these mononuclear octahedral Co(II) complexes participate in the assembly of the overall lattice of **2**.

3) $[Co(H_2O)_2\{N(CH_2COO)(CH_2PO_3H)(CH_2PO_3)\}Co(NH_3)_2(H_2O)_3]^0$ is a dinuclear complex comprised of two Co(II) centers. One of the two Co(II) ions serves as a central metal ion in the component containing three water molecules and two molecules of ammonia. Thus, a mixed oxygen-nitrogen coordination sphere is

formulated with five out of six positions being occupied by these monodentate ligands. The sixth coordination opposition of the octahedral complex anion is taken up by the oxygen of one of the phosphonate groups of the adjacently located $NTAP^{4-}$ ligand attached to the second mononuclear Co(II) complex unit. In the latter mononuclear unit, also of octahedral coordination sphere, the central metal ion is bound by a) one N,N-bis(phosphonomethyl) glycinate ($^{=}O_3P\text{-}CH_2\text{-}N(CH_2COO^{-})\text{-}CH_2\text{-}PO_3H^{-}$) $HNTAP^{4-}$ ligand and b) two water molecules. Specifically, the $HNTAP^{4-}$ ligand employs the two phosphonate groups as well as the carboxylate group to bind to the metal ion through one of the oxygen of the corresponding groups. An additional position in the octahedral coordination sphere is occupied by the tertiary amine nitrogen. One of the terminal phosphonates bound to the Co(II) ion is singly deprotonated. The second phosphonate group is doubly deprotonated. It is the latter phosphonate group, the remaining oxygen terminal of which serves as a bridge to the abutting mononuclear complex described above as being part of the dinuclear assembly. Two of the dinuclear assemblies are present in the structure of compound **2**.

The Co-O distances in the equatorial plane of the octahedron are of similar length, despite the variable nature of the ligands, which utilize their oxygens as terminal anchors to Co(II). In contrast, the corresponding axial Co-O bond lengths are longer than the equatorial ones by 0.04 to 0.07 Å. Given the fact that high-spin Co(II) octahedral complexes are strongly characterized by Jahn-Teller distortions, it is very likely that here, too, such analogous distortions arise in complex **2**, and are exemplified in bond distance variations alluded to above. The Co-O distances in three species in **1** are similar to those observed in other mononuclear octahedral Co(II) sites, among which are those in $(NH_4)_4[Co(C_6H_5O_7)]_2$ (2.051(2)-2.157(2) Å) (**3**),[1] $[Co\{COOCH_2CH(OH)COO\}] \cdot 3H_2O$ (2.067(3)-2.136(3) Å) (**4**),[2] the phosphonate derivatives $[Co(NH_3CH_2PO_3)_2(H_2O)_2]$ (2.104(4)-2.121(4) Å) (**5**),[3] $[Co(HO_3PC(CH_3)(OH)PO_3H)_2(H_2O)_2]$ $[NH_2(C_2H_5)_3]_2$ (2.064(2)-2.179(2) Å) (**6**),[4] and $[Co(OPMe_3)_3(H_2O)_2]I_2 \cdot [Co(OPMe_3)_3(H_2O)_3]I_2$ (1.87(6)-2.18(4) Å) (**7**)[5] for the octahedral site).

The angles within the equatorial are in the range 87.18(1)-92.16(1) °, and hence fairly close to the ideal octahedral angle of 90°. Similar is the angle variation observed between the axial donor atoms and those in the equatorial plane (range: 86.91(9)-93.09(9) °). The aforementioned angle values are similar to those observed in (**1**)-(**5**) and the heterometal complexes $[Cu(HO_3PC(CH_3)(OH)PO_3H)_2]^{2-}$ (84.7-95.3° and 87.8-

92.2°, respectively) and $[Zn(HO_3PC(CH_3)(OH)PO_3H)_2]^{2-}$ (85.0-95.0° and 88.6-91.4°, respectively).[6]

Hydrogen bonding interactions are present in the crystal structure of **2** (Table 3 and Fig. 2). These interactions involve the coordinated water molecules, the imino nitrogen and the phosphonate oxygen and hydroxyl moieties on the $NTA2P^{5-}$ ligands. Collectively, the hydrogen bonds generate an extensive network, which likely contributes to the overall stability of the crystal lattice in **2**. The lattice water molecules are located in the pores and are also involved in hydrogen bonding.

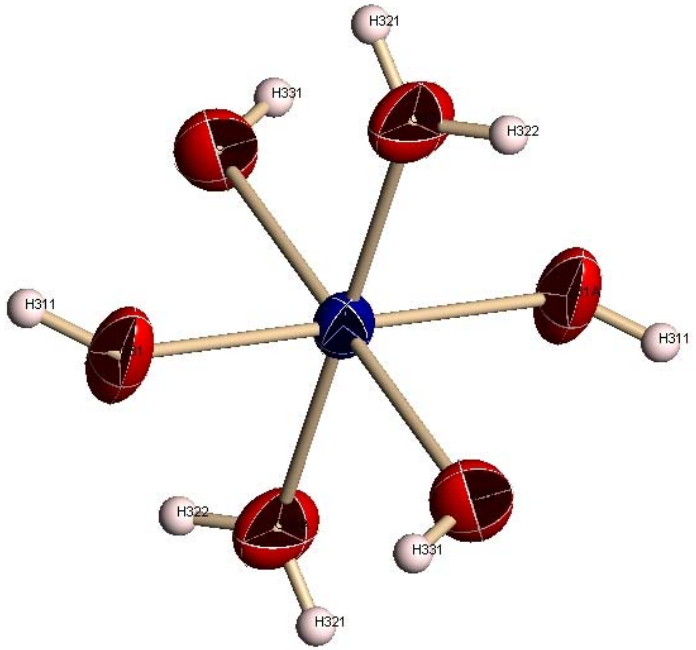

Fig.1 (a) -X-ray structure of $[Co(H_2O)_6]^{2+}$

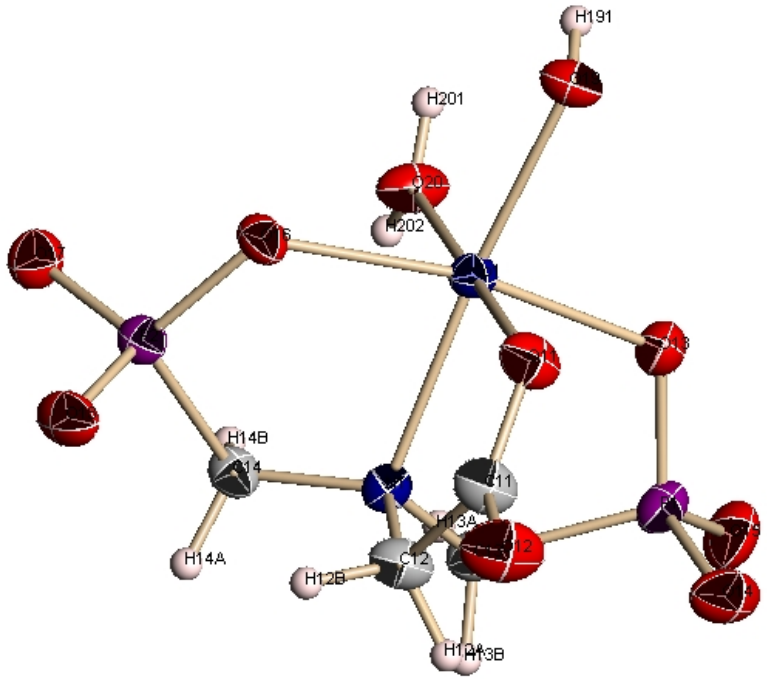

Fig.1(b) -X-ray structure of $[Co\{N(CH_2COO)(CH_2PO_3)_2\}(H_2O)_2]^{3-}$

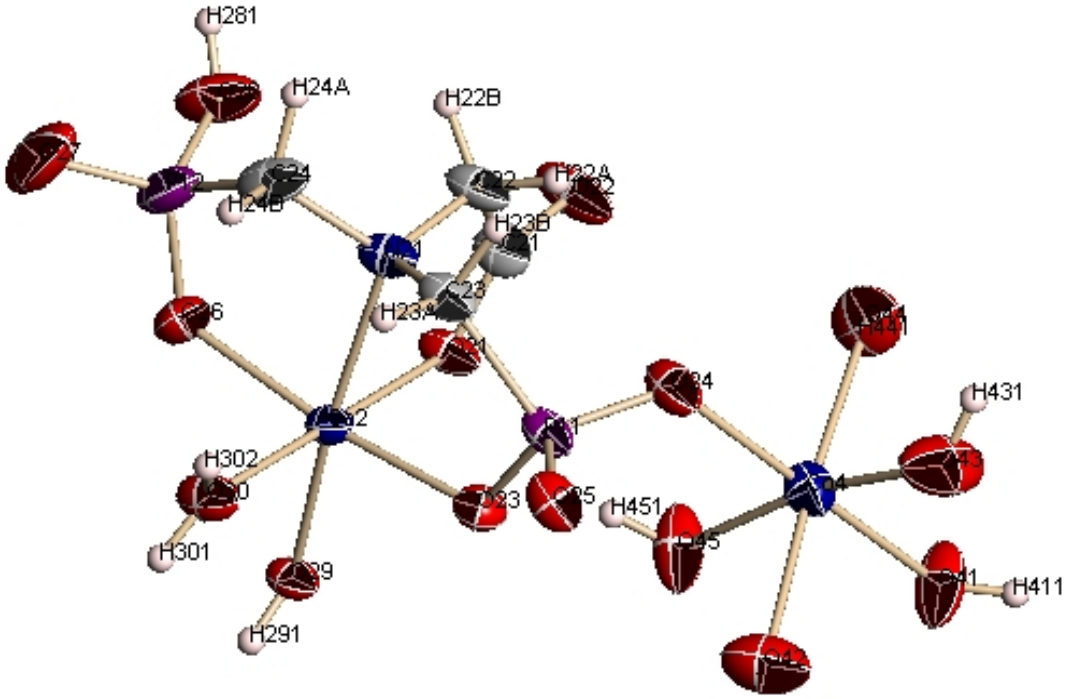

Fig.1(c) -X-ray structure of $[Co(H_2O)_2\{N(CH_2COO)(CH_2PO_3H)(CH_2PO_3)\}Co(NH_3)_2(H_2O)_3]^0$

Table 1. Summary of Crystal, Intensity Collection and Refinement Data for $(NH_4)_4[Co(H_2O)_6][Co(H_2O)_2\{N(CH_2COO)(CH_2PO_3H)(CH_2PO_3)\}Co(NH_3)_2(H_2O)_3]_2$ $[Co\{N(CH_2COO)(CH_2PO_3)_2\}(H_2O)_2]_2 \cdot 10\ H_2O \cdot 1.36\ CH_3CH_2OH$ (**2**).

Empirical formula	$C_{18.72}H_{122.16}Co_7N_{12}O_{63.36}P_8$
Formula weight	2190.11
Temperature, ˚K	300(2)
Wavelength	Mo K_α 0.71073
Space group	$P\bar{1}$
a (Å)	11.835(3)
b (Å)	12.377(3)
c (Å)	14.862(4)
α, deg	106.500(5)
β, deg	91.320(5)
γ, deg	108.001(5)
V, ($Å^3$)	1970.6(9)
Z	1
D_{calcd}/D_{measd} (Mg m^{-3})	1.845/1.85
abs. coeff. (μ), mm^{-1}	1.722
R indices [1]	$R = 0.0545$, $R_w = 0.1046$ [2]

[1] R values are based on F values, R_w values are based on F^2.

$$R = \frac{\sum \| F_o | - | F_c \|}{\sum (|F_o|)} \quad , \quad R_w = \sqrt{\sum \left[w(F_o^2 - F_c^2)^2 \right] \Big/ \sum \left[w(F_o^2)^2 \right]}$$

(2) [5226 refs I>2σ(I)]

Table 2. Bond lengths [Å] and angles [deg] in complex **2**.

Co(1)-O(11)	2.060(3)	O(11)-Co(1)-O(20)	178.78(15)
Co(1)-O(20)	2.072(3)	O(11)-Co(1)-O(19)	88.95(13)
Co(1)-O(19)	2.091(3)	O(20)-Co(1)-O(19)	90.68(13)
Co(1)-O(13)	2.091(3)	O(11)-Co(1)-O(13)	92.16(14)
Co(1)-O(16)	2.147(3)	O(20)-Co(1)-O(13)	89.01(14)
Co(1)-N(11)	2.166(4)	O(19)-Co(1)-O(13)	91.02(13)
P(1)-O(15)	1.508(4)	O(11)-Co(1)-O(16)	88.49(14)
P(1)-O(14)	1.525(4)	O(20)-Co(1)-O(16)	90.43(13)
P(1)-O(13)	1.528(3)	O(19)-Co(1)-O(16)	100.02(13)
P(1)-C(13)	1.821(5)	O(13)-Co(1)-O(16)	168.95(12)
P(2)-O(18)	1.513(3)	O(11)-Co(1)-N(11)	83.00(13)
P(2)-O(17)	1.520(4)	O(20)-Co(1)-N(11)	97.41(13)
P(2)-O(16)	1.541(3)	O(19)-Co(1)-N(11)	171.68(13)
P(2)-C(14)	1.832(5)	O(13)-Co(1)-N(11)	87.18(14)
O(11)-C(11)	1.264(6)	O(16)-Co(1)-N(11)	81.95(13)
O(12)-C(11)	1.248(5)	O(26)-Co(2)-O(23)	170.67(15)
N(11)-C(12)	1.481(6)	O(26)-Co(2)-O(29)	94.53(15)
N(11)-C(13)	1.485(6)	O(23)-Co(2)-O(29)	94.72(13)
N(11)-C(14)	1.495(6)	O(26)-Co(2)-O(21)	91.81(15)
C(11)-C(12)	1.535(6)	O(23)-Co(2)-O(21)	89.27(14)
Co(2)-O(26)	2.073(4)	O(29)-Co(2)-O(21)	90.80(13)
Co(2)-O(23)	2.074(4)	O(26)-Co(2)-O(30)	88.35(15)
Co(2)-O(29)	2.084(3)	O(23)-Co(2)-O(30)	90.43(14)
Co(2)-O(21)	2.085(3)	O(29)-Co(2)-O(30)	90.04(14)
Co(2)-O(30)	2.117(3)	O(21)-Co(2)-O(30)	179.13(15)
Co(2)-N(21)	2.193(4)	O(26)-Co(2)-N(21)	86.10(17)
P(11)-O(25)	1.509(4)	O(23)-Co(2)-N(21)	84.92(15)
P(11)-O(24)	1.524(4)	O(29)-Co(2)-N(21)	171.57(14)
P(11)-O(23)	1.536(4)	O(21)-Co(2)-N(21)	80.78(14)
P(11)-C(23)	1.828(5)	O(30)-Co(2)-N(21)	98.38(14)
P(12)-O(27)	1.494(5)	O(31)′-Co(3)-O(32)	92.13(18)
P(12)-O(26)	1.515(4)	O(31)-Co(3)-O(32)	7.87(18)
P(12)-O(28)	1.565(4)	O(31)′-Co(3)-O(33)	91.10(16)
P(12)-C(24)	1.803(7)	O(31)-Co(3)-O(33)	88.90(16)
O(21)-C(21)	1.261(6)	O(32)-Co(3)-O(33)	88.30(15)
O(22)-C(21)	1.245(6)	O(32)′-Co(3)-O(33)	91.70(15)
O(24)-Co(4)	2.066(4)	O(43)-Co(4)-O(24)	94.85(17)
N(21)-C(24)	1.486(7)	O(43)-Co(4)-O(41)	89.42(18)
N(21)-C(23)	1.487(7)	O(24)-Co(4)-O(41)	174.32(16)
N(21)-C(22)	1.496(6)	O(43)-Co(4)-O(45)	169.80(18)
C(21)-C(22)	1.530(7)	O(24)-Co(4)-O(45)	89.54(15)
Co(3)-O(31)	2.049(4)	O(41)-Co(4)-O(45)	86.85(16)
Co(3)-O(32)	2.085(4)	O(43)-Co(4)-N(44)	91.51(19)
Co(3)-O(33)	2.129(4)	O(24)-Co(4)-N(44)	88.91(16)
Co(4)-O(43)	2.063(4)	O(41)-Co(4)-N(44)	87.24(18)
Co(4)-O(41)	2.074(4)	O(45)-Co(4)-N(44)	97.79(19)
Co(4)-O(45)	2.080(4)	O(43)-Co(4)-N(42)	85.76(19)
Co(4)-N(44)	2.128(4)	O(24)-Co(4)-N(42)	94.77(17)
Co(4)-N(42)	2.162(4)	O(41)-Co(4)-N(42)	89.27(19)
O(81)-C(81)	1.47(15)	O(45)-Co(4)-N(42)	84.70(19)
C(81)-C(82)	1.55(18)	N(44)-Co(4)-N(42)	175.59(19)
O(71)-C(71)	1.44(20)		
C(71)-C(72)	1.56(30)		

Table 3. Hydrogen bonds in complex **2.**

D-H(Å)	H...A(Å)	D...A(Å)	<(DHA) (deg)	Interaction
0.80	1.90	2.678(5)	164.5	O19-H191...O17_$1
0.80	1.92	2.718(5)	171.1	O19-H192...O21
0.82	1.97	2.779(4)	165.8	O20-H201...O16_$1
0.81	1.89	2.695(5)	172.9	O20-H202...O22_$1
0.84	1.65	2.468(5)	162.8	O28-H28...O14_$2
0.82	1.90	2.693(5)	163.9	O29-H291...O25_$3
0.83	1.97	2.749(4)	156.6	O29-H292...O11
0.83	2.06	2.688(5)	132.4	O30-H301...O23_$3
0.82	2.00	2.800(5)	166.8	O30-H302...O12_$3
0.80	1.87	2.612(5)	153.8	O31-H311...O14
0.82	1.89	2.686(5)	164.8	O31-H312...O25_$3
0.82	1.90	2.721(5)	175.1	O32-H321...O91_$4
0.82	1.80	2.617(6)	171.0	O32-H322...O27_$5
0.81	2.12	2.862(6)	151.1	O33-H331...O25_$3
0.82	2.12	2.920(5)	166.5	O41-H411...O18_$7
0.82	1.92	2.698(5)	157.0	O41-H412...O18
0.81	1.84	2.648(6)	173.4	O43-H431...O15_$8
0.82	2.12	2.855(7)	149.8	O43-H432...N97_$9
0.89	2.25	2.992(7)	140.5	N44-H44A...O94_$3
0.89	2.07	2.864(6)	147.6	N44-H44C...O92_$1
0.84	1.99	2.727(5)	145.2	O45-H452...O16
0.83	2.08	2.874(5)	159.0	O91-H911...O15_$8
0.78	2.01	2.785(5)	171.8	O91-H912...O24
0.82	2.07	2.870(5)	164.8	O92-H921...O17_$1
0.83	2.13	2.809(5)	139.3	O92-H922...O13
0.84	1.92	2.751(7)	173.4	O93-H931...O26
0.85	1.92	2.771(6)	179.2	O94-H941...O15_$11
0.82	1.97	2.770(7)	163.5	O94-H942...O22_$3
0.88	2.14	2.879(6)	140.4	O95-H951...O18
0.84	2.01	2.829(6)	166.8	O95-H952...O92_$10
0.90	2.06	2.675(6)	124.9	N97-H973...O17_$11

$1 -x+1, -y+1, -z ; *$2* x-1, y, z ; *$3* -x+1, -y+1, -z+1 ; *$4* x+1, y+1, z
$5 -x+1, -y+2, -z+1 ; *$6* -x+2, -y+2, -z+1 ; *$7* -x+1, -y, -z ; *$8* x-1, y-1, z ;
$9 -x+1, -y, -z+1; $10 x, y-1, z ; *$11* x, y, z+1

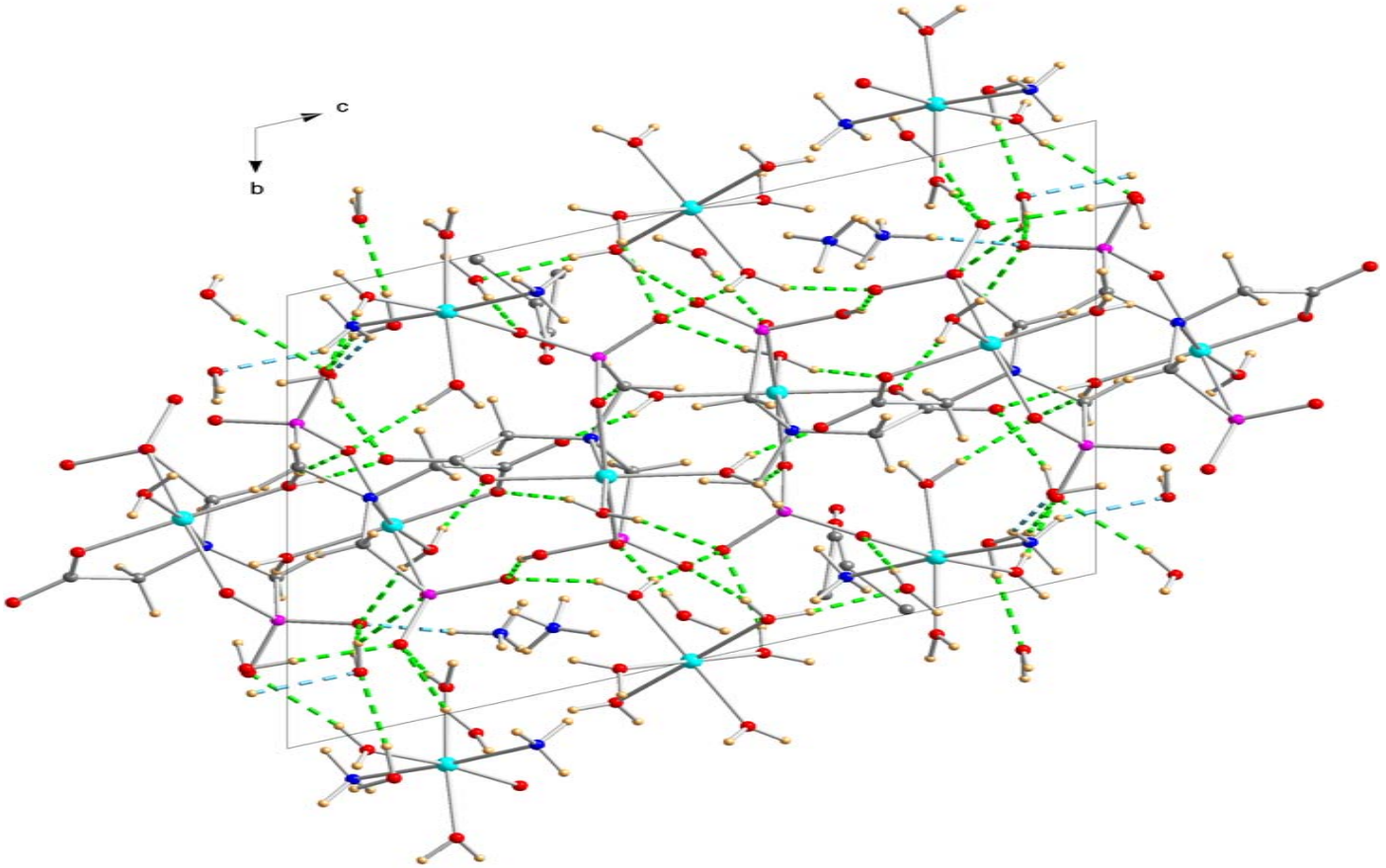

Fig. 2 Hydrogen bonding interactions in the crystal structure of **2.** The view of the structure is down the crystallographic *a* axis.

4.3.2 Electronic spectroscopy

UV/Visible spectra of the crystals were recorded on a Hitachi U-2001 spectrophotometer in the 200-1000 nm range. The UV-Visible spectrum of **2** was recorded in water and is depicted in Fig. 3 and Fig. 4. The spectrum exhibits two major peaks at λ_{max} = 551, and λ_{max} = 525, a subtly discernible shoulder around 478 and a distant shoulder around 228 nm. The absorption features are most likely d-d transitions in origin, typical for a Co(II) d^7 octahedral species. The multiple structured band around 500 nm arises from a number of causes, but primarily to admixture of spin forbidden transitions to doublet states mainly derived from ^2G and ^2H and may also be due to spin-orbit coupling.[7] It is very difficult to attribute the observed electronic features to any one of the species described in the overall assembly of compound **2**. Undoubtedly, however, the individual contributions of the components in **2** are reflected in the overall spectrum. More synthetic experimental work is obviously needed to isolated the discrete species present in **2** and delineate their individual electronic signature in the UV/Visible.

2

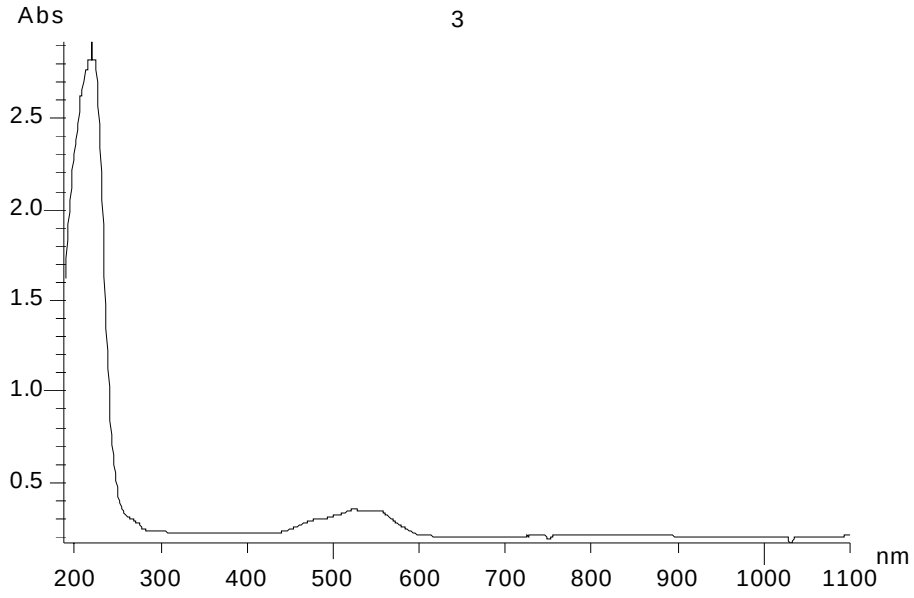

Fig. 3 UV/Visible spectrum of complex **2**, at the concentration c = 1.97mM, in the range 200-1100 nm.

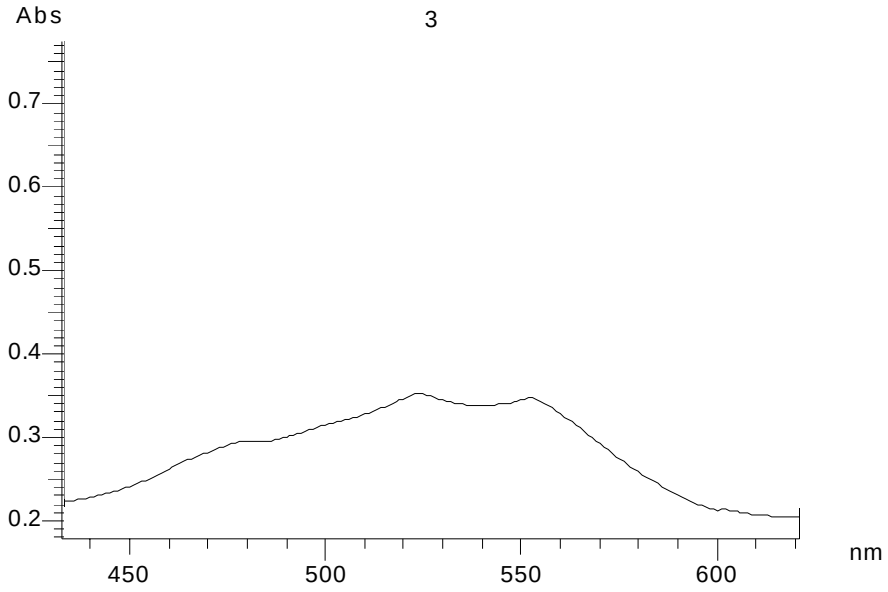

Fig. 4 UV/Visible spectrum of complex **2**, at the concentration c = 1.97mM, in the range 400-600 nm.

4.3.3 FT-IR spectroscopy.

FT-infrared measurements were taken on a Perkin-Elmer 1760X FT-IR spectrometer. The FT-infrared spectrum of **2** is depictated in Fig. 5. The FT-infrared spectrum of compound (**2**) in KBr, exhibits strong absorptions for the various vibrationally active groups. Specifically, absorptions for the PO_3 groups are observed for the antisymmetric stretching vibrations $\nu_{as}(PO_3)$ between 1105 and 980 cm^{-1}. A symmetric stretching vibration $\nu_s(PO_3)$ is observed in the range 980 - 920 cm^{-1}. The observed PO_3 groups vibrations appear to be shifted to lower frequency values in comparation to the corresponding vibrations in free N,N-bis(phosphonomethyl) glycine acid, thus indicating changes in the vibrational status of the ligand upon coordination to the Co(II) ion(Fig. 5).[8,9] The antisymmetric stretching vibration $\nu_{as}(COO^-)$ is present for the carboxylate group in the range 1685-1648 cm^{-1}. Symmetric vibration $\nu_s(COO^-)$ for the same group are present the range 1385-1338. The observed COO groups vibrations appear to be shifted to lower frequency values in comparation to the corresponding vibrations in free N,N-bis(phosphonomethyl) glycine acid. The broad absorption at 3000 cm^{-1} is due to the O-H stretching vibration of the hydration water molecule. The above described tentative assignments are, also, in agreement with previous results reported for iminophosphonate containing complexes of various metals.[10]

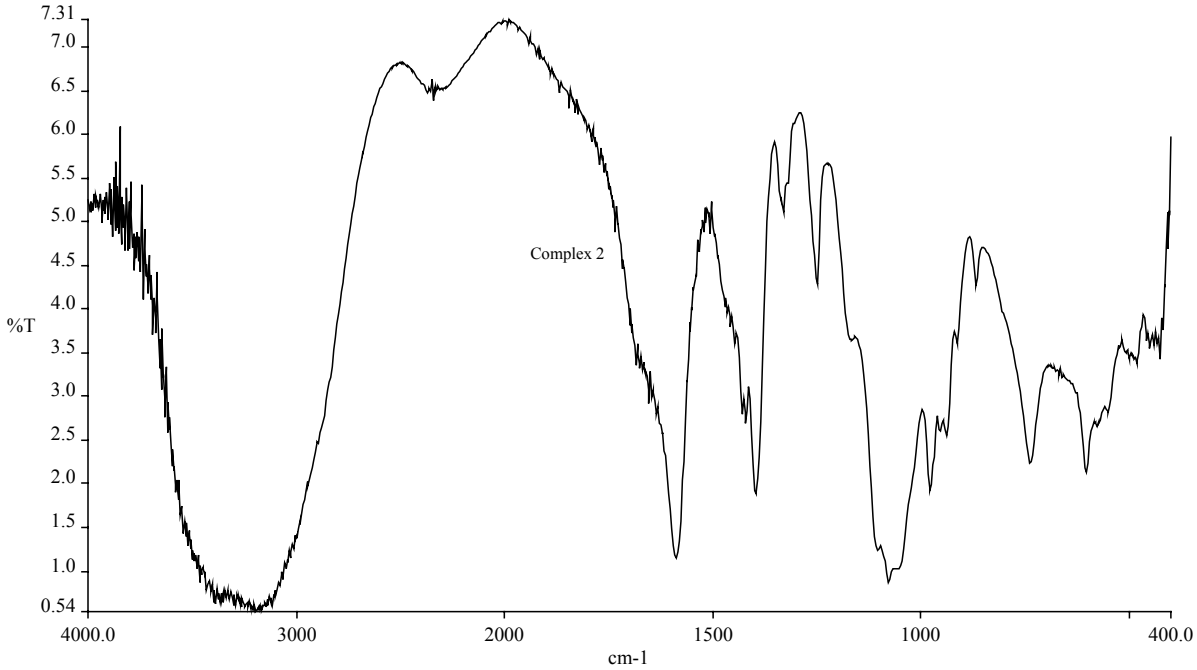

Fig. 5 The FT-infrared spectrum of $(NH_4)_4[Co(H_2O)_6][Co(H_2O)_2\{N(CH_2COO)(CH_2PO_3H)(CH_2PO_3)\}\ Co(NH_3)_2(H_2O)_3]_2$ $[Co\{N(CH_2COO)(CH_2PO_3)_2\}(H_2O)_2]_2 \cdot 10\ H_2O \cdot 1.36\ CH_3CH_2OH$ **(2).**

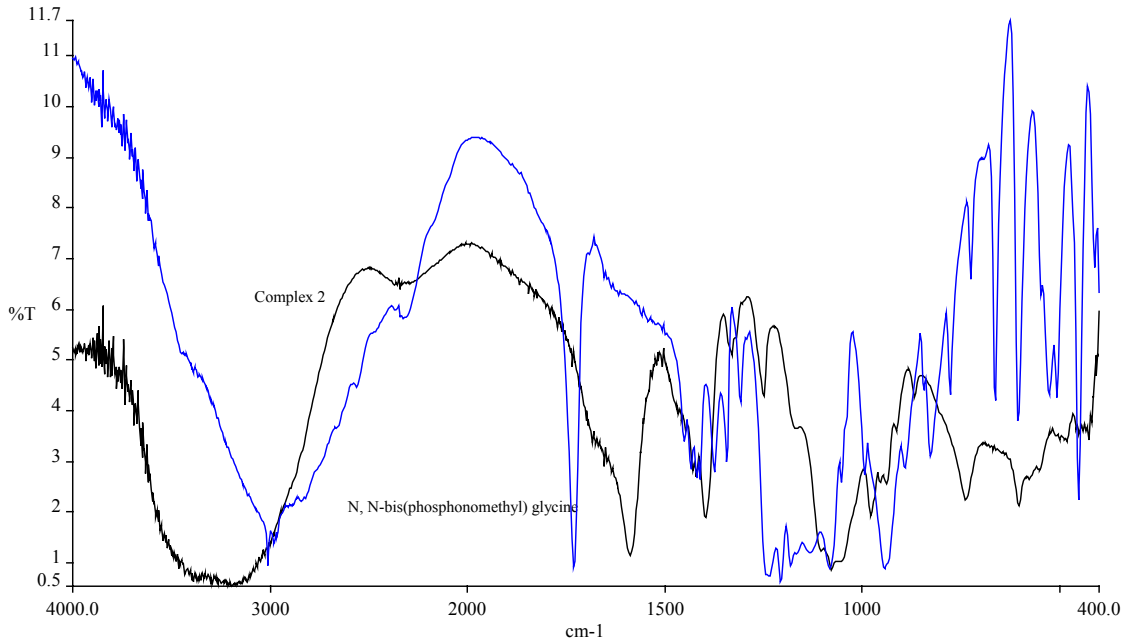

Fig. 6 Comparison between the FT- infrared spectra of compound **2** and N,N-bis(phosphonomethyl) glycine.

3.4 Cyclic Voltammetry

All electrochemical experiments were performed at 25°C using a three-electrode potentiostatic system. The potentials are reported with reference to a Ag/AgCl electrode placed in the same compartment containing the supporting electrode. The aqueous electrolyte solutions were rigorously deoxygenated with argon.

The cyclic voltammogram of complex **2** at scan rate 0.1 $V \cdot s^{-1}$ is shown in Fig. 7. The E_{pa} and i_{pa} were determined from the cyclic voltammograms at different scan rates (0.5, 0.2, 0,1, 0.05 V/sec). The studied system is an irreversible process. This is based on the following observations: the ratio of the cathodic-to-anodic peak currents i_{pc}/i_{pa} is zero, E_{pa} shifts with scan rate toward more positive potential, and the current function defined as (peak current)/(scan rate)$^{1/2}$(concentration) changes with scan rate. An oxidation wave detected at Ea = 0.978 V corresponds to the Co^{II}-Co^{III} couple.

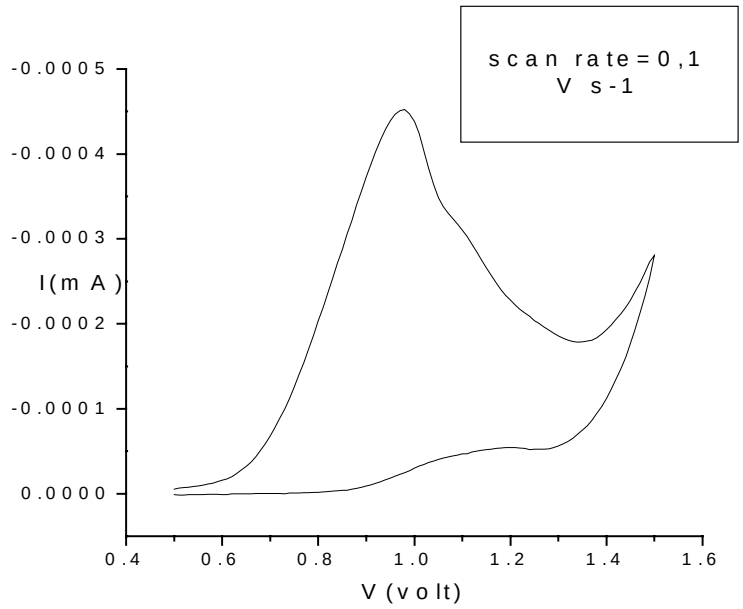

Fig. 7 Cyclic voltammogram (scan rate 0.1 V s^{-1}) of 1.8 M solution of complex **2** in water with KNO_3 as the supporting electrolyte.

4.4 DISCUSSION

Facile aqueous reactions of Co(II) ion with N,N,-bis(phosphonomethyl) glycine acid, at pH ≈ 5.5, with a metal to ligand stoichiometry of 1 : 1 led to the isolation of complex **2**. The latter complex reveals basic structural attributes of aqueous mononuclear Co(II) sites in low molecular mass species of potential biological relevance. Complex **2** is an unusual and unique assembly of species, with its structure consisting of discrete assemblies of mononuclear and dinuclear complexes of Co(II). Two factors appeared to play a role in the isolation of the final product: (a) the pH of the aqueous solution, in which the reaction was run. pH specificity allowed the product to be synthesized and isolated (b) the employment of aqueous ammonia in the adjustment of pH. Raising the pH with the aid of alkali such as KOH and NaOH, in aqueous solution, resulted in precipitates of noncrystaline nature. The synthesis and isolation of **2** in a reproducible fashion constitutes a major advancement in the relevant chemistry of Co(II) with phosphonates.

The crystallographic data support an octahedral coordination sphere for the two mononuclear complexes and the dinuclear complex of Co(II), which are present in the crystal lattice of complex **2**. The latter assertion was confirmed by the FT-IR data on complex **2**.

The octahedral coordination sphere of Co(II) is generated by different ligands in the complexes, which are present in the crystal lattice, specifically: (a) water in the case of $[Co(H_2O)_6]^{2}$; (b) N,N-bis(phosphonomethyl) glycinate and two water molecules in the case of $[Co\{N(CH_2COO)(CH_2PO_3)_2\}(H_2O)_2]^{-3}$; (c) in the case of the dinuclear specie, N,N-bis(phosphonomethyl) glycinate and two water molecules coordinate to one Co(II) center, the other Co(II) has five out of six positions being occupied by three water and two ammonia molecules. The sixth coordination of the complex anion is taken up by the oxygen of one of the phosphonate groups of the adjacently located $NTAP^{4-}$ ligand attached to the second mononuclear Co(II) complex unit. Variable modes of phoshonate coordination were previously observed in metal organophosphonate complexes containing the phosphonate ligand terminals in varying deprotonation states.[11] In solution the retention of the octahedral coordination environment in what has been suggested by the spectroscopic data, substantiates the contention that the particular metal ion could interact with phosphonate containing ligands in an aqueous solution. It

remains to be seen whether species of the herein proposed nature or similar to it represent bioavailable forms of Co(II), which can elicit interactions at the cellular level.

4.5 LITERATURE

1. Matzapetakis, M.; Dakanali, M.; Raptopoulou, C. P. ; Tangoulis, V. ; Terzis, A.; Moon, N. ; Giapintzakis, J. ; Salifoglou, A. *J. Biol. Inorg. Chem.* **2000**, *5*, 469-474.
2. Kryger, L.; Rasmussen, S. E.; *Acta Chem. Scand.* **1972**, *26*, 2349-2359.
3. Glowiak, T.; Sawka-Dobrowolska, W.; Jezowska-Trzebiatowska, B. *Inorg. Chim. Acta,* **1980**, *45*, L105-L106.
4. Sergienko, V. S. ; Aleksandrov, G. G.; Afonin, E. G. *Zh. Neorg. Khim.* **1997**,*42*, 1291-1296.
5. Godfrey, S. M.; Kelly, D.G.; McAuliffe, C. A.; Pritchard, R.G. *J. Chem. Soc., Dalton Trans.,* **1995**, 1095-1101.
6. Sergienko, V. S.; Afonin, E. G.; Aleksandrov, G. G. *Zh. Neorg. Khim.***1998**, *43*,1002-1007.
7. Lever A. B. In: *Inorganic Electronic Spectroscopy*; 2nd Edition. Elsevier: Amsterdam, **1984**, pp. 480-485.
8. (a) Corbridge, D. E. C. *J. Appl. Chem.* **1956**, *6*, 456-465.
   (b) Gore, R. C. *Discuss. Faraday Soc.* **1950**, *9*, 138-143.
   (c) Bell, J. V.; Heisler, J.; Tannenbaum, H.; Goldenson, J. *J. Am. Chem. Soc.* **1954**, *76*, 5185- 5189.
   (d) Thomas, L. C.; Chittenden, R. A.; *Spectrochim. Acta* **1964**, *20*, 467-487.
9. (a) McIvor, R. A.; Hubley, C. E. *Can. J. Chem.* **1959**, *37*, 869-876.
   (b) Thomas, L. C.; Chittenden, R. A *Chem. Ind. (London)* **1961**, 1913.
10. (a) Sagatys, D. S.; Dahlgren, C.; Smith, G.; Bott, R. C.; Willis, A. C. *Aust. J. Chem.* **2000**, *53*, 77-81.
    (b) Shoval, S.; Yariv, S. *Agrochimica* **1981**, *25*, 377-386.
    (c) Subramanian, V.; Hoggard, P. E. *J. Agric. Food Chem.* **1988**, *36*, 1326-1329.
11. (a) Sergienko, V. S.; Aleksandrov, G. G.; Afonin, E. G.; *Kristallografiya*, **2000**, *45*, 262- 256.
    (b) Smith, P.H.; Raymond, K. N. *Inorg. Chem.*, **1988**, *27*, 1056-1061.
    (c) Fenot, P.; Darriet, J.; Garrigou-Lagrange, C. J. *Mol. Struct.* **1978**, *43*, 49-60.

5. POTENTIOMETRIC AND SPECTROPHOTOMETRIC MEASUREMENTS OF CO(II) WITH NTA AND ITS PHOSPHONIC DERIVATIVES

5.1 INTRODUCTION

The metal binding capacity of nitrilotriacetic acid (NTA) and its phosphonic derivatives has been widely studied both with divalent and trivalent metal ions.[1-7] The complex formation of N-phosphonomethyliminodiacetic acid (NTAP) was first reported as early as 1949 by Schwarzenbach *et al*., concurrently with those of aminopolycarboxylates (APCs).[8] Several studies on the complex formation of such N-bonded mixed acetic-methylphosphonic acids have been reported.[9-12] The values of the protonation constants for NTAP do not vary much in these reports. However, those of NTA2P show large disparities because of the very high value of the first protonation constant.

The N-(phosphonomethyl)-iminodiacetic acid (NTAP), N,N-bis(phosphonomethyl)glycine (NTA2P) and nitrilo-tris(methylphosphonic acid) (NTA3P) ligands differ from nitrilotriacetic acid (NTA) in the stepwise replacement of carboxylic by phosphonic groups.

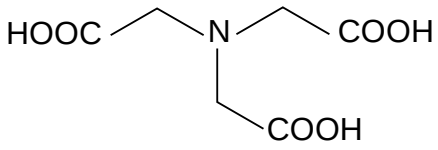

NTA

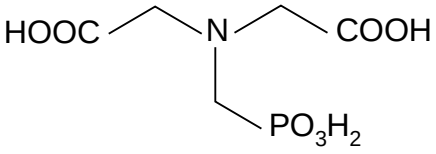

NTAP

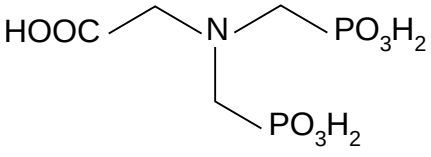

NTA2P

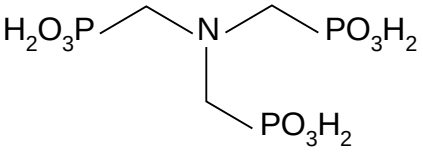

NTA3P

5.2 COMPUTER PROGRAMS AND POTENTIOMETRY

5.2.1 PSEQUAD computer program

PSEQUAD is a comprehensive program for the evaluation of **P**otentiometric and/or **S**pectrophotometric **EQ**uilibrium data **U**sing **A**nalytical **D**erivatives. Potentiometry and spectrophotometry are the most popular experimental techniques for equilibrium studies.[13] This program can handle both types of experimental data either separately or simultaneously.

The program is written in standard FORTRAN 66 language. Therefore, the input/output processes are exclusively based on the "field" conception of the FORTRAN's FORMAT command. The field conception stipulates that each individual input datum must have an exact position and length in the input file. The equilibrium system can be described through the mass-balance equations as shown below:

$$C_t = \sum_{j=1}^{n} \alpha_{jt} \cdot [S_j] = \sum_{j=1}^{n} \alpha_{jt} \cdot \beta_j \cdot \prod_{i=1}^{k} [c_i]^{\alpha_{ji}} \qquad (t = 1 \ldots k) \quad (1)$$

where:

Ct - the total concentration of the *t*th component,

n - the number of species in the system, including the components,

Sj - the *j*th species present in the system,

k - the number of components in the system,

c_i - the equilibrium (free) concentration of the *i*th component,

β_j- is the formation constant of the *j*th species,

α_{ji} - are the stoichiometric numbers, giving the number of the *i*th component in the *j*th species. α_{ji} is called the composition matrix .

The stoichiometric numbers are arranged in k columns and n rows, forming the composition or α matrix of the system.

There are two main steps in the calculations:

1. the solution of Eq. (1) for the unknown free concentrations. The calculation of the unknown free concentration is based on the standard Newton-Raphson procedure. The iteration terminates when:

$$\left|\frac{C_i^{exp} - C_i^{calc}}{C_i^{exp}}\right| \leq 5 \cdot 10^{-4} \quad (2)$$

for all of the concentrations.

2. refinement of the formation constants and/or molar absorptivities.

The program additionally lists:

-The back-calculated data and the deviation between the measured and calculated data (residuals).

- The program gives a complete output, including the concentration distribution of each species.

-The program provides only the concentration distribution in the output besides the calculated parameters.

5.2.2 HySS computer program

HySS (**Hy**perquad **S**imulation and **S**peciation) is a computer program written for the Windows Operating System on personal computers which provides[14]:

- a system for simulating titration curves
- a system for providing speciation diagrams.

For equilibria in solution, which are considered as generalized acid–base equilibria, it is usual to measure the equilibrium constants for the individual reactions and to calculate the species concentrations by solving the mass-balance equations.

At the center of any calculation, the concentrations of the free reagents, [*A*], [*B*] etc., are determined by solving the mass-balance equations:

$$T_A = [A] + \sum_i a_i \beta_i [A]^{a_i} [B]^{b_i} \ldots + \sum_j p_j C_j \quad (3)$$

$$T_B = [B] + \sum_i a_i \beta_i [A]^{a_i} [B]^{b_i} \ldots + \sum_j q_j C_j \quad (4)$$

where

A, *B*, etc. are reagents

a, *b*,… *p*, *q*, etc. are stoichiometric indices

b represents equilibrium constants and

the quantities *C* represent molar concentrations of insoluble species (quantity of solid divided by the volume of the solution) if any are present.

Associated with each insoluble species is a solubility product:

$$K_j = [A]^{p_j} \cdot [B]^{q_j} .... \quad (5)$$

Initially it is assumed that there is no precipitate present and the free concentrations are calculated with the C terms omitted from the mass-balance equations. If there is a possibility for formation of a precipitate, the concentration product is compared with the corresponding *Kj*. If the concentration product is larger than the corresponding *Kj*, not only is the *C* term included, but an additional equation is also added to the set:[15]

$$\ln K_j = p_j \cdot \ln[A] + q_j \cdot \ln[B] + ... \quad (6)$$

and the free concentrations are recalculated. When a solid is present, the set of mass-balance and solubility equations is solved, according to the Newton–Raphson method, by iteratively solving the set of linear equations obtained from the partial derivates of the mass and solubility equations.

There are no limits imposed on the number of reagents, complexes or partially soluble products that may be present. Three types of calculations may be performed:

- simulation of a titration curve
- calculation of species concentrations in a range of conditions
- speciation for a single set of conditions (single data points).

The main novelty in HySS is the complete flexibility with which the conditions may be specified for speciation calculations. All of the speciation diagrams presented in this work were performed with the aid of the HySS computer program.

5.3 DETERMINATION OF THE PROTONATION CONSTANTS OF THE LIGANDS

5.3 1. EXPERIMENTAL PART

Reagents and methods

All experiments were carried out in the open air, at room temperature. All the ligands used in the experiments were Aldrich products of puriss quality and were used without further purification. KOH was also purchased from Aldrich. Nano-pure quality water was used for all the experiments.

Potentiometric measurements of the ligands were performed with a Metrohm 713 pH meter equipped with a Metrohm 6.0234.100 combined glass electrode, which was calibrated for hydrogen ion concentration according to Irving.[16] A pK_w ($pK_w = - \lg[H^+] \cdot [OH^-]$) value of 13.76 was determined through a strong acid strong base titration. The protonation constants of the studied ligands were calculated with the aid of the SUPERQUAD computer program. The protonation constants were determined by pH-metric titrations of a 25 mL sample. The titrations were performed from pH 2.0 up to pH 12, with a carbonate free KOH solution of known concentration (*ca* 0.2 $mol \cdot dm^{-3}$) under a purified argon atmosphere. During the titrations, the temperature was maintained at 25 ± 0.1^oC. The ionic strength was adjusted with KCl to 0.2 $mol \cdot dm^{-3}$. The summary of the titration data used to calculate the protonation constants is presented in Table 1.

Table 1. Summary of the titration data used for the calculation of the protonation constants[a]

System	C_A (mol·dm^3)	pH domain	n
Proton-NTA	0.0040	2.0880-11.727	61
	0.0020	2.0980-11.703	56
	0.0040	2.0850-11.690	61
	0.0048	2.0150-11.685	63
Proton-NTAP	0.0020	2.297-11.678	66
	0.0040	2.046-11.680	79
	0.0048	2.023-11.651	82
Proton-NTA2P	0.0040	2.007-11.658	81
	0.0020	2.289-11.664	72
	0.0040	2.004-11.640	81
	0.0096	1.883-11.645	91
Proton-NTA3P	0.0040	2.121-11.639	85
	0.0020	2.412-11.665	77
	0.0096	1.756-11.694	98

[a] The initial concentrations are expressed in mmol·dm^{-3}; *n* represents the number of experimental observations in each titration.

5.3.2 RESULTS AND DISCUSSIONS

The results of the pH-metric titration of the ligands are shown in Fig. 1. The mean number of protons bound to the ligand ($\bar{n}$) (Fig. 2), is obtained from the pH using the equation:

$$\bar{n}_{obs} = \frac{\left(rc_A - c_{OH} - [H^+] + [OH^-]\right)}{c_A} \quad (1)$$

where c_{OH} and c_L are the total concentrations of the KOH titrated and ligand H_rA, respectively. The calculated values of the mean number of protons bound to the ligand, ($\bar{n}_{calc}$) are given by Eq. 2, using the protonation constants of the ligand, $K_n=[H_nA]/[H^+][H_{n-1}A]$, where $\beta_n = \prod K_n$.[17]

$$\bar{n}_{calc} = \sum n[H_nA]/c_A = \sum n\beta_n[H^+]^n /(1 + \sum \beta_n[H^+]^n) \quad (2)$$

A set of K_n giving the minimum sum of the squares of the deviations [$=\sum(\bar{n}_{obs} - \bar{n}_{calc})^2$] was obtained by a non-linear regression analysis, with the aid of the SUPERQUAD computer program.

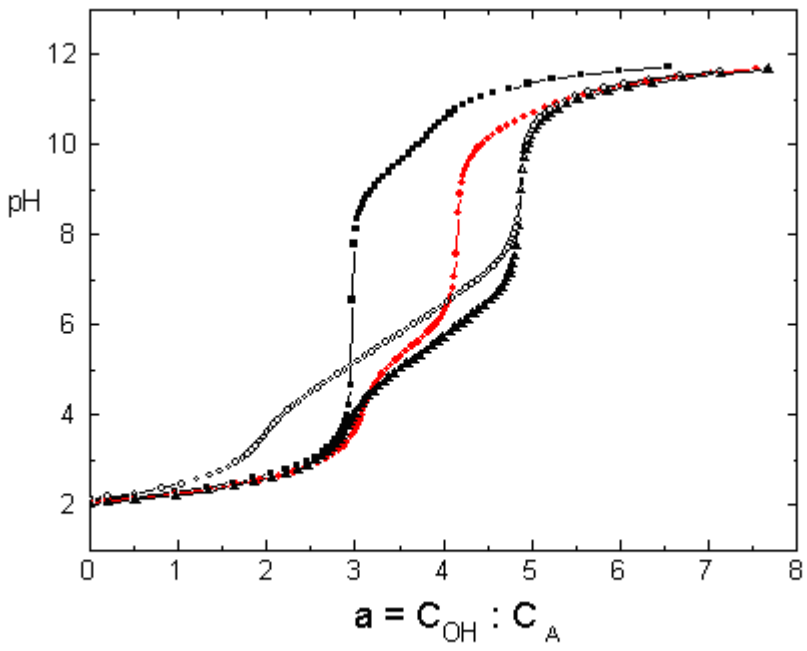

Fig. 1 pH titration curves of NTA (solid squares), NTAP (solid circles), NTA2P (solid down triangles) and NTA3P (open circles) at 25°C, ionic strength I = 0.2M (KCl).

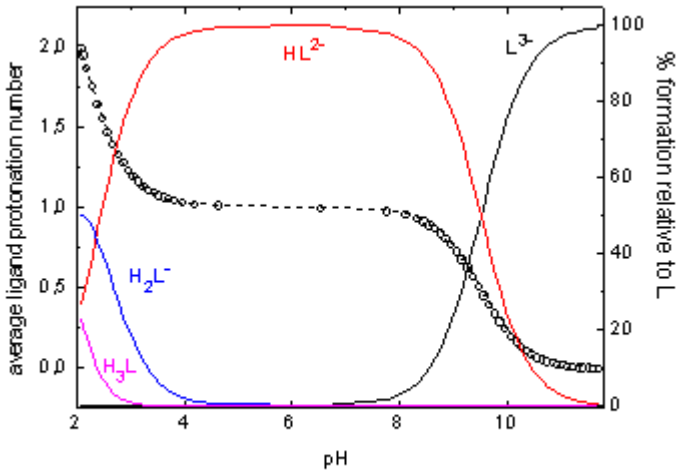
average ligand protonation number
% formation relative to L
pH
HL2-
L3-
H2L-
H3L

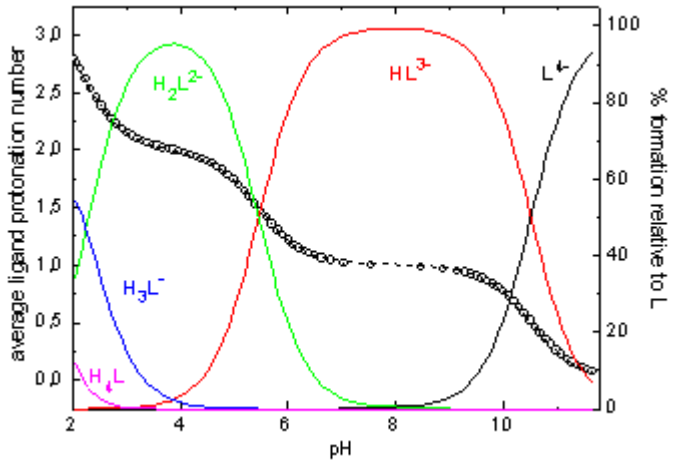
average ligand protonation number
% formation relative to L
pH
H2L2-
HL3-
L4-
H3L-
H4L

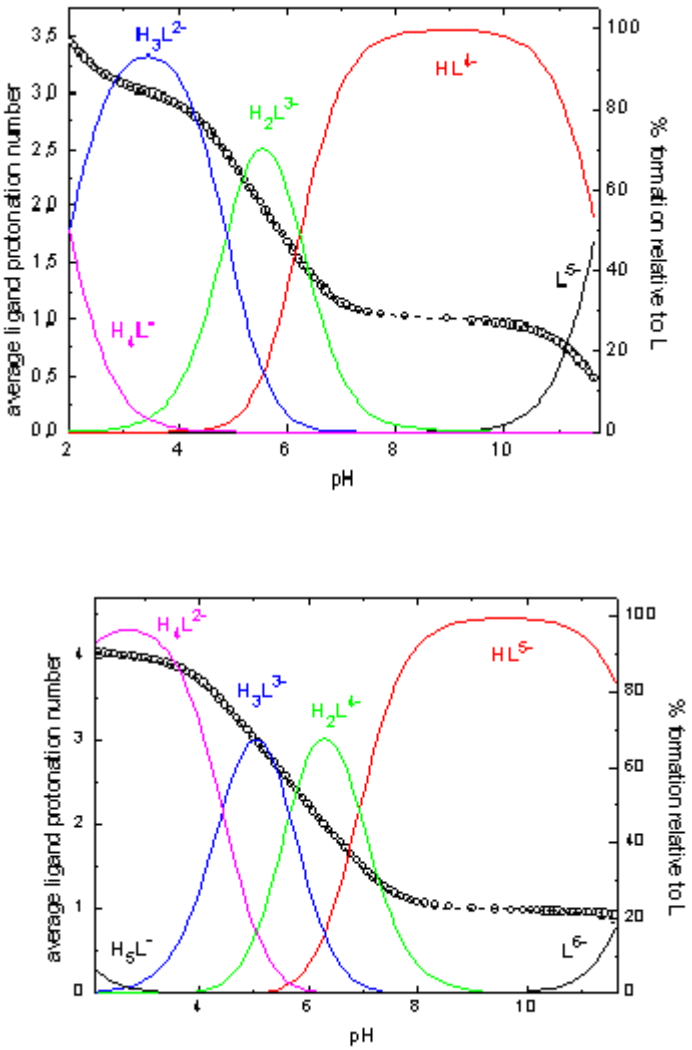

Fig. 2 Speciation curves of the ligands (NTA - C_L = 0.003714M; NTAP - C_L = 0.0042428 M; NTA2P - C_L = 0.0038884 M; NTA3P - C_L = 0.00391 M), experimental curve (open circle), calculated curve (dotted line).

A very good agreement between the experimental curve and the calculated curve (Fig. 2), proves that for all systems involved, the values calculated for the global protonation constants with the aid of the SUPERQUAD computer program are correct.

The protonation constants of nitrilotriacetic acid and its phosphonic derivatives are presented in Table 2. The protonation constants listed in Table 2 are in reasonable good agreement with those in earlier reports.[18-24]

The results indicate that the first protonation occurs on the nitrogen atom. The ensuing protonations take place on the oxygen atoms of the phosphonate groups and are followed by protonation of the carboxylate groups. The most basic donor of all the ligands is the tertiary amino group, with pK values of 9.51, 10.52, 11.71 and 12.30 (see Table 2). The next most basic groups are the phosphonates (PO_3H^-), which deprotonate in the pH range of 4.5-7.2. The carboxylic functions (COOH) are deprotonated in the pH range 1.38 - 2.36. The remaining PO_3H_2 groups are very weakly basic. The corresponding log *K* values are around or less than 1 and can be determined by pH potentiometry, only with rather high uncertainties (a value of 1.23 has been reported in the past).[4] The basicity increases with increasing number of phosphonic functions due to their negative charge and electron repelling effect.

Table 2. Protonation (log *K*) constants of nitrilotriacetic acid and its phosphonic derivatives at t = 25°C and I = 0.2M (KCl).

	NTA	**NTAP**	**NTA2P**	**NTA3P**
log *K*(N)	9.51	10.52	11.71	12.3
log *K*(PO_3H^-)	–	5.45	6.23	6.92
log *K*(PO_3H^-)	–	–	4.88	5.66
log *K*(PO_3H^-)	–	–	–	4.42
log *K*(CO_2^-)	2.36	2.25	2.00	–
log *K*(CO_2^-)	1.75	1.38	–	–
log *K*(CO_2^-)	–	–	–	–
log *K*(PO_3H_2)	–	–	–	0.94

5.4 DETERMINATION OF THE FORMATION CONSTANTS OF Co(II) COMPLEXES

5.4.1 EXPERIMENTAL PART

Reagents and methods

All experiments were carried out in the open air, at room temperature. The Co(II) stock solution was prepared from recrystallized $CoCl_2 \cdot 6H_2O$. All the ligands used in the experiments were Aldrich products of puriss quality and were used without further purification. KOH was also purchased from Aldrich. Nano-pure quality water was used for all reactions run.

A) POTENTIOMETRIC MEASUREMENTS

Potentiometric measurements of the ligands in the presence of cobalt Co(II) were performed with a Metrohm 713 pH meter equipped with a Metrohm 6.0234.100 combined glass electrode, which was calibrated for hydrogen ion concentration according to Irving. The stability constants of cobalt Co(II) with the studied ligands, $\beta_{pqr} = [M_pA_qH_r] / [M]^p[A]^q[H]^r$ were calculated with the aid of the PSEQUAD[25] computer program. The stability constants of the cobalt Co(II) complexes were determined by pH-metric titrations of a 25 mL sample. Ligand to metal ion molar ratios of 4:1, 4:2, 4:4, 2:1, 2:2 were employed in titrations. During the titrations, the temperature was maintained at 25 ± 0.1^oC. The ionic strength was adjusted with KCl to 0.2 $mol \cdot dm^{-3}$. Titrations were performed from pH 2.0 up to pH 12, with a carbonate free KOH solution of known concentration (*ca* 0.2 $mol \cdot dm^{-3}$) under a purified argon atmosphere. The summary of the titration data used to calculate the formation constants for cobalt Co(II) – NTA and its phosphonic derivative complexes are presented in Table 3-6.

Table 3. Summary of the titration data used for the calculation of the formation constants of cobalt Co(II) – NTA complexes [a]

System	C_{Co}(mol·dm^3)	C_A (mol·dm^3)	C_H (mol·dm^3)	pH domain	n
Co(II) - NTA	0.003657	0.003728	0.015628	2.106-11.747	53
	0.002032	0.003728	0.015628	2.123-11.725	65
	0.001016	0.003728	0.015628	2.139-11.738	67
	0.001828	0.001936	0.00789	2.359-11.728	45
	0.001016	0.001936	0.00789	2.370-11.785	51

Table 4. Summary of the titration data used for the calculation of the formation constants of cobalt Co(II) - NTAP complexes [a]

System	C_{Co}(mol·dm^3)	C_A (mol·dm^3)	C_H (mol·dm^3)	pH domain	n
Co(II)- NTAP	0.00307	0.003272	0.015628	2.075-11.795	75
	0.002032	0.003272	0.015628	2.085-11.729	78
	0.001016	0.003272	0.015628	2.096-11.729	79
	0.001828	0.001936	0.007893	2.335-11.782	65
	0.001016	0.001936	0.007893	2.352-11.722	66

Table 5. Summary of the titration data used for the calculation of the formation constants of cobalt Co(II) – NTA2P complexes [a]

System	C_{Co}(mol·dm^3)	C_A (mol·dm^3)	C_H (mol·dm^3)	pH domain	n
Co(II)-NTA2P	0.002717	0.004099	0.024501	2.051-11.713	77
	0.002032	0.003888	0.023319	2.071-11.731	78
	0.001016	0.003888	0.023319	2.077-11.775	80
	0.001828	0.001944	0.011659	2.336-11.740	65
	0.001016	0.001944	0.011659	2.342-11.717	69

Table 6. Summary of the titration data used for the calculation of the formation constants of cobalt Co(II) – NTA3P complexes [a]

System	C_{Co}(mol·dm^3)	C_A (mol·dm^3)	C_H (mol·dm^3)	pH domain	n
Co(II)-NTA3P	0.003657	0.00391	0.01949	2.188-11.725	76
	0.002032	0.00391	0.01949	2.183-11.723	82
	0.001016	0.00391	0.01949	2.192-11.756	84
	0.001828	0.001975	0.009822	2.457-11.789	68
	0.001016	0.001975	0.009822	2.475-11.767	74

[a] The initial concentrations are expressed in mmol·dm^{-3}; *n* represents the number of experimeNTAl observations in each titration.

B) SPECTROPHOTOMETRIC MEASUREMENTS

The relativity of the pH-metrically determined stability constants was checked spectrophotometrically. A special titration cell was used for these measurements, having a light tube with quartz windows on both ends (path length = 3.005 cm) built into a conventional water-jacketed potentiometric cell. All measurements and operations of the spectropolarimeter were computer controlled. The temperature was maintained at $25 \pm 0.3^{o}C$ with circulating water. The spectral range covered was 400-800 nm. Spectra were collected at various pH values for solutions containing ligand to metal ion molar ratios of 4:8 and 4:16. The burette used was a Metrohm 736 GP Titrino equipped with two DOSIMAT 685 units. UV/Visible spectra were recorded on a Hewelett-Packard 8452 diode-array spectrophotometer.

5.4.2 RESULTS AND DISCUSSION

A set of formation constants for the metal complexes and their successive protonation constants, defined by $K_{MH_mA} = [MH_mA] / [H][MH_{m-1}A]$, were evaluated, with the aid of the PSEQUAD computer program, taking into account the hydrolysis of the metal ions. In all of the cases the hydroxo complexes, CoA(OH) forms at high pH. The formation constant of a hydroxo complex is defined by $K_{M(OH)A} = [M(OH)A]/[MA] \cdot [OH]$.

The formation constants of cobalt Co(II) complexes calculated separately from potentiometric and spectrophotometric titrations are presented in Table 7. The formation constants of cobalt (II) complexes calculated from both potentiometric and spectrophotometric titrations are presented in Table 8.

Table 7. The formation constants of cobalt Co(II) complexes (log β) of nitrilotriacetic acid and its phosphonic derivatives at T = 25°C and I = 0.2M (KCl).

	NTA		NTAP		NTA2P		NTA3P	
Species	Sp	pH	Sp	pH	Sp	pH	Sp	pH
$CoAH_3$	-	-	-	-	-	-	27.91(1)	27.96(1)
$CoAH_2$	-	-	-	-	22.40(1)	22.47(1)	24.36(1)	24.40(2)
CoAH	-	-	16.08(1)	16.14(1)	17.94(1)	18.03(2)	19.46(1)	24.51(2)
CoA	9.79(1)	9.83(1)	11.01(1)	11.06(2)	12.51(1)	12.62(2)	13.62(1)	13.69(2)
$CoAH_{-1}$	-1.44(1)	-1.33(2)	-0.49(1)	-0.33(3)	0.22(1)	0.09(9)	1.44(2)	1.51(3)
CoA_2	13.78(1)	13.81(4)	13.51(1)	13.73(6)	-	-	-	-

Sp=Spectrophotometry
pH=pH-metry

Table 8. The formation constants of cobalt Co(II) complexes (log β) of nitrilotriacetic acid and its phosphonic derivatives at T = 25°C and I = 0.2M (KCl).

	NTA	NTAP	NTA2P	NTA3P
$CoAH_3$	–	–	–	27.94
$CoAH_2$	–	–	22.42	24.38
CoAH	–	16.11	17.97	19.49
CoA	9.80	11.04	12.55	13.67
$CoAH_{-1}$	-1.41	-0.45	0.25	1.48
CoA_2	13.76	13.54	-	–
Number of points	281	363	356	384
Fitting parameter[a]	$3.16 \cdot 10^{-3}$	$2.85 \cdot 10^{-3}$	$2.45 \cdot 10^{-3}$	$3.19 \cdot 10^{-3}$
p*K*($CoAH_3$)	–	–	–	3.56
p*K*($CoAH_2$)	–	–	4.45	4.89
p*K*(CoAH)	–	5.07	5.42	5.82
p*K*(CoA)	11.21	11.49	12.30	12.19

[a] Average difference between the experimental and calculated titration curves expressed in mL of the titrant.

In table 8, $pK(CoAH_n) = p\beta(CoAH_n) - p\beta(CoAH_{n-1})$, where **n**- number of substituted phosphonate groups.

The NTA –like ligands are potentially tetradentate metal ion binders. It is worth noting that only 1:1 complexes are formed with most of the metal ions,[26, 27] There can be diverse binding modes for the ligands in the protonated complexes. The ligands can coordinate to Co(II) via the carboxylates in the NTA and through the carboxylates and phosphonate groups in the complexes of mixed carboxylic – phosphonic derivatives. The coordination of all phosphonate groups to Co(II) in the NTA3P complexes is not likely, because of the high electrostatic repulsion between the phosphonate arms.

Formation of protonated complexes $CoAH_n$ can be deduced from the pH-metric and spectrophotometric titrations. The more carboxylate groups are replaced by phosphonate groups the higher the tendency is for the ligand to form protonated complexes. In the case of NTA, no protonated complexes are formed. For its mixed carboxylic-phosphonic derivatives, CoAH and $CoAH_2$ appear in high quantities, while for NTA3P even the $CoAH_3$ species forms at very low pH. The bis complex CoA_2 is forming only in the cases of NTA and NTAP. Owing to the high affinity of the NTA-like ligands for Co(II), complex formation reactions between the metal ion and the protonated forms of the ligand are almost complete at acidic pH values and free Co(II) ion is present at rather low concentrations at the starting pH values. In spite of this, pH-metry can be applied for the determination of stability constants, as the equilibrium system is better "fixed" to the uncomplexed Co(II)-hydroxo species in the high pH range.

In all of the protonated species formed in the weekly acidic pH range, the amino group remains probably coordinated to the metal. As the pH increases, the protonated forms undergo further deprotonation, resulting in the formation of CoA complexes in which the amino group is coordinated, as that is observed in the solid state for NTA2P. In the Co(II) – NTA system, deprotonation of CoA species starts after pH 6 and results in the formation of the hydroxo species $CoAH_{-1}$. For the NTA phosphonic derivatives, NTAP and NTA2P deprotonation occurs after pH 8, while for NTA3P deprotonation occurs after pH 6, resulting in the formation of the hydroxo species $CoAH_{-1}$.

The relatively low protonation constants and the slight changes in the visible spectral parameters indicate that the nitrogen donor remains coordinated and the proton(s) reside(s) on the oxygen donor phosphate and/or carboxylate functions.[26] This is in contrast to what was reported for the alkaline – earth complexes of these ligands, when the first protonation process was assumed to occur on the tertiary-N donor.[28]

The titration curves were evaluated with different potential speciation models. The best fit between the experimental and calculated titration curves was obtained by

considering the species in Table 8. The speciation curves were evaluated with aid of the HySS computer program. Speciation curves for the complexes formed in the Co(II)-NTA, Co(II)-NTAP, Co(II)-NTA2P, Co(II)-NTA3P systems as a function of pH are shown in Fig.3.

The speciation distribution curves for the system Co(II)-NTA (Fig. 3 a)) indicate that complex formation starts at pH≈2 with the 1:1 deprotonated species CoA, this species being the dominant one in the pH range 4 - 6. At the physiological pH 7.4, in the system, there are two species present, the deprotonated species CoA and the bis complex CoA_2, which starts to form at pH 6. After pH 10, the hydoxo complex CoA(OH) starts to form. Of the potential species proposed, the ones at high concentrations are (a) CoA, which represents 100% of the total species fraction in solution in the pH range 4-6, and (b) CoA_2 which appears to be 90% of the total species fraction in solution at pH values greater than 10.

The speciation distribution curves for the system Co(II)-NTAP (Fig. 3 b)) indicate that complex formation starts with the monoprotonated species CoAH approximately at pH 2. Upon pH increase, deprotonation of the ligand takes place and the 1:1 deprotonated species CoA grows into the potential biodistribution scheme. CoA is the major species at the physiological pH (7.4). The bis complex species CoA_2 starts to form at pH 8, with a maximum (about 30%) at pH 11. In the case of NTAP, the bis complex species starts to form at a higher pH than in the case of NTA and the maximum for this species is considerably lower in the case of NTAP (30% in comparation with 90% in the case of NTA). The hydoxo complex CoAOH starts to form at pH values greater than 10. Of the potential species proposed, the ones at high concentrations are (a) CoAH, which appears to be 90% of the total species fraction in solution around pH range 4, and (b) CoA, which represents approx. 100% of the total species fraction in the pH range 7-9.

In the case of the Co(II)-NTA2P system, the speciation distribution curves (Fig. 3 c)) indicate that complex formation also starts at pH≈2, with the doubleprotonated species $CoAH_2$. Upon pH increase, deprotonation of the ligand takes place, the monoprotonated species CoAH starts to form at pH 3, with a maximum (about 60%) at pH 5. In the pH range 4 – 12, the 1:1 deprotonated species CoA forms and it is the major species at the physiological pH 7.4. The hydroxo complex CoAOH forms at pH values greater than 10. The bis complex species was also considered in the speciation calculation, but it was rejected by the computer program. Of the potential species proposed, the ones at high concentrations are (a) $CoAH_2$, which appears to be 70% of the total species fraction in

solution around pH 4, and (b) CoA, which represents almost 100% of the total species fraction in the pH range 7.5-10. Since complex **1**, isolated in the solid state at pH 5.5-6, contains a dinuclear species, the nuclearity of the complex in solution was carefully checked. When the presence of dinuclear species, like Co_2A or Co_2A_2, was evoked in addition to the mononuclear species CoA, the former species were rejected. Only when either the dinuclear species Co_2A or Co_2A_2 was assumed, with the monomer omitted from the speciation model, did the fit between the experimental and calculated titration curves decrease considerably. These facts, along with the electronic spectra, which indicate the formation of a single species around $pH \approx 8$, suggest that that formation of the dinuclear species Co_2A_2 in solution, at least in the concentration range studied, can be excluded.

Overall, therefore, the binary system Co(II) - N, N-bis(phosphonomethyl)glycine (as that is shown in the speciation curves depicted in Figure 2 c), can be described adequately by considering the presence of species $[CoAH_2]^{-1}$, $[CoAH]^{2-}$, its deprotonated form $[CoA]^{3-}$ and the fully deprotonated form $[CoLOH]^{4-}$.

It should be mentioned that, in the herein-described speciation scheme, the resulting species are proposed to be octahedral, with the generated vacant coordination sites on each potential complex occupied by solvent water molecules. On the basis of such geometry around Co(II), coordination proceeds via both the phosphonate groups through one of its deprotonated hydroxides, the tertiary nitrogen atom as well as the carboxylate group.

The speciation distribution curves for the system Co(II)-NTA3P (Fig. 3 d) indicate that complex formation starts with the species $CoAH_2$ at $pH \approx 2$. Upon pH increase, deprotonation of the ligand takes place and the monoprotonated specie (CoAH) starts to form at pH 2.5. Between the pH range 3 – 8 the 1:1 deprotonated species (CoA) forms with a maximum content (approx. 55%) at pH 5.5. The hydroxo complex $CoAH_{-1}$ starts to form at pH 4. At the physiological pH 7.4 in the system, there are two species, the deprotonated species CoA and the hydroxo complex $CoAH_{-1}$, the last one being the major species until the end of titration (approx. pH 12). Other chemically reasonable species, such as CoA_2H_{-2} or $CoAH_{-2}$, were also considered in the speciation calculation but were rejected by the computer program. Of the potential species proposed, the ones at high concentrations are (a) CoAH, which appears to be 60% of the total species fraction in solution around pH 4.5, and (b) $CoAH_{-1}$, which represents 100% of the total species fraction after pH 7.

a)

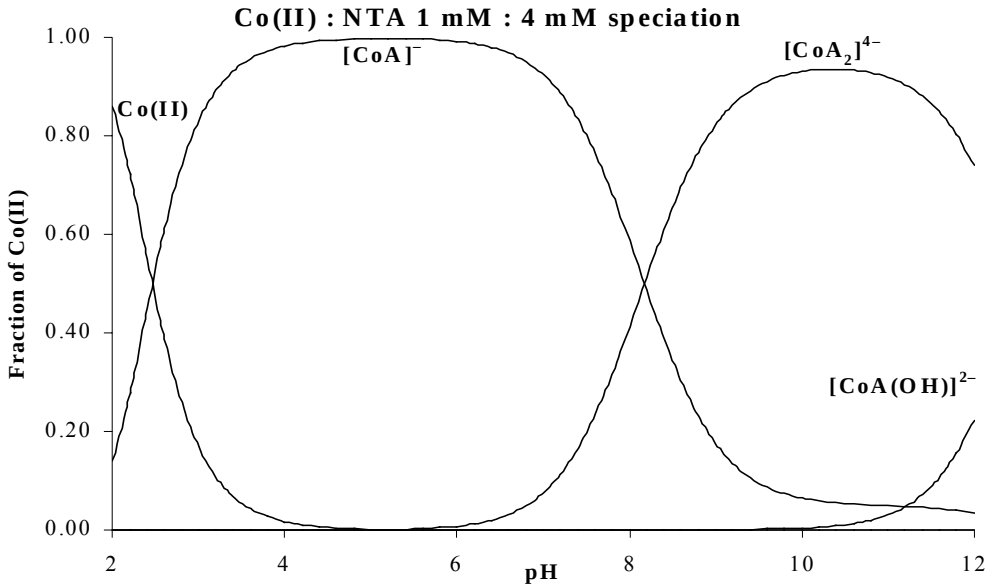
Co(II) : NTA 1 mM : 4 mM speciation
Fraction of Co(II)
1.00
0.80
0.60
0.40
0.20
0.00
2
4
6
8
10
12
pH
Co(II)
[CoA]⁻
[CoA₂]⁴⁻
[CoA(OH)]²⁻

b)

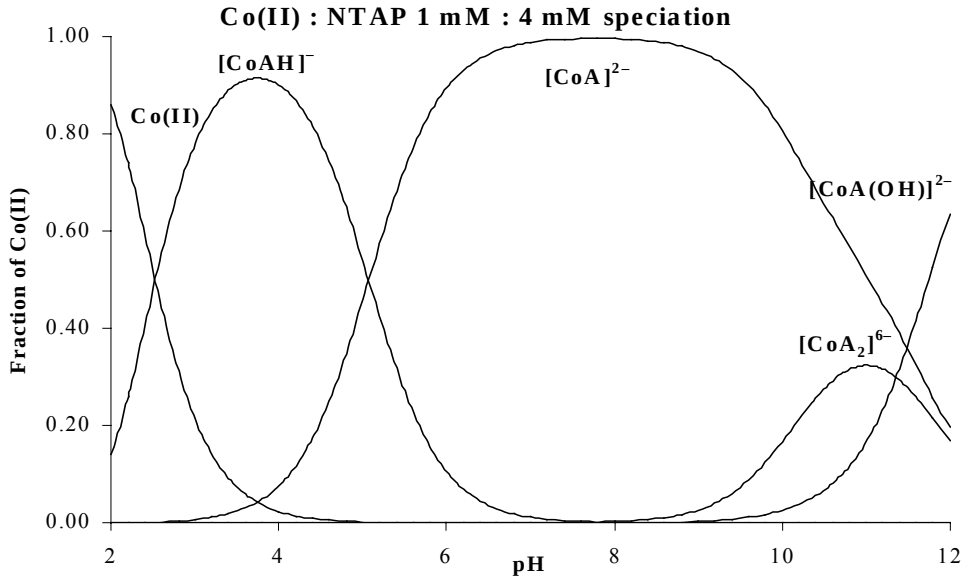
Co(II) : NTAP 1 mM : 4 mM speciation
Fraction of Co(II)
1.00
0.80
0.60
0.40
0.20
0.00
2
4
6
8
10
12
pH
Co(II)
[CoAH]⁻
[CoA]²⁻
[CoA(OH)]²⁻
[CoA₂]⁶⁻

c)

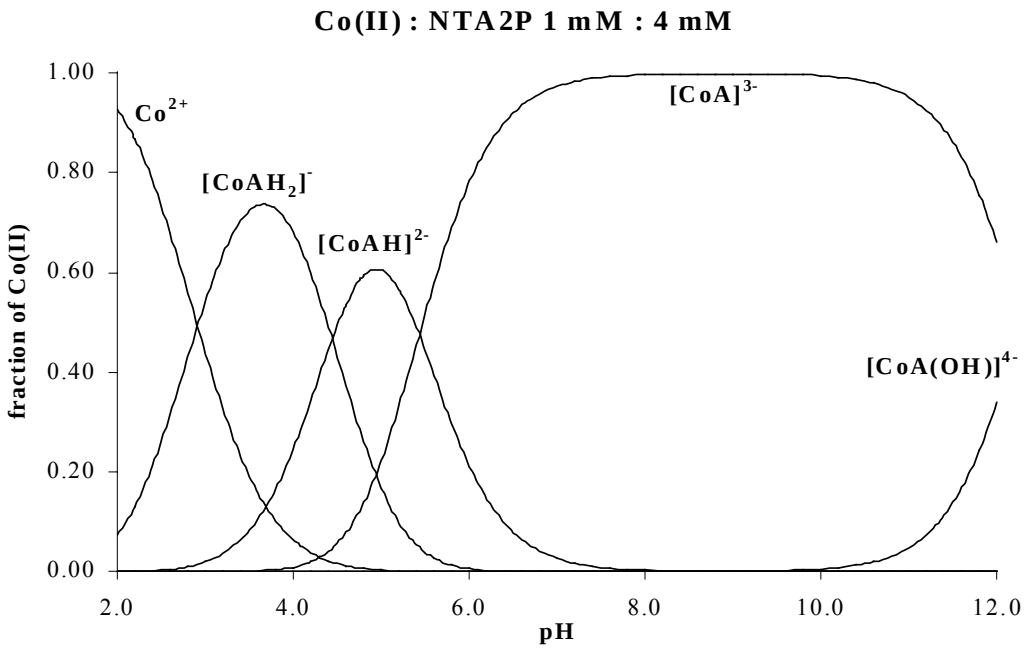

d)

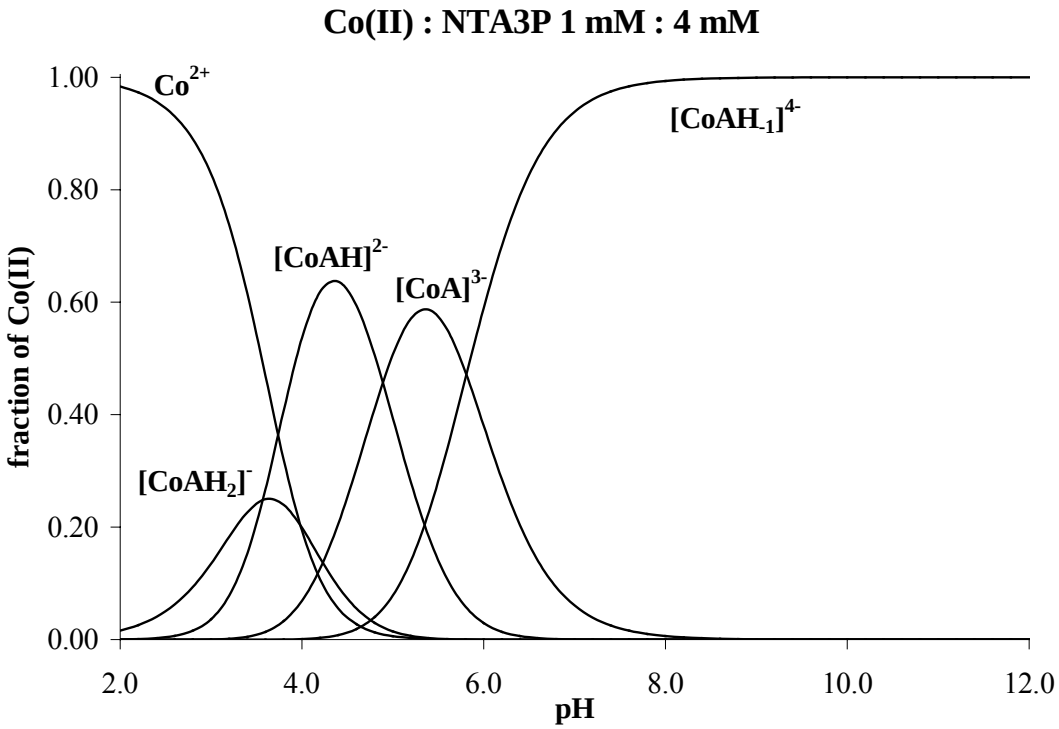

Fig. 3 Speciation distribution diagrams for a) Co(II)-NTA, b) Co(II)-NTAP, c) Co(II)-NTA2P, d) Co(II)-NTA3P systems at 1:4 mM ratio.

The absorption spectra obtained at various pH values and containing cobalt and ligands in known amounts, have been utilized for a quantitative evaluation of the speciation curves. The absorption spectra of the complexes formed in the Co(II)-ligand systems are depicted in Fig. 4. The values of the formation constants of cobalt Co(II) complexes obtained from the spectrophotometric measurements are in very good agreement with the values obtained from the pH-metric measurements (see Table 7.). According to the spectrophotometric titrations, the same complexes form in the Co(II)-NTA, Co(II)-NTAP, Co(II)-NTA2P and Co(II)-NTA3P systems as predicted by the potentiometric titrations. The excellent agreement suggests the absence of any bias in the results.

a)

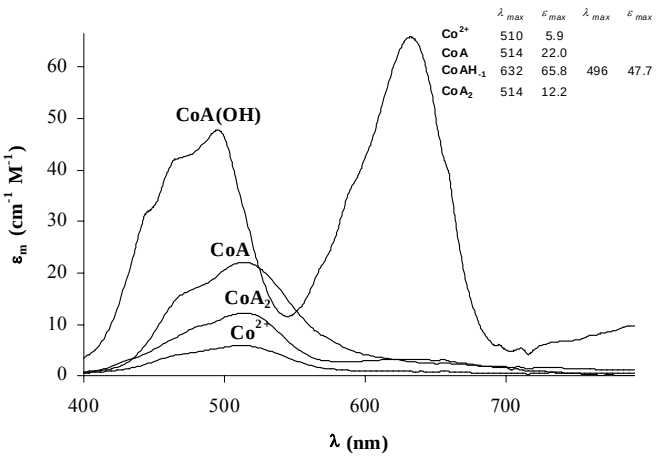

Species	λ_{max}(nm)	ε_{max}($cm^{-1}M^{-1}$)	λ_{max}(nm)	ε_{max}($cm^{-1}M^{-1}$)
Co(II)	510	5.9	-	-
CoA	514	22.0	-	-
CoA(OH)	632	65.8	496	47.7
CoA_2	541	12.2	-	-

b)

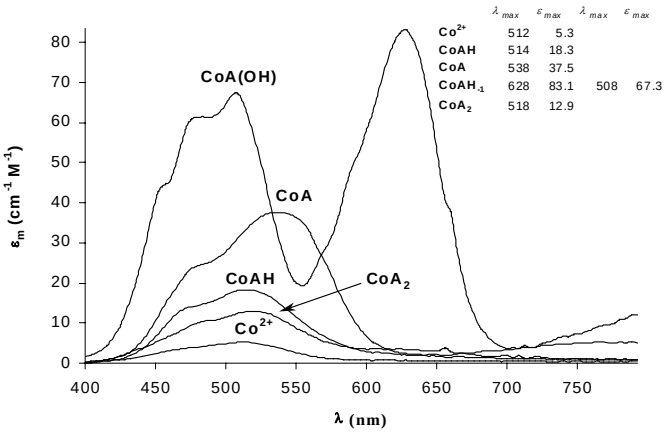

Species	λ_{max}(nm)	ε_{max}($cm^{-1}M^{-1}$)	λ_{max}(nm)	ε_{max}($cm^{-1}M^{-1}$)
Co(II)	512	5.3		
CoAH	514	18.3		
CoA	538	37.5		
CoA(OH)	628	83.1	508	67.3
CoA_2	518	12.9		

c)

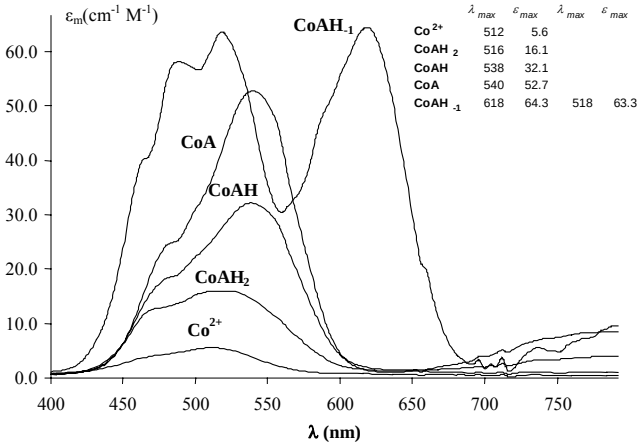

Species	λ_{max}(nm)	ε_{max}($cm^{-1}M^{-1}$)	λ_{max}(nm)	ε_{max}($cm^{-1}M^{-1}$)
Co(II)	512	5.6		
$CoAH_2$	516	16.1		
CoAH	538	32.1		
CoA	540	52.7		
CoA(OH)	618	64.3	518	63.3

d)

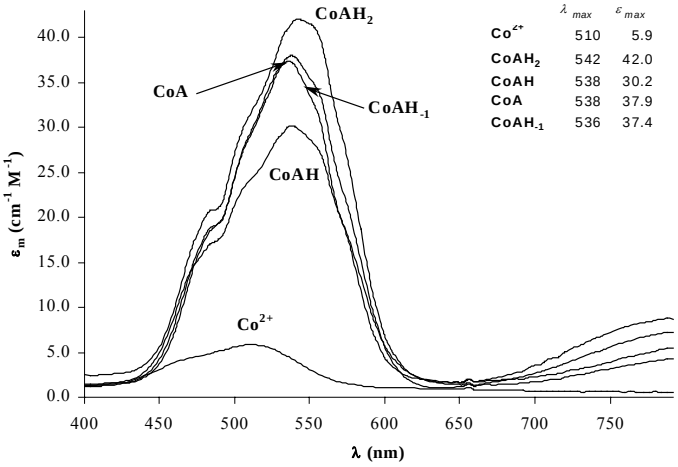

Species	λ_{max}(nm)	ε_{max}($cm^{-1}M^{-1}$)
Co(II)	510	5.9
$CoAH_2$	542	42.0
CoAH	538	30.2
CoA	538	37.9
CoA(OH)	536	37.4

Fig. 4 Absorption spectra of the complexes formed in the a) Co(II)-NTA, b) Co(II)-NTAP, c) Co(II)-NTA2P, d) Co(II)-NTA3P systems.

5.5 CONCLUSIONS

Detailed speciation studies suggested the presence of the following species in the studied systems:

a) The Co(II)- nitrilotriacetic acid (NTA) system can be described by considering the presence of a deprotonated species $[CoA]^{1-}$, a bis complex $[CoA_2]^{4-}$ and the fully deprotonated form $[CoAOH]^{2-}$.

b) The Co(II) - N-(phosphonomethyl)-iminodiacetic acid (NTAP) system can be described by considering the presence of a monoprotonated specie $[CoAH]^{1-}$, its deprotonated form $[CoA]^{2-}$, the fully deprotonated form $[CoAOH]^{2-}$ and the bis complex $[CoA_2]^{6-}$.

c) The Co(II) - N, N-bis(phosphonomethyl)glycine) (NTA2P) system can be described well by considering the presence of a doubleprotonated specie $[CoAH_2]^{1-}$, a monoprotonated species $[CoAH]^{2-}$, its deprotonated form $[CoA]^{3-}$ and the fully deprotonated form $[CoAOH]^{4-}$.

d) The Co(II) - nitrilo-tris(methylphosphonic acid) (NTA3P) system can be described adequately by considering the presence of a doubleprotonated specie $[CoAH_2]^{2-}$, a monoprotonated specie $[CoAH]^{2-}$, its deprotonated form $[CoA]^{3-}$ and the fully deprotonated form $[CoAOH]^{4-}$.

The phosphonic derivatives act as very effective ligands towards Co(II). The data, listed in Table 8 and Fig. 5, indicate that the stability of the complexes increases with increasing number of the more basic phosphonates. Co(II) forms the least stable complexes with NTA and NTAP, while the complexes with NTA2P and NTA3P have the highest stability. For comparison, the stability constants of the respective complexes of Cu(II)[26], VO(IV)[27] and Al(III)[29] are also shown in Fig. 5. A comparison of pK(MA) values (depicted in Fig. 5) for Co(II), Cu(II), VO(IV), Al(III) complexes reveals several differences in the coordination behaviour of these metal ions with the studied ligands. Al(III) forms the least stable complexes with NTA and its phosphonic derivatives, while Co forms the most stable complexes.

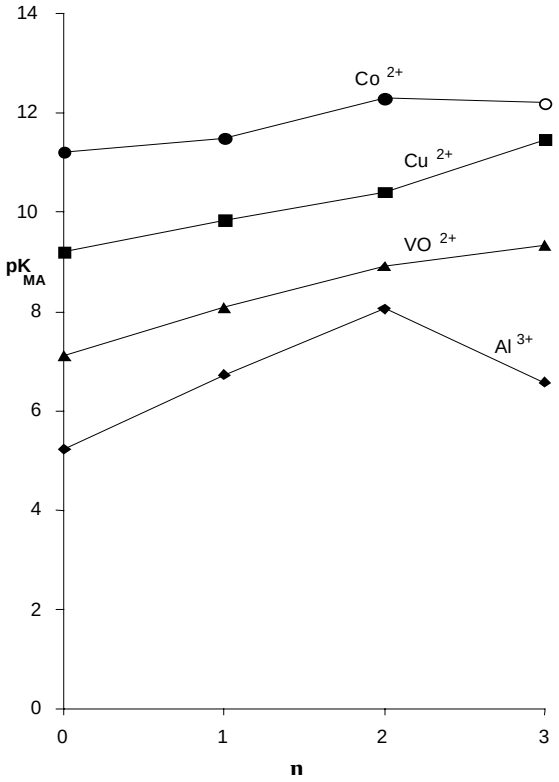

Fig. 5 Comparison of pK (CoA), pK (CuA), pK (VOA), pK (AlA) values for NTA complexes of mixed phosphonic-carboxylic derivates. **n**- number of substituted phosphonate groups.

By plotting pCo(II) (pCo(II) = log [Co(II)]) as a function of pH at two different ligand to metal molar ratios (4mM : 4mM and 4mM : 1mM) in Fig. 6, it can be seen that at low pH NTA is the most effective binder, but upon pH increase (approx. pH = 6) NTA3P becomes the most effective binder for Co(II).

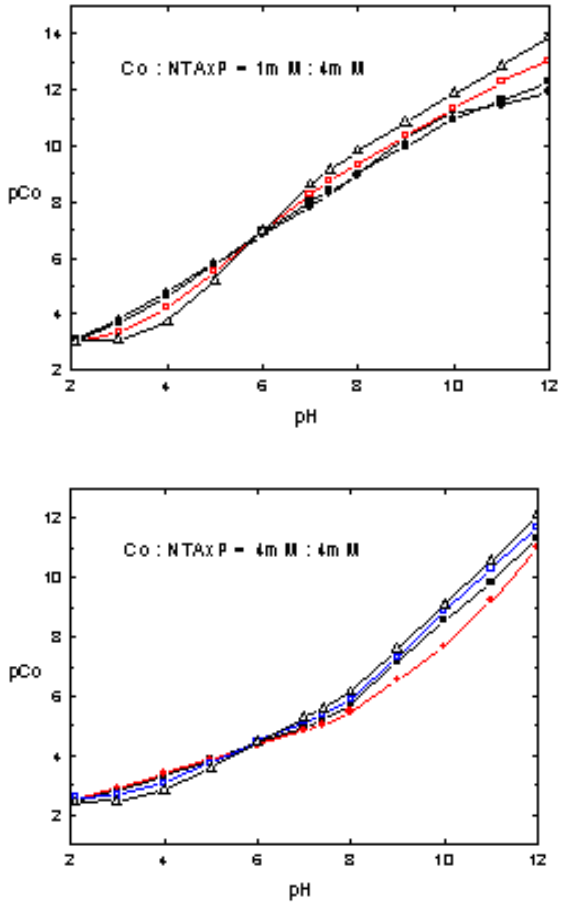

Fig. 6 Plots of pCo(II) as a function of pH at two different ligand to metal molar ratio (4mM : 4mM and 4mM : 1mM). (solid circles – NTA; solid squares – NTAP; open squares – NTA2P; open up triangles – NTA3P)

More reliable measurements for the metal binding ability of the ligands are the conditional stability constants or free (uncomplexed) metal ion concentrations (pM) under specific conditions. The most effective binder for Co(II) (the highest pCo value) is NTA3P, followed by NTA2P, NTAP and NTA, as that can be seen from the Fig. 7.

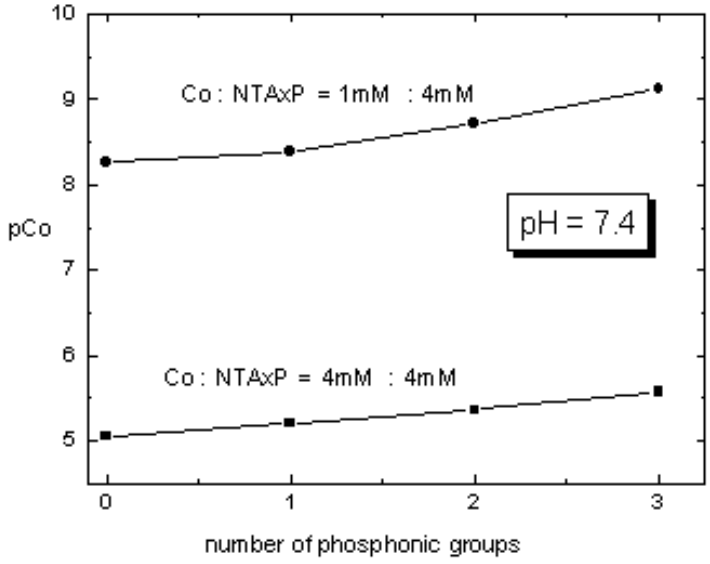

Fig. 7 – Influence of phosphonic group numbers of NTAxP on pCo values at physiological pH and at two values of Co : NTAxP ratios

5.6 LITERATURE

1. Martell M. A.; and Smith, R. M. *Critical Stability Constants,* Vol. V. Plenum, New York, **1982**, p. 183.
2. Motekatis, R. J.; and Martell, A. E. *J. Coord. Chem*., **1985**, *14*, 138.
3. Smith, P. H.; and Raymond, K. N. *Inorg. Chem.*, **1988**, *27*, 1056.
4. Katkov, A. P.; Matkovskaya, T. A.; Krutikova, N. I.; Monakhov ,A. S.; and Dyatlova, N. M. *Zh Neorg Khim*., **1991**, *36*, 693.
5. Dhansay, M. A.; and Linder, P. W. *J. Coord. Chem*., **1993**, *28*, 133.
6. Pangunoori, R.; and Ram, K. *Orient. J. Chem*., **1994**, *10*, 9.
7. Popov, K. I.; Anderegg J.; and. Popova, I. A. *Russ. J. Coord. Chem*., **1998**, *24*, 396.
8. Schwarzenbach, G.; Ackermann H.; and Ruckstuhl, P.*Helv. Chem. Acta*, **1949**, *32*, 1175.
9. Westerback, S.; Rajan, K. S.; and Martell, A. E. *J. Am. Chem.,* **1965**, *87*, 2567.
10. Carter, R. P.; Carroll R. L.; and Irani, R.R. *Inorg. Chem.,* **1967**, *6*, 939.
11. Piculikova, Z.; Muchova A.; and Majer, J.*Acta. Fac. Pharm. Univ. Comenianae,* **1987**, *41*, 83.
12. Rao, G. M.; Pangunoori, R.; and Ram, K. *J. Indian Chem. Soc.,* **1997**, *74*, 94.
13. Zekany, L.; Nagypal, I.; *Computational Methods for the Detrmination of Stability Constants,* Plenum Press, Ney York, **1985**.
14. Martell, A. E.; Hancock, R. D. ACS *Symp. Ser.,* **1994**, *565*, 240-247.
15. Alderighi, L.; Gans, P.; Ienco, A.; Peters, D.; Sabatini, A.; Vacca, A. *Coordination Chemistry Reviews*, **1999**, *184*, 311-318.
16. Irving, H. M.; Miles M.G.; and Petit, L.D. *Anal. Chim. Acta*, **1967**, *38*, 475
17. Ichikawa T.; and Sawada, K. *Bull. Chem. Soc. Jpn.*, **1997**, *70,* 829-835.
18. Motekaitis R. J.; and Martell, A. E. *Inorg. Chem*., **1980**, *19*, 1646
19. Kornev, V.; Valayaeva, V.; Mukanov, I. *Zhur. Phys. Khim*., **1978**, *52,* 1132
20. Israeli, J.; Cecchetti, M. *Can. J. Chem*., **1968**, *46,* 3821-3835
21. Nikitina, L; Karmasina, L.; Dyatlova, N. *Zhur. Neorg. Khim*.,**1974**,*19*, 1671.
22. Motekaitis, R. J.; and Martell, A. E. *J. Coord. Chem*., **1985**, *14*, 139
23. Dhansay, M. A.; and Linder, P.W. *J. Coord. Chem.*, **1993**, *28*,133
24. Jazowska-Bojczuk, M.; Kiss, T.; Kozlowski, H.; Decock P.; and Barycki, J. J. *Chem. Soc., Dalton Trans.*, **1994**, 811.

25. Zekany, L.; Nagypal, I.; and Peintler, G. PSEQUAD for Chemical Equilibria, Technical Software Distributions, Baltimore, MD, **1991**
26. Buglyo, P.; Kiss, T.; Dyba, M.; Jezowska-Bojczuk, M.; Kozlowski H.; and Bouhsina, S. *Polyhedron*, **1997**, *16*(*19*), 3447-3454.
27. Sanna, D.; Bodi, I.; Bbouhsina, S.; Micera G.; and Kiss, T. *J. Chem. Soc., Dalton Trans*, **1999**, 3275.
28. Kiss, T.; Lazar I; .and Kafarski, P. *Metal Based Drugs*, **1994**, *1*, 247.
29. Kilyen, M.; Lakatos, A;. Latajka, R.; Labadi, I.; Salifoglou, A.; Raptopoulou, C.P.; Kozlowski H.; and Kiss, T. *J. Chem. Soc., Dalton Trans*, **2002**, 3578-3586.

6. CONCLUSIONS

6.1 Correlation between speciation and structural studies

A detailed speciation study of the binary system Co(II) – N,N-bis(phosphonomethyl)glycine was carried out under varying Co(II) and N,N-bis(phosphonomethyl)glycine molar ratios throughout the pH range. For a better understanding of the system mentioned above, speciation studies of Co(II) – NTA phosphonate derivatives were carried out under varying cobalt(II) and ligand molar ratios throughout the pH range.

Four major species arise from the derived speciation of Co(II)–N,N-bis(phosphonomethyl)glycine system. One of them is the deprotonated species $[CoA]^{3-}$ This species begins to form around pH 4 and at pH 6 is the predominant specie. Being aware of the possibilities in the coordination environment around Co(II) ion of this species in water, it would not be unreasonable to envisage a coordination sphere comprised of both ligand phosphonates (through one of the deprotonated hydroxides), the corboxylate group, the tertiary nitrogen atom as well as bound water oxygen around Co(II). The pH at which this species starts to dominate is 6, where the synthetic reaction was run, leading to the isolation of an assembly of species, complex **2**. A species presenting the structural characteristics of the one mentioned above is part of this assembly ($[Co\{N(CH_2COO)(CH_2PO_3)_2]^{3-}$). Unfortunately, from the speciation studies only one species present in complex **2** ($[CoA]^{3-}$) could be determined.

At higher pH values (> 10) the hydroxo complex CoA(OH) starts to form upon the deprotonation of a water molecule in the coordination sphere of Co(II).

In the low pH range, two species arise: the doubleprotonated species $[CoAH_2]^{1-}$ and the monoprotonated species $[CoAH]^{2-}$. The speciation studies begin at pH 2 with the synthetic reaction leading to the isolation of complex **1** having been run at a pH value lower than 2. Thus, this species has not been included in the speciation studies.

$[Co\{N(CH_2COO)(CH_2PO_3)_2]^{3-}$ complex is a good example of a well-characterized species of potential biological relevance. This being the major species around the physiological pH, it may reflect a form of Co(II) which is potentially relevant to forms exerting influence on biochemical events related to toxic effects at the cellular level and aberrant physiological symptoms in human helth.[1-3]

Overall, the herein-developed chemistry suggests that, in the wide spectrum of pH-variable aqueous solution, different species exist with variable solubility profiles, thus

forging their isolation in the crystalline form, in the presence of specific counterions (K^+, Na^+, NH_4^+).

6.2 Final Conclusions

As a representative metal binder, the organophosphonate ligand, N,N,-bis(phosphonomethyl) glycine was employed in aqueous reactions with Co(II), ultimately leading to the isolation of two complexes at two different pH values.

Facile aqueous reactions of Co(II) ion with N,N-bis(phosphonomethyl) glycine acid in the presence of ammonia led to the isolation of complex **$[Co(C_4H_9O_8NP_2)_2(H_2O)_2] \cdot 2H_2O$** (**1**) at low pH. At higher pH values 5.5-6 aqueous reactions of Co(II) ion with N,N-bis(phosphonomethyl) glycine acid in the presence of ammonia led to the isolation of the complex assembly

$(NH_4)_4[Co(H_2O)_6][Co\{N(CH_2COO)(CH_2PO_3)_2\}(H_2O)_2]_2[Co(H_2O)_2\{N(CH_2COO)(CH_2PO_3H)(CH_2PO_3)\}Co(NH_3)_2(H_2O)_3]_2 \cdot 10\ H_2O \cdot 1.36\ CH_3CH_2OH$ (**2**).

With assessment of the structural features observed in both **1** and **2,** the following observations can be made:

1. The Co(II) ions in both species achieve a stable octahedral coordination. Different ligands are employed to satisfy the octahedral environment around the Co(II) ion ($(H_2O_3P\text{-}CH_2\text{-}N\ (CH_2COOH)\text{-}CH_2\text{-}PO_3H_2$, H_2O, NH_3).
2. Complex **1** is comprised of mononuclear units linked together through water molecules of crystallization and an extensive network of hydrogen bonds. The mononuclear Co(II) ion resides in a distorted octahedron.
3. Complex **2** is an unusual and unique assembly of species, with its structure consisting of discrete assemblies of mononuclear and dinuclear complexes of Co(II).
4. The charge on the mononuclear complex **1** is zero, while the charges of the species present in complex **2** are +2, 0 and -3. ($[Co(H_2O)_6]^{2+}$, $[Co(H_2O)_2\{N(CH_2COO)(CH_2PO_3H)(CH_2PO_3)\}Co(NH_3)_2(H_2O)_3]^0$, $[Co\{N(CH_2COO)(CH_2PO_3)_2\}(H_2O)_2]^{3-}$).

Complexes **1** and **2** constitute proof of species arising from simple speciation distributions of binary systems between Co(II) and simple phosphonate ligands.[4-6] The retention in solution of the octahedral coordination environment in what has been suggested by the spectroscopic data, substantiates the contention that the particular metal ion could interact with phosphonate containing ligands in an aqueous solution.

Spectroscopic studies combined with cyclic voltammetry, and EPR data in the solid state and in solution formulate the speciation signature of the investigated binary systems, with projections covering the existence of other species arising in a pH-dependent fashion across the pH physiological range.

The overall physical and chemical properties of the cobalt complexs synthesized and characterized, represent the basis of understanding the behaviour of cobalt in biologically relevant media. It remains to be seen whether species of the herein proposed nature or similar to it represent bioavailable forms of Co(II), which elicit interactions at the cellular level not unlike the ones involved in biological processes.

6.3 LITERATURE

1. Kusaka, Y.; Jokohama, K.; Sera, Y.; Yamamoto, S.; Sone, S.; Kyono, H.; Shirakawa, T.; Golo, T. *J. Int. Med*, **1986**, 43, 474-485.
2. Moorhouse, C. P.; Halliwell, B.; Grootveld, M.; Gutteridge, J. M. C. *Biochim. Biophys. Acta,* **1985**, 843, 261-268.
3. Robison, S. H.; Cantoni, O.; Costa, M. *Carcinogenesis,* **1982**, 3, 657-662.
4. Mootz, D.; Wunderlich, H. *Acta Cryst.***1980**, *B 36*, 445-447.
5. Mammano, N. J.; Templeton, D. H.; Zalkin, A. *Acta Cryst.* **1977** *B33*, 1251-1254.
6. Corradi, A. B.; Palmieri, C. G.; Nardelli, M.; Pellinghelli, M. A.; Tani, M. E. V. *J. Chem. Soc. Dalton Trans.* **1973**, 655-658.

ACKNOWLEDGEMENTS

This study has been carried out at the University of Crete, Department of Chemistry, Greece and at the University of Szeged, Department of Analytical and Coordination Chemistry, Hungary under the supervision of Assoc. Prof. A. Salifoglou.

First of all I would like to thank my supervisor, Assoc. Prof. A. Salifoglou for his constant interest, and critical advice in this academic work. My special thanks go to Prof. T. Kiss and to T. Jakusch who supervised the experimental work carried out at the University of Szeged. I would also like to thank V. Tangoulis for performing the EPR experiments and the Dimokritos group for the X-ray structures.

I would like to give my thanks to the members of the postgraduate program "Applied Molecular Spectroscopy" for making it possible for me to finalize my Master work at the University of Crete.

I would like to thank Prof. Athanassios Coutsolelos, Assoc. Prof. Apostolis Rizos, and Assoc. Prof. Athanassios Salifoglou for agreeing to be on my committee.

I would like to express my deep gratitude to my parents for their support, understanding, and encouragement. Mirela, Maria and Niko many thanks for your friendship.

.